UNIVERSITÀ DEGLI STUDI DI PADOVA

Dipartimento ICEA

MASTER THESIS IN ENVIRONMENTAL ENGINEERING – SOIL PROTECTION COURSE

ANALYSIS OF THE THERMO-PHYSICAL PROPERTIES OF SOILS AND ROCKY MATERIALS IN TRENTO AREA RELATED TO USE OF THE SUBSOIL AS A THERMAL ENERGY STORAGE

Relatore: Prof. Raffaele Sassi
Correlatore: Prof. Antonio Galgaro
Dott.ssa Eloisa Di Sipio

Laureando: Martino Ruggeri

ANNO ACCADEMICO 2013 / 2014

Summary

1. Introduction

The aim of the thesis is to provide an overview of the thermal properties of rocks and soils in the area of the municipality of Trento, for a better implementation of Thermal Energy Storage (TES) system. This thesis is part of a larger project of the Bruno Kessler Foundation in collaboration with the University of Padova to investigate the feasibility of TES technology for house heating. Bruno Kessler Foundation (FBK) is the research institute of the Trento Province, and works in the fields of science, technology and humanistic studies. FBK has been operating since 2007, and promotes and carries out research in areas of interest for the provincial development and carries out its activities with the goal of being recognized as a national and international center of excellence.

The term “geothermal” is derived from the greek “geos” = earth and “thermos” = heat, from which the literal meaning is “Heat of the Earth”. Therefore geothermal energy means the one contained as heat in the ground, and whose only manifestation is temperature.

There are various types of geothermal systems (defined as any underground resource which it can exchange heat). Initially they were considered only the hydrothermal ones, with a thermal tank represented by subsoil in which the heat is propagated by convection because of the convective motions of the fluids contained. It can be water dominant (with lower energy content, in that case there is also conduction) or vapor-dominated (with very high energy content).
The systems with a temperature higher than 150°C are called “high-enthalpy” and are exploited for the production of electricity: the first exploitation of the Earth's heat to generate electricity took place in Larderello in Tuscany by Prince Piero Ginori Conti in the years 1904-05, and the first commercial geothermal power plant was installed there in 1911.
Low-enthalpy systems have a temperature lower than 150°C (Norden, 2011), and are used mainly for the heating of buildings.
The soil, because of its moderate thermal inertia, even at low depth is less influenced by the daily and seasonal temperature fluctuations. Below 10 m of depth its temperature can be considered constant throughout the year, due to the balance between the heat flow that comes from the Earth's mantle and core, the contribution of solar energy to the earth's surface, and sometimes the contribution of the available energy from groundwater (Verrone, 2009). In the framework of low-enthalpy field, the thermal properties of the ground can be exploited could be used to cool building in summer and warm them in winter. This heat energy may be tapped either by:
• pumping groundwater from a borehole and extracting heat from it via a heat pump. This method is best suited to permeable rocks and wells with a high yield (open loop).
• circulating a fluid through a closed hose system down the borehole. The fluid is warmed to the temperature of the rocks and, on its return to the surface, may be sent through a heat

pump (closed loop).

In most Italian regions, regardless of the type of rock, the geological structure and stratigraphy, at about 15 m depth the available temperature is between 12° and 16°C, while below the temperature increases by an average of 3°C per 100 m, according to the geothermal gradient. Usually the heat stored in rocks 500 m deep is about 25 - 30°C and 35 - 45°C at 1000 m (Chieco, 2011).
Also, subsoil can be used as a thermal storage to store heat during the summer for winter house heating. Different types of rocks and soils have different behaviors in accumulating heat; in this thesis the thermal properties of some types of rocks and soils are studied.

2. Geological outline

The area of the municipality of Trento is in the Trentino-Alto Adige region, North of Italy. It is located in the Adige valley, that crosses the Alps in N-S direction towards the Garda lake. The geological map of the area is described at the scale of 1:50000 into 060 Trento sheet. The city of Trento is located at center of a wide syncline extending between the Calisio Mt. and the Marzola Mt; easternward the structure opens into the Valsugana Valley.

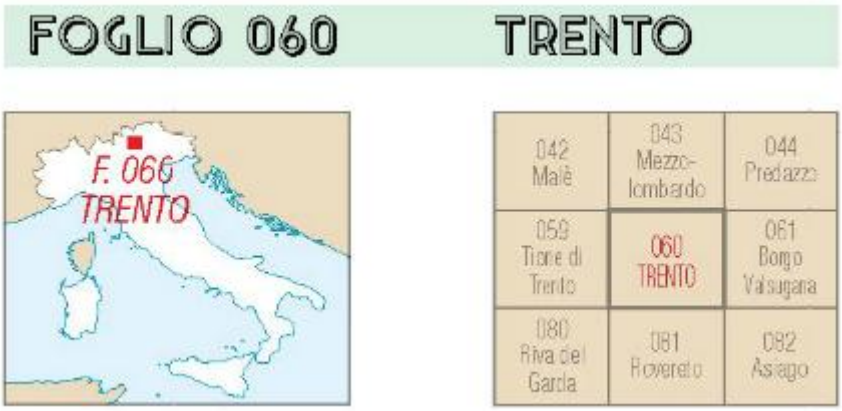

Figure 2.1: Ubication of Trento and its geological sheet.

The variety of landscapes, that passes from elevated culminations (Paganella Mt.) to ample valleys with characters of highland (Terlago area) and then to the Adige furrow, is mainly the result of the erosional and depositional processes connected to the last glacial expansions. The surface hydrography is strictly related to lithology and tectonics, resulting in narrow and deep valleys, as well as asymmetrical and wide alluvial valleys. The Adige River represents the main watercourse of the territory.

Rocks exclusively belong to the Southern Alps structural domain. The oldest rocks are represented by the Pre-Permian crystalline Basement (Valsugana Unit), mainly composed by phyllites. The crystalline basement is crossed by a series of Lower Permian sub-volcanic bodies of various composition.

Figure 2.2: Geological map of Trento. The red circle shows the city of Trento (Avanzini et al., 2010).

The overlying volcanic rocks are represented by a sequence of lava and ignimbrites, with varying chemical composition (from andesitic to rhyolitic). In the central sector (Valley of Cembra), their estimated thickness is of about 2000 m (Avanzini et al., 2010). The Adige volcanic district is related to an important extensional tectonics that took place in the Early Permian. The master fault is the Calisio Paleoline, an E verging fault with several antithetic W-verging normal faults (Linea del Fersina, Linea di Pinè). These faults bound the effusion area of different volcanic bodies which become more recent toward NE. Several volcanic events linked to the extensional tectonics are recognizable in space and time: the final event (rhyolitic ignimbrites of the Formazione di Ora) is probably connected to a general calderic sinking. The Valsugana Line represent the tectonic southern border of the volcanic district.

The sedimentary formations mainly crop out in the southern and western sector of the Sheet and include units from the Upper Permian to the Lower Oligocene; important and continuative tectonics is recorded in their variations of facies and thickness.

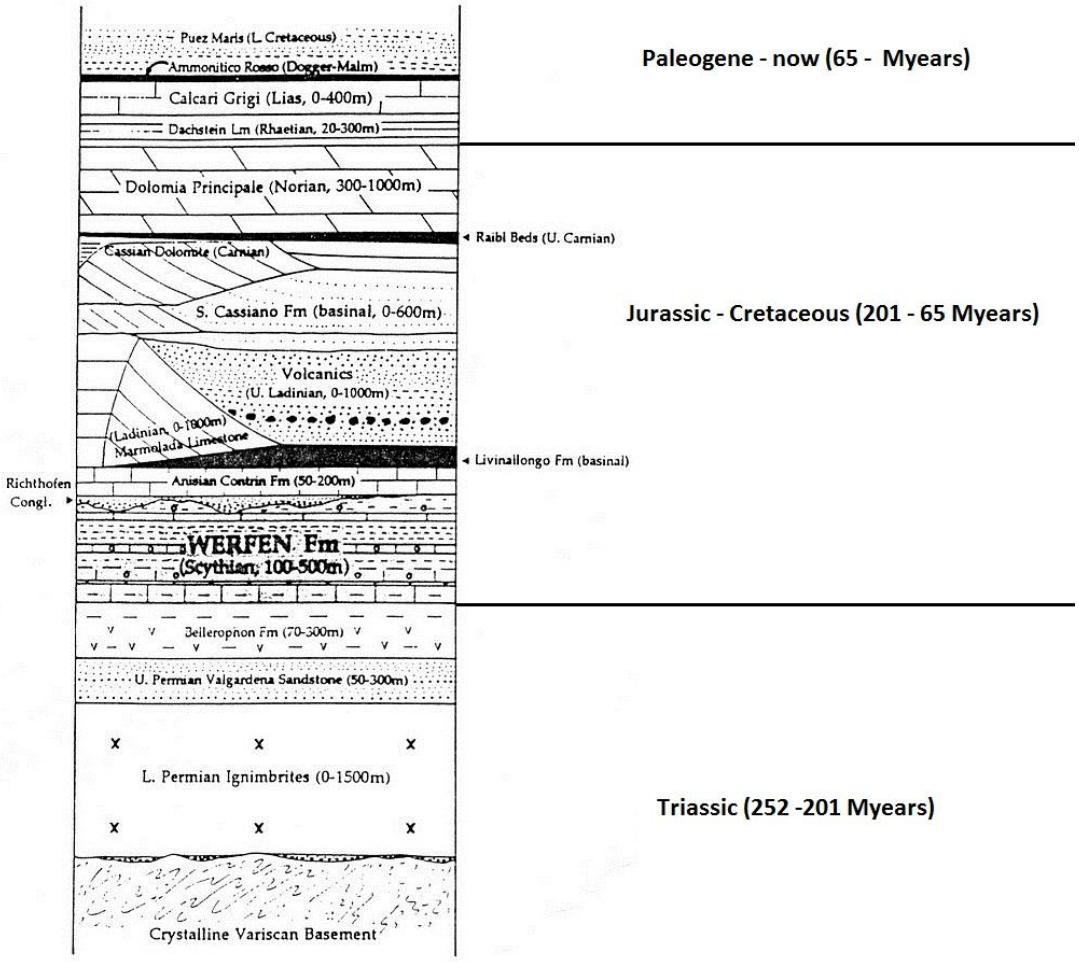

Figure 2.3: Stratigraphic column of Dolomites, in the area of Trento (from siripro.com).

Permian formations are represented by alluvial (Val Gardena sandstone) and marginal marine deposits outcropping near Trento and in the Valsugana.

During the Mesozoic rifting the Adige volcanic district turns into a structural high (Trento Platform). The stratigraphic evolution of the Trento Platform during the Jurassic is characterized by its inundation at the end of the Early Jurassic. Two main stages may be thus recognized, each one represented by a typical sedimentary package: the thick Calcari Grigi Group corresponds to the first phase of shallow-water sedimentation, during the Early Jurassic; the second phase, corresponding to the pelagic sedimentation on the top of the drowned Trento platform, is summarized by the Rosso Ammonitico Veronese Formation. Cretaceous to Paleocene sediments follows in the eastern side of the Adige Valley (Maiolica Fm. Scaglia Variegata alpina Fm., Scaglia Rossa Fm.).

In the Eocene the inherited structural arrangement originated a new Carbonate Platform (Calcare di Torbole, Calcare di Malcesine, Calcare di Nago) and a basic volcanic activity took place (Basalto della Vallagarina).

The Quaternary is mainly represented by Pleistocene deposits left by the Adige glacier, by Late glacial deposits related to the withdrawal phases (fluvioglacial deposits, glacial contact) and by slope and alluvial deposits (Avanzini et al., 2010).

3. The analytical approach

3.1 TES technology

Energy storage is necessary for the large-scale utilization of renewable energy. The reason is that renewable energy is abundantly available when the demand is low. So, heat is available in air, ground, and water during the warm season while the heating demand mainly occurs during the cold season. In a similar way the cold of the winter would be useful during the summer.
Systems for seasonal storage of thermal energy are therefore used to balance the difference in supply and demand. Such systems could be also used to store industrial waste heat between seasons.
There are three main types of thermal energy storage:
• *sensitive heat storage:* when a storage medium is heated or cooled. Usually this has a relatively low energy density. Large storage tanks are often buried so as not to occupy space on the surface and use the land as an insulator. Also subsoil itself is used as storage (rock or soil), or underground water bodies: these applications are possible due to their relatively low cost, and are called Underground Thermal Energy Storage (UTES).
• *latent heat storage:* the phase change of a substance (for example ice-water, paraffin and salt hydrates) is able to release energy without any change of temperature. These substances have a storage capacity of 5-15 times greater than sensitive heat storage, but they have higher costs.
• *thermochemical heat storage:* the energy is stored in reversible chemical reactions and can reach densities from 3 to 12 times greater than the accumulation of sensible heat (in some cases even 20 times higher). It is able to provide thermal energy at different temperatures of release, but it depends on the properties of a specific thermochemical reaction (Pomarè, 2013).

Since large volumes are needed for large storage volumes Underground Thermal Energy Storage (UTES) are commonly used. With respect to other geothermal system, TES requires more attention regarding the study of heat dispersion due to the higher temperatures involved.
The most common thermal storage systems used are ATES, BTES, and CTES; that stand for Aquifer Thermal Energy Storage, Borehole Thermal Energy Storage, and Cavern Thermal Energy Storage.
UTES systems could to be used to save energy and environment in many more countries. One reason that this technology has not been promoted is probably that it not a product for export and thus has no economic incentive. For example, ground heating/cooling systems are almost unknown in North Africa, although the local conditions in many areas are more favorable than in Sweden (Nordell et al., 2007).

3.1.1 ATES

In an ATES system thermal energy is stored in the groundwater and the porous matrix through which the groundwater flows. Heat is transferred to the ground by the groundwater, which is pumped from and to a number of extraction/injection wells. In the heating charging mode, extracted water from the cold wells is pumped to a heat exchanger where it is heated (usually by heat from thermal solar panels) before injected into the warm wells. The groundwater flows through the ground towards the extraction while warming up the matrix. The temperature velocity is half of that of the water velocity which means that the water volume of the aquifer is pumped twice before the aquifer is fully charged (Nordell et al., 2007).

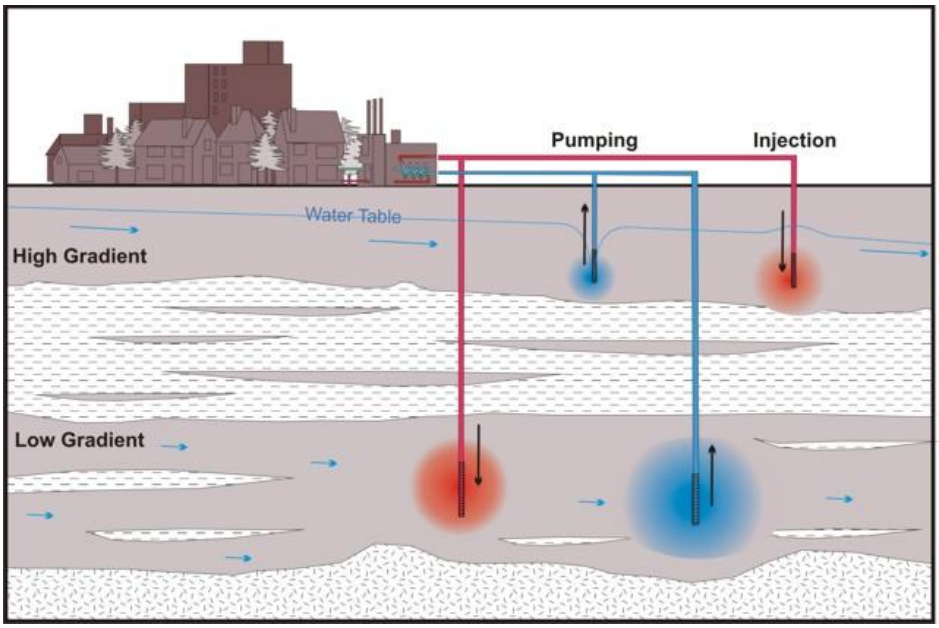

Figure 3.1: Example of ATES (from sfu.ca).

When extracting the heat the pumping is reversed and the heat is extracted from the warm wells. Also in this case a heat exchanger is used to transfer the heat to the heat distribution system. ATES systems use large scale storage mainly for seasonal storage, but also for short term storage. Most ATES are used for cooling, though more recent systems are used for both heating and cooling. Such systems usually include a heat pump, which delivers the heat while the cooling often is by free cooling (direct use of groundwater).
ATES systems require suitable geology (permeable soils/sands) and favorable groundwater conditions. Occurring problems are usually related to water chemistry problems (Nordell et al., 2007).

3.1.2 BTES

These are usually for both heating and cooling. This energy efficient technology is very ecological since extracted heat is renewable energy that is passively stored from ground

surface. These systems are most efficient if low-temperature heat distribution systems are used. Large-scale BTES are mainly used for seasonal heat storage. Typical heat sources are industrial waste heat or solar heat. The most favorable system is high temperature storage for low temperature applications, where no heat pump or additional heating is required.
Storage temperatures up to about 80-90°C are used in BTES, though low temperature systems are most common. Occurring heat losses from such systems depends on the bedrock properties, temperature, geometry, and volume (Nordell et al., 2007).
The technical solutions for boreholes are three:
- Vertical geothermal probes, heat exchangers, with typical lengths from 50 to over 350 m,
- Coils in the ground, heat exchangers placed horizontally at 1-2 m deep in loose soil,
- Energy piles, heat exchangers integrated into the foundation piles of the building with typical depth of a few tens of meters (Verrone, 2009).

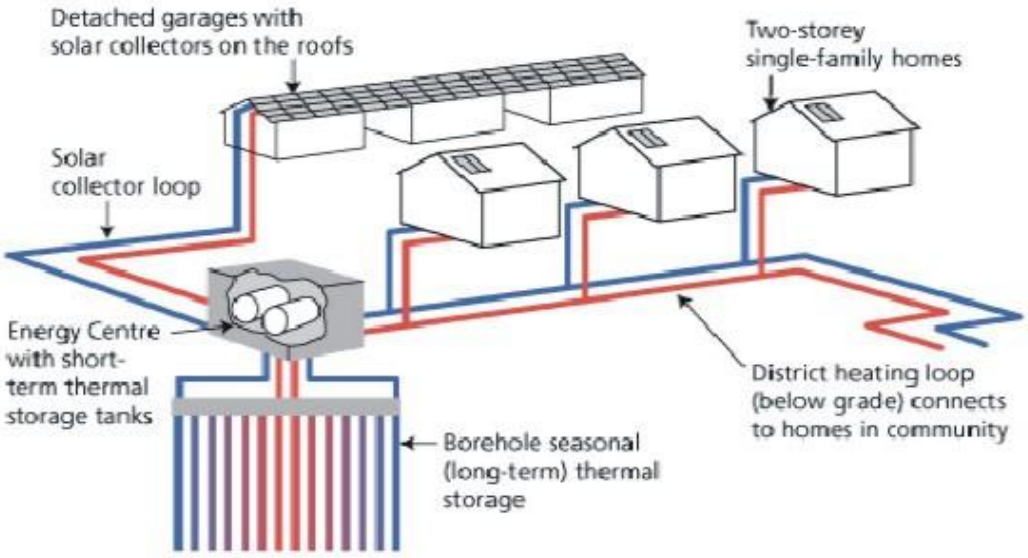

Figure 3.2: example of BTES (from onenesspublishing.com).

In areas where the larger land areas are available, horizontal pipe systems are used for the extraction of heat and cold. In colder climates heat pumps are used to extract the heat during the winter while the ground is used for direct cooling (no cooling machines) during the summer. In a warmer climate the situation would be the opposite, the heat of the cooling machines is dumped into the ground and this heat is used for direct heating during the winter season. In the most favorable case the ground could be used for both direct cooling and direct heating. This means that the heat and cold is extracted by circulating water through a buried pipe system. The horizontal pipe system in the ground is placed in many different ways. If large land areas are available the pipes are normally placed in lines with a few m spacing over the area. If smaller areas are available the pipe is placed in a more compact manner. Different types of collectors are available.
The idea with more compact forms of ground heat collectors is to reduce the land area use. Several pipes in the same ditch means that the total pipe length is increased, while the length of the ditch is reduced.

3.1.3 CTES

The rock cavern heat storage (CTES) has the advantage of very high injection and extraction powers (just a matter of pump capacity), while the disadvantage is its high construction costs. It is possible to use old rock caverns, previously used for oil storage, and convert them for high temperature water storage (Nordell et al., 2007).

While presenting advantages from the point of view of energy, these systems may represent a potential risk to groundwater aquifers. During terebration of wells, they may be compromised if the natural water barriers separating the shallow and deep aquifers are brought into contact with each other, causing the hydrochemistry mixing and sometimes contamination.
The risks are not only related to the construction phase, but also to the management and include (Verrone, 2009):

- Possible chemical contamination of the water pumped back into the groundwater due to leaks in the hydraulic circuit (for BTES),
- Quantitative changes of chemical species dissolved in groundwater induced by the temperature change,
- Changes in the microbiological content of the groundwater,
- Changes in the dynamics of groundwater, especially with discharges of significant size (especially for ATES).

The thermal pollution may result in a change in the chemistry of the groundwater because with the temperature changes, the ability of water dissolution of minerals increases; the most susceptible are also the most soluble such as iron, calcium and hydrogencarbonates that may change the chemical composition.

3.2 Thermal properties of rocks

3.2.1 Thermal conductivity

Thermal conductivity λ is a physical property governing heat transfer. It describes how much heat flows across a unit cross-section of a material along a unit distance per unit temperature decrease per unit time; in other words, the ability of a material to transmit heat. Its dimension is W m^{-1} K^{-1}. Thermal conductivity λ in steady-state thermal conduction and transient heat diffusion in most of the Earth's crust and mantle is caused by scattering of quantized lattice vibrations, the phonons, and by diffusive radiation of photons. These two processes are described by phonon thermal conductivity λ_p and radiative thermal conductivity, λ_r, respectively (Clauser, 2011). The most important for the aim of the thesis is phonon thermal conductivity, because radiative process becomes relevant for very high temperatures (Clauser, 2011), while all laboratory measures are taken at room temperature.
Mathematically thermal conductivity is defined by Fourier's law:

(3.1) $$q = - \lambda \nabla T$$

Where:
λ is the thermal conductivity;
T is the temperature;
q is the heat flow density; it is a vector.

Thermal conductivity λ is an intrinsic property of the material. For minerals it is more constrained than that of rocks, due to the well-defined crystal structure and chemical formula for each mineral.
Rocks are less well defined. In fact, there are many factors that influence the value of thermal conductivity, in different ways. The main ones are anisotropy, mineral content, porosity, pore fluid and saturation. These factors are variable for each rock, but Clauser (2011) summarized the controlling parameters of rock thermal conductivity for the four main diagenetic classes of rocks (sedimentary, volcanic, plutonic and metamorphic) in a statistical manner.

For sedimentary rocks, thermal conductivity is mainly controlled by porosity and sediment type.
For volcanic rocks, porosity is the controlling factor on thermal conductivity.
Plutonic and metamorphic rocks are generally much less porous. The controlling factor is the dominant mineral phase; the feldspar content affects λ.
For metamorphic rocks, it is the quartz content which controls thermal conductivity .

3.2.1.1 Variation with anisotropy

Anisotropy is defined as the property of being directionally dependent, as opposed to isotropy, which implies identical properties in all directions. It can be defined as a difference, when measured along different axes, in a material's physical or mechanical properties.
In general, thermal conductivity parallel to the direction of layering or foliation is greater than thermal conductivity in the perpendicular direction. The factor of anisotropy A_λ is defined as the ratio $\lambda_{parallel}/\lambda_{normal}$, and generally falls into the range 0,9-3, with most values between 1-2 (Clauser, 2011; Popov et al., 1999).

(3.2) $$A_\lambda = \lambda_{parallel}/\lambda_{normal}$$

where:
A_λ is the anisotropy factor;
$\lambda_{parallel}$ is the thermal conductivity measured parallel to the foliation;
λ_{normal} is the thermal conductivity measured normal to the foliation.

Thermal conductivity for many rocks is approximately isotropic, particularly for volcanic and plutonic rocks. In these cases the heat flow in the subsoil will be predominantly vertical (assuming no significant tectonic phenomena). Instead, thermal conductivity of many sedimentary and metamorphic rocks is strongly anisotropic, and lateral heat flow will be significant. Hence information on anisotropy is often needed, requiring laboratory measurements in different directions (Clauser et al., 1995).
Anisotropy exists on several scales:
(1) On the microscopic scale, because many minerals are anisotropic.
(2) On the laboratory scale, the thermal conductivity of many rocks is also anisotropic.
However, even if rocks are composed of anisotropic minerals, random orientation of the crystals may make the rock's thermal conductivity appear isotropic macroscopically.
(3) On a larger scale, if rocks are exposed to folding or other tectonic processes, the thermal conductivity of the resulting rock formation may be either isotropic or anisotropic.

3.2.1.2 Variation with temperature

Since the pioneering experiments, thermal conductivity of minerals and rocks is known to decrease with temperature, generally with its inverse (Clauser, 2011).
The decrease is primarily due to the decrease of phonon thermal conductivity λ_p with temperature and to a smaller degree to thermal cracking. Since the thermal expansion coefficient increases with temperature (but differently for all minerals), differential expansion may create contact resistances between mineral grains. For single-mineral aggregates, a linear relationship between temperature and thermal resistivity, λ^{-1}, discriminates between contributions which depend on temperature T and others which do

not, such as micro-cracks, grain boundaries, shape and orientation of crystals and their fragments (Clauser et al., 1995):

(3.3) $$\lambda^{-1}(T) = c_1 + c_2 T$$

where
λ is the thermal conductivity (in W m^{-1} K^{-1});
T is the temperature (in K);
c_1 and c_2 are numerical constants.

By measuring thermal conductivity λ and plotting its inverse, thermal resistivity λ^{-1}, versus temperature, constants c_1 and c_2 are obtained from intercept and slope of a linear regression. (Clauser et al., 1995)

3.2.1.3 Variation with pressure

The effect of pressure is different in two distinct pressure ranges. First, fractures and micro-cracks (developed during stress release after sampling) begin to close with increasing pressure. This reduces thermal contact resistance as well as porosity which is usually filled with a low conductivity fluid. This process, which tends to decrease thermal conductivity, ends when a pressure of about 15 MPa is reached. A further pressure increase to 40 MPa does not affect thermal conductivity significantly. If pressure is increased further, however, a second process becomes effective: the reduction of intrinsic porosity, i.e. voids which are not created by stress release, hence with an increase of thermal conductivity (Clauser et al., 1995).

3.2.1.4 Variation with porosity

For large porosity (i.e. Φ>>1%) thermal conductivity of the saturating fluid affects significantly the bulk rock thermal conductivity. The influence varies with the thermal conductivity of the saturants, e.g. water, oil, natural gas, air, but generally when porosity increases thermal conductivity decreases.
The effect of partial saturation is different for porous or fractured rocks. In porous rocks, porosity comprises both bulk pore space and bottlenecks formed by the contact between individual grains. Dry bottlenecks act as thermal contact resistances between grains, while the bulk pore volume contributes proportionally to the effective rock thermal conductivity. In fractured rocks, in contrast, there are no bottlenecks between grains as in porous rocks, and the small void volume in the fractures corresponds to the bulk pores space of porous rocks (Clauser et al., 1995).

3.2.2 Heat capacity

When a material at a given temperature is placed in contact with another material at a higher temperature, energy is transferred to the cooler one and its temperature rises. The ratio of the amount of energy transferred to change the temperature is called heat capacity (Gangyan et al., 2003). If Q is the amount of heat transferred and the temperature increases from T_0 to T, the heat capacity at constant pressure is given by:

(3.4) $$C_P = Q/(T-T_0)$$

Where :
C_P is the heat capacity [J K^{-1}];
Q is the heat flux;
T_0 is the starting temperature;
T is the temperature.

Specific heat capacity c_P is used more often, and is defined by heat capacity per unit mass:

(3.5) $$c_P = C_P/m$$

Where:
c_P is the specific heat capacity [J kg^{-1} K^{-1}];
C_P is the heat capacity;
m is the mass.

Volumetric heat capacity, also termed volume-specific heat capacity, describes the ability of a given volume of a substance to store internal energy while undergoing a given temperature change, but without undergoing a phase change (Verrone, 2009). It is different from specific heat capacity in that the volumetric heat capacity depends on the volume of the material, while the specific heat is based on the mass of the material. If given a specific heat value of a substance, one can convert it to the volumetric heat capacity as the product of specific heat capacity c_P and density ρ or as the ratio of thermal conductivity λ and thermal diffusivity κ:

(3.6) $$c_\rho = \rho\, c_P = \lambda/\kappa$$

Where:
c_ρ is the volumetric heat capacity [J m^{-3} K^{-1}];
c_P is the specific heat capacity;
ρ is the density;
λ is the thermal conductivity;
κ is the thermal diffusivity.

3.2.3 Thermal diffusivity

Thermal diffusivity κ is a physical property governing transient heat diffusion. It is defined by the ratio of thermal conductivity and thermal capacity, its dimension is $m^2 s^{-1}$.

If both conductivity and thermal capacity are known, thermal diffusivity κ can be calculated from:

(3.7) $$\kappa = \lambda/(\rho\, c_P).$$

Where:
κ is the thermal diffusivity;
λ is the thermal conductivity ;
c_P is the specific heat capacity ;
ρ is the density.

As thermal diffusivity is the ratio of thermal conductivity and thermal capacity, it is also influenced by the variation of density and specific heat capacity. This is of particular interest with respect to the variation with temperature. The reason is the opposite behavior of thermal conductivity and heat capacity with respect to temperature. While between 0 and 300°C thermal conductivity of rocks decreases in general, thermal capacity (the product of density and specific heat capacity) increases (Mottaghy et al., 2008).

The transient heat transport equation for an isotropic solid without any source of heat generation is governed by thermal diffusivity:

(3.8) $$\nabla^2 T = (1/\kappa) \cdot \partial T/\partial t$$

Where:
$\nabla^2 = \partial^2/\partial x^2 + \partial^2/\partial y^2 + \partial^2/\partial z^2$ is Laplace's operator;
T is the temperature;
κ is the thermal diffusivity;
t is the time.

Therefore, an exact knowledge of the thermal diffusivity of rocks is of particular importance when studying the thermal regime of the Earth's crust.

3.2.3.1 Variation with temperature

Thermal diffusivity κ of rocks varies even more strongly with temperature than thermal conductivity λ. This is caused by the opposite behavior of thermal conductivity and thermal capacity ($\rho\ c_P$) with respect to temperature. Because of several self-compensating factors, thermal capacity ($\rho\ c_P$) with few exceptions generally varies within ±20 % of 2,3 MJ m^{-3} K^{-1} for the great majority of minerals and rocks (Clauser et al., 1995). A linear regression of thermal capacity as a function of temperature yields also a linear relationship.
Thus, thermal diffusivity can be derived from thermal conductivity and vice versa.

3.2.3.2 Variation with other factors

Micro-cracks and grain boundaries give rise to increased thermal resistance and to a reduction of the mean free path of radiation due to scattering of radiation (Clauser, 2011).

3.3 Density and porosity measurements

The procedure for density and porosity measurements was done following the UNI EN 1936 standard, “Natural stone test method - Determination of real density and apparent density, and of total and open porosity”.
For density and porosity measurements the instrumentation required is:
-ventilated stove, to dry the samples,
-drier
-vacuum pump
-a weighting scale with a precision of 0,001 g (Mettler PM400).

Figure 3.3: PM400 balance

The samples (at least 3 for each lithology) are dried in a fan-forced oven at a temperature of (70±5)°C, then they are stored in a drier (Fig. 3.4) for other 24 hours until they reach room temperature.

Figure 3.4: the samples in the drier

Every specimen is weighted (m_d, dry mass), and then put into a container in which, with a vacuum pump, pressure is decreased until (2,0±0,7) kPa = (15±5) mm Hg. This pressure is maintained for 24 hours in order to eliminate air in the specimen pores. After that, demineralized water at room temperature (20±5°C) is gradually introduced. The water velocity should be regulated so that the specimen will be totally submerged in about 15 minutes. The pressure is maintained constant for the following 24 hours.

Subsequently, the pressure is taken to the atmospheric pressure value. Every sample is now weighted in water and the value of submerged mass is registered (m_h); then the specimen have a quick passage through a humid towel and the saturated mass m_s is determined.

Figure 3.4: the vacuum pump apparatus in function

The open pores volume (in mm) is expressed by the equation:

(3.9) $$V_0 = 1000^* (m_s - m_d)/\rho_{rh}$$

where:
V_0 is the open pores volume;
m_s is the saturated mass;
m_d is the dry mass;
ρ_{rh} is the water density.

The apparent volume (in mm) is expressed by the equation:

(3.10) $$V_b = 1000^* (m_s - m_h)/\rho_{rh}$$

where:
V_b is the apparent volume;
m_s is the saturated mass;
m_h is the submerged mass;
ρ_{rh} is the water density.

That can be also calculated on the basis of the sample's dimensions. Water density ρ_{rh} is derived depending for water temperature, in the following table.

Table 3.1: Values of density dependent on temperature

Temperature (°C)	Density (g/l)
0	0,99986
5	0,99999
10	0,99972
12	0,99952
14	0,99927
16	0,99897
18	0,99862
20	0,99823
22	0,9978
24	0,99732
26	0,99681
28	0,99625
30	0,99567
35	0,99406
40	0,99224
45	0,99024
50	0,98807
60	0,98324
70	0,97781
80	0,97183
90	0,96534
100	0,95838

Therefore, once measured the room temperature T, it is possible to select the right value to be used in equations (3.9) and (3.10).
The apparent density (in kg/m^3) is expressed by the ratio between the mass of the dry sample and its apparent volume, with the equation:

(3.11) $$\rho_b = \rho_{rh}\, m_d/(m_s - m_h)$$

where:
ρ_b is the apparent density;
ρ_{rh} is the water density;
m_d is the dry mass;
m_s is the satured mass;
m_h is the submerged mass.

The open porosity (in %) is expressed as the ratio between the open pores volume and the apparent volume of the sample, with the equation:

(3.12) $$\Phi o = (m_s - m_d)/(m_s - m_h)$$

where:
Φo is the open porosity;
m_s is the saturated mass;
m_d is the dry mass;
m_h is the submerged mass.

For the purpose of the thesis, the apparent density and the open porosity are considered equal to the actual density and porosity.

3.4 Thermal analyses

There are two main categories in which methods of measuring thermal conductivity can be divided, dynamic and static, depending on whether the temperature distribution within the sample is time dependent or not. For both methods, the solution of the thermal equation depends on the geometry of the sample, on the heat source and on the sink (Gangyan et al., 2005).

3.4.1 Static method

In static or steady state methods the thermal conductivity is obtained from Fourier's law for heat transport by measurement of the temperature gradient ∇T and heat flow q. In its simplest form the sample is a cylinder and heat flow circulates in an axial direction. The isotherms are planes perpendicular to the cylindrical axis. This is the basis of the so-called linear flow method. There are inevitably heat losses, and it is difficult to ensure that the temperature gradient is always perpendicular to the cross-sectional area. If the heat losses from the cylindrical surface of the sample are negligible, then the thermal conductivity is determined by

(3.13) $$\lambda = Q\,L / A\,(T_1-T_2)$$

Where:
λ is the thermal conductivity;
Q is the heat flow;
L is the length of the cylindrical sample;
A is the cross-sectional area of the sample;
(T_1-T_2) is the difference of temperature between the two ends of the sample.

In general, measurement of the heat flow rate Q and of the cross sectional area A presents no problem. However, it is necessary to pay more attention to the measurement of temperature gradient

(3.14) $$\partial T/\partial x = (T_1-T_2) /L$$

Where:
$\partial T/\partial x$ is the temperature gradient;
(T_1-T_2) is the difference of temperature between the two ends of the sample;
L is the length of the cylindrical sample.

3.4.2 Dynamic method

In dynamic or non-steady state methods, the temperature distribution throughout the sample varies with time, therefore the complete differential equation of heat flow is necessary. If the experimental time is short, heat losses have a smaller influence on the measurement than in the steady state method. Dynamic methods can be divided into two categories, transitory or periodic, if the thermal energy is supplied to the sample as a single step function (constant source) or with a modulation of fixed period. As a consequence the temperature changes in the sample are either transitory or periodic.

For measurements of the thermal conductivity of poor conductors, such as rocks and some building construction materials, using the steady state method requires a very long time to reach equilibrium. Therefore the dynamic method of measurement is more appropriate. The transient line heat-source probe, the so-called thermal conductivity probe, is commonly used.

This method employs a linear heat source, normally an electrically-heated fine wire, and a temperature sensor placed alongside of it and embedded in the material under test. When a constant heat q per length unit is supplied by the heater, the temperature rise T after time t at a point from the heat source in solid of infinite extent is given by

(3.15) $$T_1 - T_2 = q/(4 \pi \lambda) \ln (t_2/t_1)$$

Where:
(T_1-T_2) is the difference of temperature between the two ends of the sample;
q is the heat flow per length unit;
λ is the thermal conductivity;
t_i is the time.

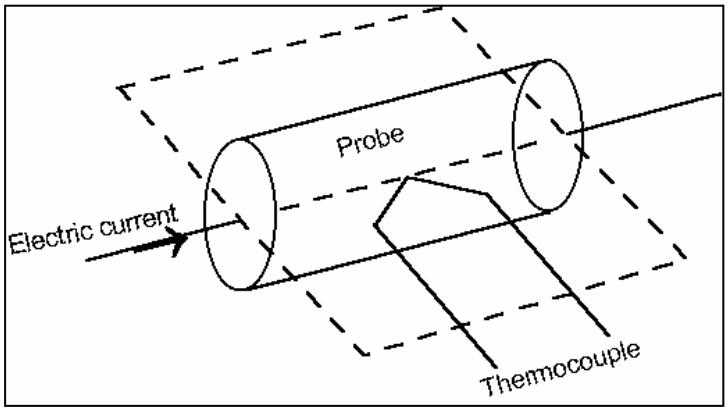

Figure 3.5: scheme of transient line heat-source probe method (Gangyan et al., 2003)

Parameters t_1 and t_2 are sampling time, with respectively temperatures T_1 and T_2.

In this way the thermal conductivity can be obtained from the slope of the temperature rise against ln(t). Alternatively, the temperature rise $\Delta T = (T_1-T_2)$ between t_1 and t_2 may be used.
In order to justify the approximations, the distance must be small and t large. Theoretically, an infinite line heater and an infinite sample are necessary, therefore the probe must have a reasonable length-to-diameter ratio and be small compared to the sample (Gangyan et al., 2005).

For the thermal analyses of rock and soil samples the instrumentation used is ISOMET 2114, a portable hand-held measuring instrument for direct measurement of heat transfer properties of a wide range of materials. It is equipped with two types of measurement probes: needle probes for unconsolidated sediments, surface probes for cohesive materials. It applies a dynamic measurement method, which enables to reduces the measurement time in comparison with steady state measurement methods.

Figure 3.6: the ISOMET 2114 instrument for thermal conductivity measurements

Measurement is based on analysis of the temperature response of the analyzed material to heat flow impulses. Heat flow is excited by electrical heating of the resistor inserted into the probe, which is in direct contact with the tested specimen. Evaluation of thermal conductivity and volume heat capacity is based on periodically sampled temperature records as function of time, provided that heat propagation occurs in unlimited medium.
The instrument measures directly thermal conductivity λ, and gives and indirect measure of thermal diffusivity κ and volumetric heat capacity c_ρ. Results can be downloaded to a computer organized in a .csv file.

Rock samples must have a flat surface of 6x6 cm minimum, possibly without fractures, dust or other disturbing factors. The surface probe is put over and the parameters of the

instruments are set:
-measurement range, that can be 0,3 – 2 W/m K or 2 – 6 W/m K;
-name of the sample;
-number of measurements for each measure, that are averaged by the instrument: 2, with interval of 60 seconds between them.

Unconsolidated sediment samples are set in a 0,5 l water bottle. The needle probe is put in and the parameters of the instruments are set:
-measurement range, that can be 0,2 – 1 W/m K or 1 – 2 W/m K;
-name of the sample;
-number of measurements for each measure, that are averaged by the instrument: 2, with interval of 60 seconds between them.

For rock samples it was taken one cycle of two measures (averaged by the instrument) for each face of the specimen, where possible, in dry conditions, and one cycle in wet conditions. For unconsolidated sediments, it was taken one cycle of measures for dry samples and one cycle for wetted samples.
The instrument accuracy for the utilized measurement ranges is shown in Table 3.2.

Table 3.2: accuracy of ISOMET 2114 for the different parameters measured.

Parameter	Accuracy
Thermal conductivity	10 % of reading
Volumetric heat capacity	15 % of reading + $1*10^3$ J/m^3K

3.5 Thin sections

Thin sections of the rock samples were prepared, in order to study the mineralogical and microstructural features of considered rocks.
A suitable size rock slab for is cut from the sample with a diamond saw, and it is lapped flat and smoothed first on a cast iron lap with 400 grit carborundum, then finished on a glass plate with 600 grit carborundum.
After drying on a hot plate, a glass slide is glued to the lapped face of the slab with epoxy.
Using a thin section saw, the slab is cut-off close to the slide. The thickness is further reduced on a thin section grinder. A finished thickness of 30 microns is achieved by lapping the thin section by hand on a glass plate with 600 grit carborundum. A fine grinding with 1000 grit prior to polishing is optional.
The section is placed in a holder and spun on a polishing machine using nylon cloth and diamond paste until a suitable polish is achieved for microscope or SEM studies.

4. The samples

4.1 Choice of lithologies

It was decided to sample the rocks in the area of the municipality of Trento with an outcrop larger than 1 km^2. Then were added other lithotypes to have a more complete outlook on all types of rocks (especially magmatic and metamorphic). The lithologies chosen are also some of the most thick (from bibliographic references), for the aim of having a wide thermal storage. In Table 4.1 and Table 4.2 are shown the geologic formations and the unconsolidated sediments selected for sampling.

Table 4.1: Geological formations and rock type

Code	Formation	Lithology	Age	Thickness (m)	Area (km^2)
DPR	Dolomia Principale	dolomite	Triassico medio - inf	> 800	10,03
RTZ	Gruppo dei Calcari Grigi - Formazione di Rotzo	limestone	Giurassico - Cretacico	150	8,79
SAA	Scaglia Rossa	limestone	Giurassico - Cretacico	70	8,5
CHI	Formazione di Chiusole	limestone	Eocene inf. - Oligocene inf.	80 - 90	5,83
FMZ	Gruppo dei Calcari Grigi - Formazione di Monte Zugna	limestone	Giurassico - Cretacico	130 - 300	5,57
ARV	Rosso Ammonitico Veronese	limestone	Giurassico - Cretacico.	25 - 50	4,53
ORA	Gruppo Vulcanico Atesino - Formazione di Ora	rhyolite	Permiano inf.	200 - 800	3,74
WER_{1-2}	Formazione di Werfen - Membri di Tesero e Mazzin	marly/silty limestone, dolomite	Triassico inf..	0 - 15 (Mazzin) 40 (Tesero)	2,44
GIV_3	Formazione di Giovo - Membro del Monte Ozol	dolomite	Triassico medio - inf	180 - 200	2,13
CTR	Formazione del Contrin	dolomite	Triassico medio - inf	10 - 150	1,33
NAG	Calcare di Nago	limestone	Eocene inf. - Oligocene inf.	100	1,03
SCI	Formazione dello Sciliar	dolomite	Triassico medio - inf.	50 - 350	1,02
MCE	Calcare di Malcesine	limestone	Eocene inf. - Oligocene inf.	70	0,67
f_a	Filoni a quarzo e calcite	volcanoclastic rock	Permiano inf.	-	-

VFS	Unità della Valsugana - Filladi e Filladi quarzifere	phyillite	pre - Permiano	-	0,36
LUB	Gruppo Vulcanico Atesino - Formazione di Buss	andesite	Permiano inf.	0 - 60	0,26
ICT	Gruppo Vulcanico Atesino - Formazione del Castelliere	riodacite	Permiano inf.	50 - 100	0,08

Table 4.2: Unconsolidated sediment types

Code	Sample code	Formation	Description	Area (km^2)
1120	10B	Glacial deposit	Sands and silts weakly clayey, some pebbles	21,41
1060	20B	Alluvional/fluvioglacial deposit	Medium and fine sands	18,04
1030	27A	Landslide deposit	Coarse sands weakly silty	13,27
1010	6D	Slope deposit	Gravel and sands	10,05
1061	25A	Alluvial/fluvioglacial fan	Fine sands	8,92
1101	21A	Mixed fan: debris flow and alluvial	Coarse sands	4,54
1100	31A	Mixed deposit: debris and alluvial	Gravel, sand, clay and a small quantity of silt	2,75
1050	13A	Colluvial deposit	Clay and silt, small quantity of sand and gravel	1,75

4.2 Field collection

The outcrops were found using the GPS and the geological map of Trento. The dimension required for the rock samples was at least 10x10x10 cm, to have sufficient material for the tests but small enough for the cutting machine. For the unconsolidated sediments a minimum volume of 0,5 dm^3 was required for thermal analyses. There were taken photographs of the samples with a visual reference for the dimensions, of the outcrop and were also taken the GPS coordinates. In paragraph 4.4 the data sheets of the collected rock and unconsolidated sediment samples are shown. There were collected 34 samples of 19 different geological formations, and 9 samples of 8 soil types. After a brief control, eliminating the duplicates and wrong samplings, 21 samples for 17 formations and 8 soil types were chosen.

4.3 Sample cutting

The specimens were cut with a Struers Unitom-2 water-cooled diamond saw (Fig. 4.1) for huge cuttings, for a more precise work it was used a Struers Labotom-3 (Fig. 4.2).

Figure 4.1: the Struers Unitrom-2 saw for big cuttings.

Figure 4.2: the Struers Unitrom-3 saw for small cuttings.

The samples were cut into (Fig. 4.3):
-three cubes of approximately 3x3x3 cm, for density and porosity measures;
-two slices of 4x2x0,5 cm, for thin sections;
-one sample with a cut parallel and one normal to the stratification (if present), for thermal analyses.

Figure 4.3: Cut samples for thermal property measurements, density and porosity measurements and thin sections.

4.4 Data sheets of rock samples

Sample code: 2A
Code: f_a, quartzite and calcite veins (volcanoclastic rock)
Collection date: 31/10/2013
GPS coordinates: N 46° 03’ 44.1”, E 11° 09’ 48.3”

Figure 4.4: Photo of the outcrop

Figure 4.5: Photo of the sample

Figure 4.6: location of the outcrop

Outcrop description: a few meters in the wood next to a dirt road. It is very small and altered.

Description: Loose red rock, composed by big grains, with stripes of light green color. The sample is heavily altered, difficult to find a part not loosening.

Sample code: 4B
Code: WER, Werfen formation (limestone)
Collection date: 31/10/2013
GPS coordinates: N 46° 03’ 41.6”, E 11° 09’ 57.8”

Figure 4.7: Photo of the outcrop

Figure 4.8: Photo of the sample

Figure 4.9: location of the outcrop

Outcrop description: the sample was taken along the dirt road, near to a drywall.
Description: Mazzin member: marly limestones alternated with siltstones and silty layers, the sample is a light grey calcarenite.

Sample code: 5A
Code: WER, Werfen formation (limestone)
Collection date: 31/10/2013
GPS coordinates: N 46° 04’ 05.3”, E 11° 10’ 59.7”

Figure 4.10: Photo of the outcrop

Figure 4.11: Photo of the sample

Figure 4.12: location of the outcrop

Outcrop description: It is found along the road, 1 m meter high and about 5 m long.
Description: Mazzin member: marly limestone, brown in the weathered pert, yellow-like color with darker streaks in the interior. There are a few holes inside due to the petrogenic process.

Sample code: 6A
Code: WER, Werfen formation (limestone)
Collection date: 31/10/2013
GPS coordinates: N 46° 04’ 18.5”, E 11° 11’ 00.0”

Figure 4.13: Photo of the outcrop

Figure 4.14: Photo of the sample

Figure 4.15: location of the outcrop

Outcrop description: it is part of a larger outcrop on the slope of Cima Celva, near Cimirlo. It is about 50 m far from a turn of via Eremo on a trail.
Description: Mazzin member: micritic limestone, light grey color.

Sample code: 6C
Code: WER, Werfen formation (limestone) (?)
Collection date: 31/10/2013
GPS coordinates: N 46° 04’ 18.5”, E 11° 11’ 00.0”

Figure 4.26: Photo of the outcrop

Figure 4.17: Photo of the sample

Figure 4.18: location of the outcrop

Outcrop description: it is part of a larger outcrop on the slope of Cima Celva, near Cimirlo. It is about 50 m far from a turn of via Eremo on a trail.
Description: Mazzin member: micritic limestone, light grey color. There are visible small shiny crystals.

Sample code: 6D
Soil code: 1010, slope deposit
Collection date: 31/10/2013
GPS coordinates: N 46° 04’ 18.5”, E 11° 11’ 00.0”

Figure 4.39: Photo of the outcrop

Figure 4.20: location of the outcrop

Outcrop description: it is part of a larger outcrop on the slope of Cima Celva, near Cimirlo. It is about 50 m far from a turn of via Eremo on a trail.
Description: The soil is composed mainly by sand and gravel.

Sample code: 8A
Code: FMZ (grey limestone)
Collection date: 31/10/2013
GPS coordinates: N 46° 04’ 20.6”, E 11° 10’ 55.5”

Figure 4.21: Photo of the outcrop

Figure 4.22: Photo of the sample

Figure 4.23: location of the outcrop

Outcrop description: It is a high rock wall on the side of Cima Celva. It can be reached with a trail.
Description: Micritic bioclastic grey limestone. The weathered part is grey, the interior is light pink, with intrusions of quartz.

Sample code: 10A
Code: VFS, Valsugana unit (phyllite)
Collection date: 31/10/2013
GPS coordinates: N 46° 04’ 02.6”, E 11° 11’ 28.5”

Figure 4.24: Photo of the outcrop

Figure 4.25: Photo of the sample

Figure 4.26: location of the outcrop

Outcrop description: There are no visible outcrops, but some samples can be found near the small river where the water eroded the surface soil exposing the rock below.
Description: Phyllites with more or less quartz, sericite, muscovite, chlorite, albite, biotite and ilmenite. The grain size is usually submillimetric. The color is blue and silver; it has an evident schistosity.

Sample code: 10 B
Soil code: 1120, glacial (morenic) deposit
Collection date: 31/10/2013
GPS coordinates: N 46° 04’ 02.6”, E 11° 11’ 28.5”

Figure 4.27: Photo of the outcrop

Figure 4.28: location of the outcrop

Outcrop description: On the river banks, where the soil is not altered by vegetation, humus and weathering.
Description: Silt and sands weakly clayey, some pebbles.

Sample code: 12A
Code: DPR, main dolomite
Collection date: 31/10/2013
GPS coordinates: N 46° 04’ 10.5”, E 11° 09’ 30.4”

Figure 4.29: Photo of the outcrop

Figure 4.30: Photo of the sample

Figure 4.31: location of the outcrop

Outcrop description: on a hill near Povo, the entire hill is made of dolomite.
Description: stromatolitic dolomite, grey-pink color.

Sample code: 13A
Soil code: 1050, colluvial deposit
Collection date: 31/10/2013
GPS coordinates: N 46° 03’ 56”, E 11° 09’ 34.2”

Figure 4.32: Photo of the outcrop

Figure 4.33: location of the outcrop

Outcrop description: The sample was taken near an open car park.
Description: The soil is composed mainly by clay and silt, with a smaller component of sand and gravel

Sample code: 14A
Code: SAA, scaglia rossa (limestone)
Collection date: 31/10/2013
GPS coordinates: N 46° 04’ 24.9”, E 11° 09’ 08.4”

Figure 4.34: Photo of the outcrop

Figure 4.35: Photo of the sample

Figure 4.36: location of the outcrop

Outcrop description: along the road, just before going under a bridge. It is 1-1,5 m high and 10m long.
Description: Red micritic sheet-like limestones (5 -15 cm), with flint in the lower part and with marly interlayers. Very high fracturing anisotropy, hard to find a sample with proper dimensions.

Sample code: 15B
Code: MCE, Malcesine limestone
Collection date: 31/10/2013
GPS coordinates: N 46° 04’ 26.3”, E 11° 08’ 35.3”
Description: limestone

Figure 4.37: Photo of the outcrop

Figure 4.38: Photo of the sample

Figure 4.39: location of the outcrop

Outcrop description: on a small hill in Cognola, near a school. It is small and hidden by vegetation.
Description: Limestone, light brown with recognizable grains. A deposition anisotropy can be detected, also for the preferential orientation of fractures.

Sample code: 16A
Code: RTZ, Rotzo formation (grey limestone)
Collection date: 31/10/2013
GPS coordinates: N 46° 04’ 19.1”, E 11° 08’ 09.6”

Figure 4.40: Photo of the outcrop

Figure 4.41: Photo of the sample

Figure 4.42: location of the outcrop

Outcrop description: it is 3 m high, along the road. It is quite difficult to collect samples because the rock is compact.
Description: Bioclastic limestones stratified in sequences of variable thickness (from metric to decametric). The lower part of the sequence may contain clays.

Sample code: 17A
Code: ARV, ammonitic red (limestone)
Collection date: 31/10/2013
GPS coordinates: N 46° 04’ 20.1”, E 11° 07’ 37.6”

Figure 4.43: Photo of the outcrop

Figure 4.44: Photo of the sample

Figure 4.45: location of the outcrop

Outcrop description: very high outcrop (about 10 – 20 m) in the center of Trento, near the Buonconsiglio castle.
Description: Red and white limestone with preferential fracturing due to stratification; its name comes from the abundance of ammonite fossils.

Sample code: 18A
Code: ORA, Ora formation (rhyolite)
Collection date: 31/10/2013
GPS coordinates: N 46° 07’ 21.5”, E 11° 06’ 43.8”

Figure 4.46: Photo of the outcrop

Figure 4.47: Photo of the sample

Figure 4.48: location of the outcrop

Outcrop description: high outcrop along the road; it can be confused with an adjacent one of sandstone for the similarity of color and size of minerals/grains.
Description: Massive lapilli tuffs, with clear and regular sub-vertical crackings. Presence of phenocrysalts of quartz, plagioclase, sanidine, biotite in a red/brown matrix.

Sample code: 19A
Code: CTR, Contrin formation (dolomite) (?)
Collection date: 31/10/2013
GPS coordinates: N 46° 07’ 02.5”, E 11° 06’ 56.1”

Figure 4.49: Photo of the outcrop

Figure 4.50: Photo of the sample

Figure 4.51: location of the outcrop

Outcrop description: high outcrop along the road; it is difficult to collect a proper sample for the high grade of fractures.
Description: Dolomite of white/red color, with quartz veins. The rock is heavily fractured and it’s difficult to collect a sample of proper dimensions.

Sample code: 20A
Code: SCI, Sciliar formation (dolomite)
Collection date: 06/11/2013
GPS coordinates: N 46° 05’ 14.7”, E 11° 05’ 40.7”

Figure 4.52: Photo of the outcrop

Figure 4.53: Photo of the sample

Figure 4.54: location of the outcrop

Outcrop description: very high wall of dolomite (about 60 m), near to an apple orchard.
Description: Stratified white dolomite, with small shiny crystals.

Sample code: 20B
Soil code: 1060, alluvial/fluvioglacial deposit
Collection date: 06/11/2013
GPS coordinates: N 46° 05’ 14.7”, E 11° 05’ 40.7”

Figure 4.55: Photo of the outcrop

Figure 4.56: location of the outcrop

Outcrop description: field near to an apple orchard.
Description: The soil is composed by fine and medium sands.

Sample code: 21A
Soil code: 1101, mixed alluvial fan
Collection date: 06/11/2013
GPS coordinates: N 46° 04’ 55.1”, E 11° 06’ 05.8”

Figure 4.57: Photo of the outcrop

Figure 4.58: location of the outcrop

Outcrop description: a field in Vela hamlet.
Description: The soil is composed by coarse sands.

Sample code: 22A
Code: MCE, Malcesine formation (limestone)
Collection date: 06/11/2013
GPS coordinates: N 46° 04’ 30.6”, E 11° 06’ 25.7”

Figure 4.59: Photo of the outcrop

Figure 4.60: Photo of the sample

Figure 4.61: location of the outcrop

Outcrop description: the outcrop is under an highway bridge, and about 3 m high. It is quite altered.
Description: Badly-layered calcarenites with a predominantly nodular of well-cemented calcarenites embedded in a more marly matrix. The rock is white and quite easy to fracture.

Sample code: 23A
Code: NAG, Nago formation (limestone)
Collection date: 06/11/2013
GPS coordinates: N 46° 04’ 17.2”, E 11° 06’ 30.7”

Figure 4.62: Photo of the outcrop

Figure 4.63: Photo of the sample

Figure 4.64: location of the outcrop

Outcrop description: small outcrop along the road that leads to the monuments to Alpine soldiers.
Description: Stratified micritic limestones (10-30 cm). The rock has different colors, from light grey to yellow and white, due to the different grade of weathering.

Sample code: 24A
Code: CHI, Chiusole formation (limestone)
Collection date: 06/11/2013
GPS coordinates: N 46° 04’ 21.4”, E 11° 04’ 21.2”

Figure 4.65: Photo of the outcrop

Figure 4.66: Photo of the sample

Figure 4.67: location of the outcrop

Outcrop description: There are no visible outcrops, but some samples can be found near the small river where the water eroded the surface soil exposing the rock below. The rock can be heavily altered due to the water erosion.
Description: Micritic limestones, in thin layers (10-30 cm) and sometimes with flint nodules and beds. Presence of thin interlayers of marl and clay. Stratified light grey rock, the surface is altered by water.

Sample code: 25A
Soil code: 1061, Trento alluvial fan
Collection date: 06/11/2013
GPS coordinates: N 46° 02’ 28.4”, E 11° 07’ 30.8”

Figure 4.68: Photo of the outcrop

Figure 4.69: Photo of the sample

Figure 4.70: location of the outcrop

Outcrop description: a field near the street.
Description: The soil is composed by fine sands.

Sample code: 26A
Code: GIV3, Giovo formation, dolomite
Collection date: 06/11/2013
GPS coordinates: N 46° 01’ 16.5”, E 11° 06’ 41.1”

Figure 4.71: Photo of the outcrop

Figure 4.72: Photo of the sample

Figure 4.73: location of the outcrop

Outcrop description: 3-4 m high, along the road, the rock is fractured.
Description: Thinly layered limestone and dolomite (10-20 cm) intercalated with thin layers of mudstones with quartz and muscovite. At the top it changes to bioclastic dolomite. White, fractured rock with small shiny crystals.

Sample code: 27A
Soil code: 1030, landslide deposit
Collection date: 06/11/2013
GPS coordinates: N 46° 02’ 34.7”, E 11° 09’ 13.6”

Figure 4.74: Photo of the outcrop

Figure 4.75: Photo of the sample

Figure 4.76: location of the outcrop

Outcrop description: It is along the road, on a small slope.
Description: The soil is composed by coarse sands weakly silty.

Sample code: 28 A
Code: LUB, Buss formation (andesite)
Collection date: 06/11/2013
GPS coordinates: N 46° 03’ 26.1”, E 11° 08’ 10.2”

Figure 4.77: Photo of the outcrop

Figure 4.78: Photo of the sample

Figure 4.79: location of the outcrop

Outcrop description: along the road, it is organized in huge and stratified layers, associated to rounded and angular blocks cemented together by a matrix of the same composition.
Description: porphyric and andesitic lava. Presence of phenocrystals of plagioclase, pyroxene, amphibole, biotite and quartz in a microgranular matrix mainly composed by plagioclase. The rock is a dark grey and rounded block, it seems hard to break.

Sample code: 29A
Code: ICT, riodacite
Collection date: 06/11/2013
GPS coordinates: N 46° 03’ 19.1”, E 11° 08’ 09.4”

Figure 4.80: Photo of the outcrop

Figure 4.81: Photo of the sample

Figure 4.82: location of the outcrop

Outcrop description: along the road in banks of metric thickness; frequent levels of fine tuff and tuff breccia.
Description: Lapilli tuff, presence of phenocrystals of quartz, plagioclase, biotite and pyroxene in a felsitic matrix. The rock is dark brown, it can be broken quite easy.

Sample code: 31A
Soil code: 1100, mixed deposit
Collection date: 06/11/2013
GPS coordinates: N 46° 03’ 58.5”, E 11° 10’ 14.3”

Figure 4.83: Photo of the outcrop

Figure 4.84: location of the outcrop

Outcrop description: near a road turn, next to a small river.
Description: The soil is composed mainly by sand, clay, gravel and a smaller component of silt.

4.5 Thin sections

Thermal conductivity for some rocks can be strongly anisotropic. In order to determine if anisotropy of the studied rocks induce anisotropies in thermal conductivity, all samples have been analyzed by optical microscopy. Two thin sections for each sample, one parallel and one perpendicular to the stratification/foliation (plane xy and yz respectively in Fig. 4.85), have been studied. In particular, it was checked if microstructural features of the rocks, such as iso-orientation of grains/bioclasts/minerals determine differences in modal composition causing anisotropies in thermal conductivity.

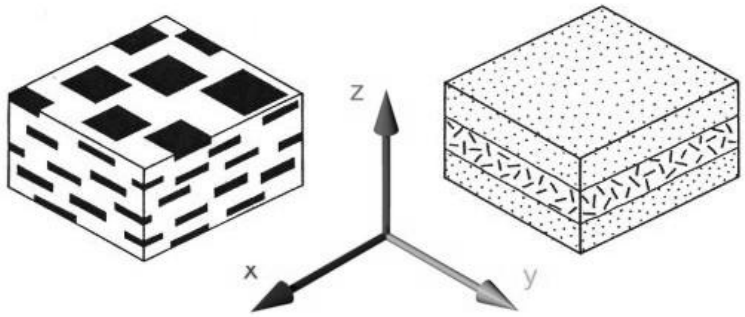

Figure 4.85: The studied rock thin sections are cut parallel an perpendicular to the horizontal anisotropy of the rock, on xy and yz planes respectively.

4.5.1 Dolomia Principale DPR (12A)

Most of the sample can be classified as a packstone (lighter portions in Fig. 4.86) because of its grain supported structure and the absence of carbonatic mud. Grains are made up by dolomite. Darker portions (top-left corner in Fig. 4.86) contains micritic mud, few dolomitic grains and rare bioclasts and can be classified as a wackstone. A faint orientation of the rock structure is visible in Fig. 4.86b). A lot of veins filled by sparitic calcite are present.
At higher magnification, we can easily distinguish the grain-supported domains (Fig. 4.87) and the mud-supported ones (Fig. 4.87b).
The structural and compositional features of the samples do not show evident differences on the two differently oriented surfaces.

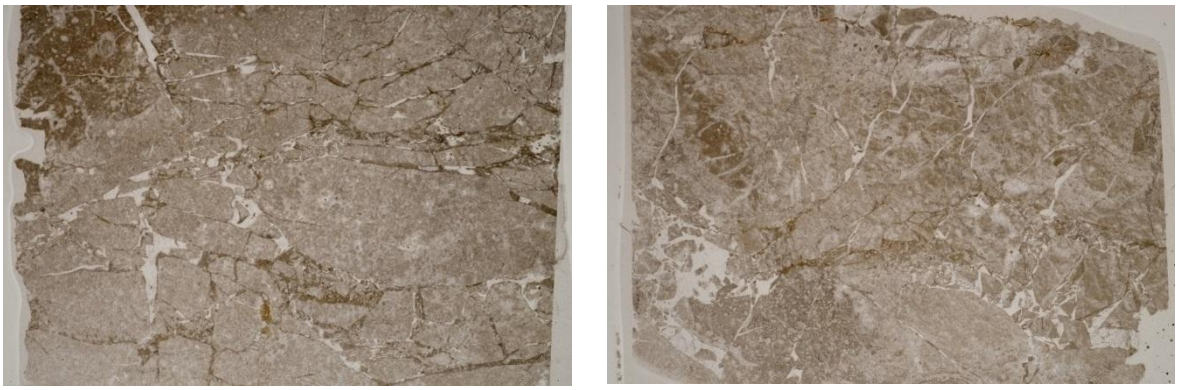

Figure 4.86: Thin sections of the sample 12A: a) section cut parallel to the stratification; b) section cut perpendicular to the stratification. Vertical side: 25 mm.

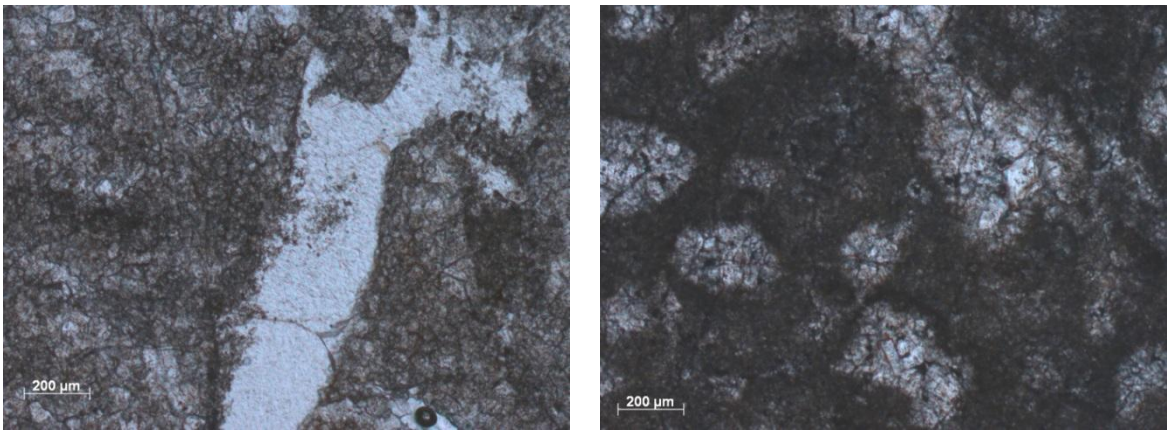

Figure 4.87: Thin sections of the sample 12A: a) grain-supported domain and a sparite vein; b) mud supported domain. The scale is on the pictures.

4.5.2 Calcari grigi RTZ (16 A)

This sample was a wackstone that partially underwent to dolomitization process. Darker areas (Fig. 4.88, 4.89a) show the original micritic composition whereas the lighter ones (Fig. 4.88, 4.89b) feature nearly complete dolomitization process. A lot of veins and channels are present.

At higher magnification, we can easily distinguish the micritic domains (4.89a) from the dolomitized portion of the rock (4.89b) where the original limestone has been totally replaced by dolomite. Where the dolomitization process is incomplete rhomb-shaped dolomite crystals are visible (4.89a).

The structural and compositional features of the samples do not show evident differences on the two differently oriented surfaces.

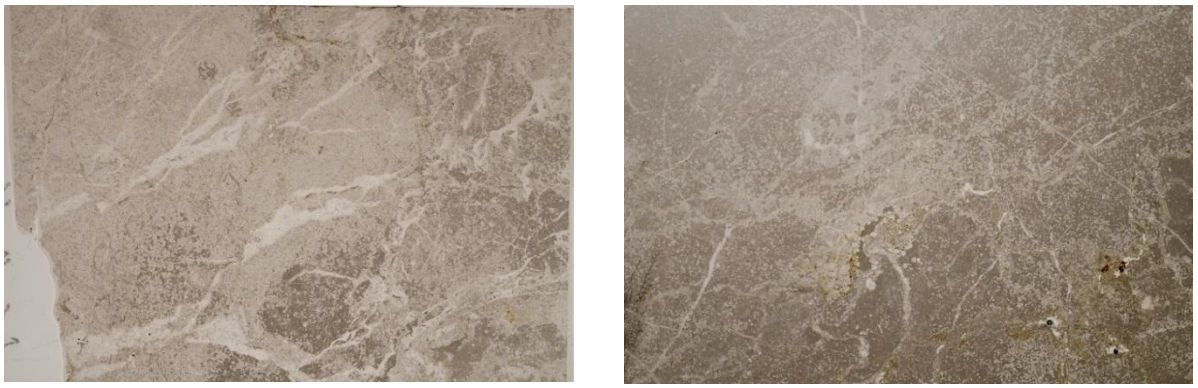

Figure 4.88: Thin sections of the sample 16A: a) section cut parallel to the stratification; b) section cut perpendicular to the stratification. Vertical side: 25 mm.

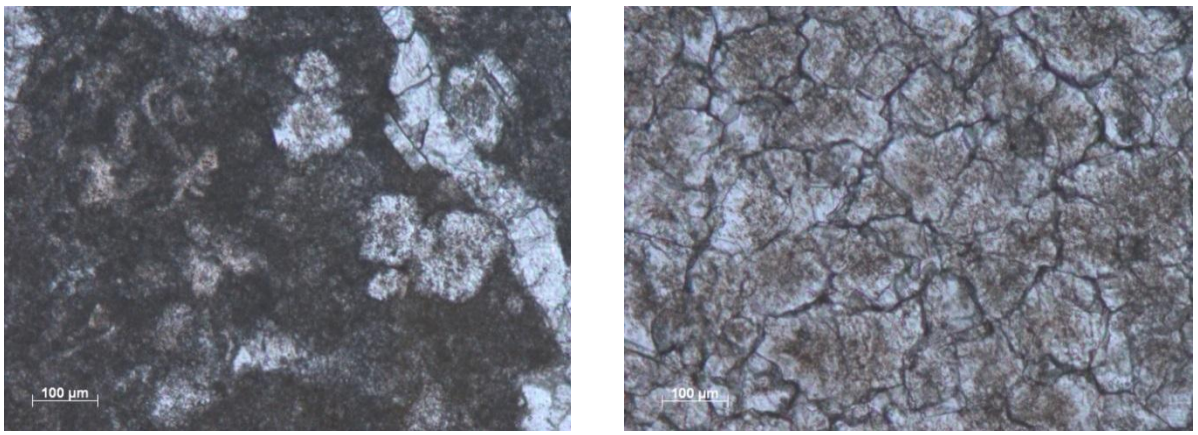

Figure 4.89: Thin sections of the sample 16A: a) micritic domain with some dolomite crystals; b) dolomite crystals replaces original limestone. The scale is on the pictures.

4.5.3 Scaglia rossa SAA (14A)

This sample features a mud-supported structure and can be classified as a wackstone. The stratification and the consequent orientation is not so evident. Some fractures approximately parallel to the stratification occur in this sample (Fig. 4.90b). Grains are mainly made up mainly by bioclasts (Fig. 4.91).
The structural and compositional features of the samples do not show evident differences on the two differently oriented surfaces.

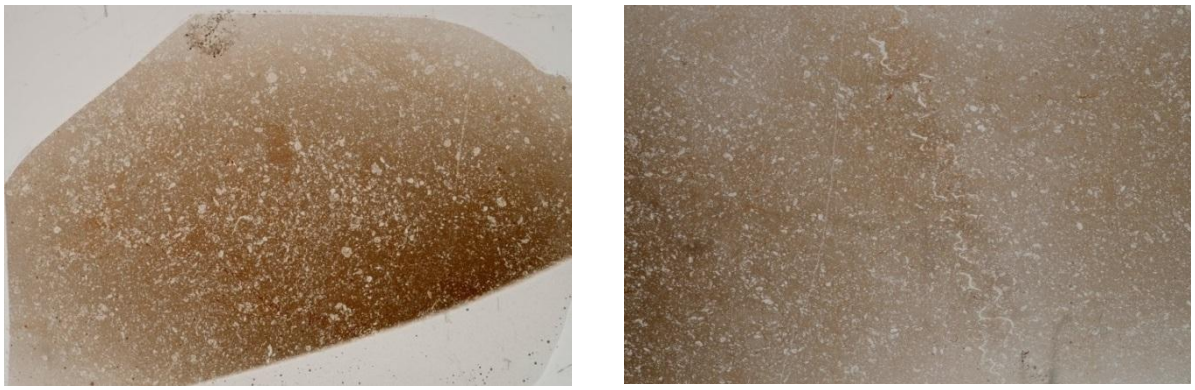

Figure 4.90: Thin sections of the sample 14A: a) section cut parallel to the stratification; b) section cut perpendicular to the stratification. Vertical side: 25 mm.

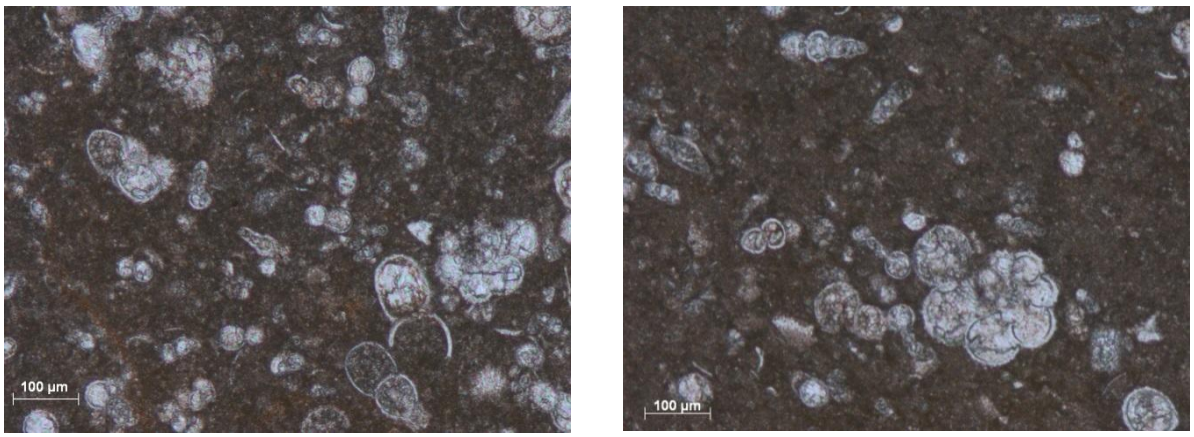

Figure 4.91: Thin sections of the sample 14A: a) bioclasts in the section cut parallel to the stratification; b) section cut perpendicular to the stratification. The scale is on the pictures.

4.5.4 Formazione di Chiusole CHI (24A)

This sample features a mud-supported structure and can be classified as a wackstone. The orientation of the structure due to the stratification is evident (Fig. 4.92b). Grains are mainly made up mainly by bioclasts (Fig. 4.93). Some rare glauconite grains are found.
At higher magnification, some oxide/hydroxide isolated grains are found. Sometimes these grains are aligned to form bands parallel to the stratification of the rock (Fig. 4.92b).

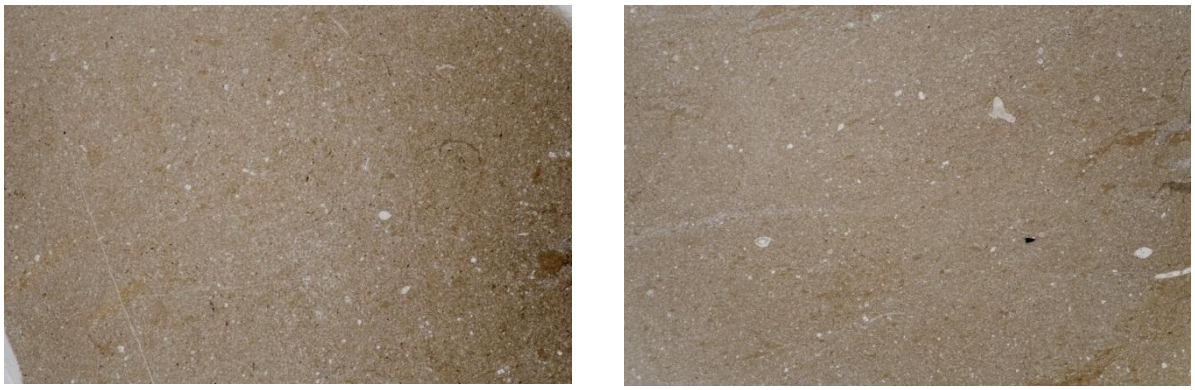

Figure 4.92: Thin sections of the sample 24A: a) section cut parallel to the stratification; b) section cut perpendicular to the stratification. Vertical side: 25 mm.

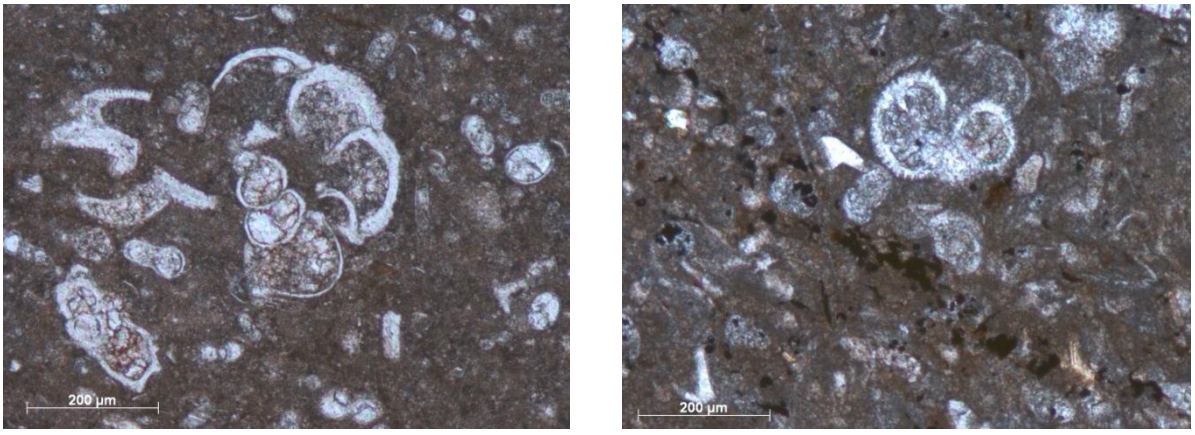

Figure 4.93: Thin sections of the sample 24A: a) bioclasts in the section cut parallel to the stratification; b) oxide oriented band parallel to the stratification. The scale is on the pictures.

4.5.5 Calcari grigi Formazione M.te Zugna FMZ (8A)

This sample features a mud-supported structure and can be classified as a wackstone. The stratification is not evident neither at millimetric scale nor at micrometric one. A lot of sparite veins occur in the samples (light portions in Fig. 4.94). Most of the veins show an irregular thickness and shape, others are thinner and constant in thickness. Grains are made up mainly by bioclasts (Fig. 4.95).
The structural and compositional features of the samples do not show evident differences on the two differently oriented surfaces.

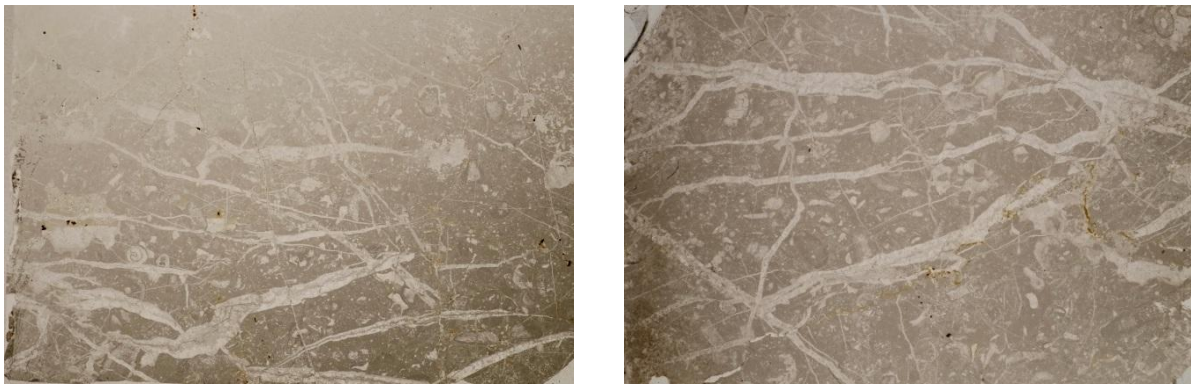

Figure 4.94: Thin sections of the sample 8A: a) section cut parallel to the stratification; b) section cut perpendicular to the stratification. Vertical side: 25 mm.

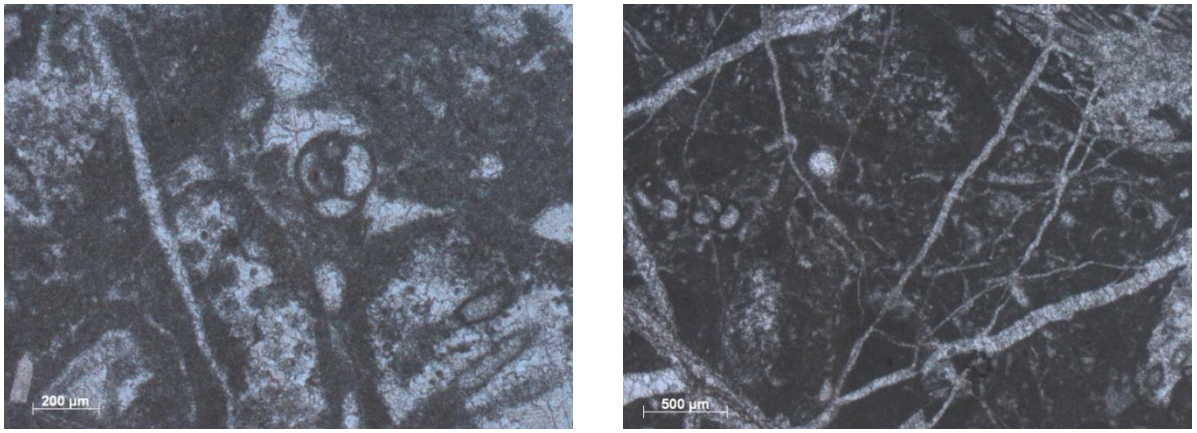

Figure 4.95: Thin sections of the sample 8A: a) bioclasts and a vein in the section cut parallel to the stratification; b) bioclasts and veins in the section cut perpendicular to the stratification. The scale is on the pictures.

4.5.6 Rosso ammonitico veronese ARV (17A)

This samples can be classified as a wackstone because of its mud-supported structure. Grains are mainly formed by small bioclasts but some dolomite grains occur as well.
Some brownish faint "shadows" are recognized (Fig. 4.96) but they do not show any peculiar orientation and relationship with the stratification of the rock. Maybe they are due to the occurrence of a small amount of oxides/hydroxides. Some fractures are present.
At higher magnification, some dolomite crystals are found (Fig. 4.97).
The structural and compositional features of the samples do not show evident differences on the two differently oriented surfaces.

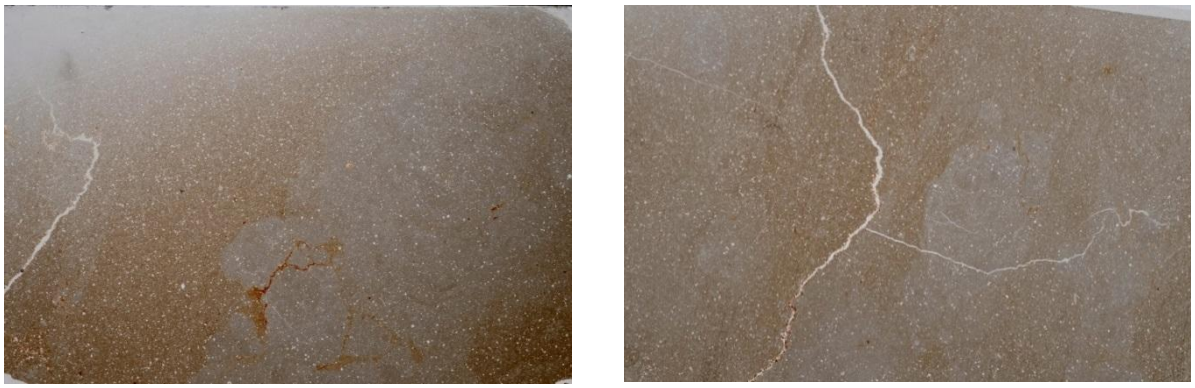

Figure 4.96: Thin sections of the sample 17A: a) section cut parallel to the stratification; b) section cut perpendicular to the stratification. Vertical side: 25 mm.

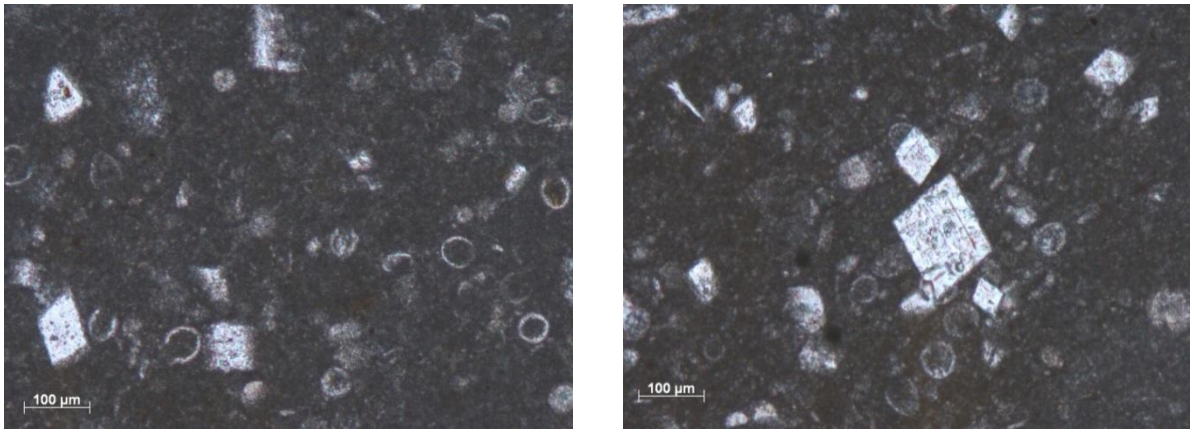

Figure 4.97: Thin sections of the sample 17A: a) bioclasts and rhomboidal dolomite crystals in the section cut parallel to the stratification; b) section cut perpendicular to the stratification. The scale is on the pictures.

4.5.7 Gruppo vulcanico Atesino - Fm Ora ORA (18A)

This acidic volcanoclastic rock is formed by large grains (40%) and cryptocrystalline groundmass (60%) (Fig. 4.98). Grains are made up by: quartz, plagioclase, alkali feldspars, volcanic rocks fragments, biotite and opaque minerals. There are cavities filled by secondary calcite.

No significative compositional differences between the perpendicular and parallel thin sections are found.

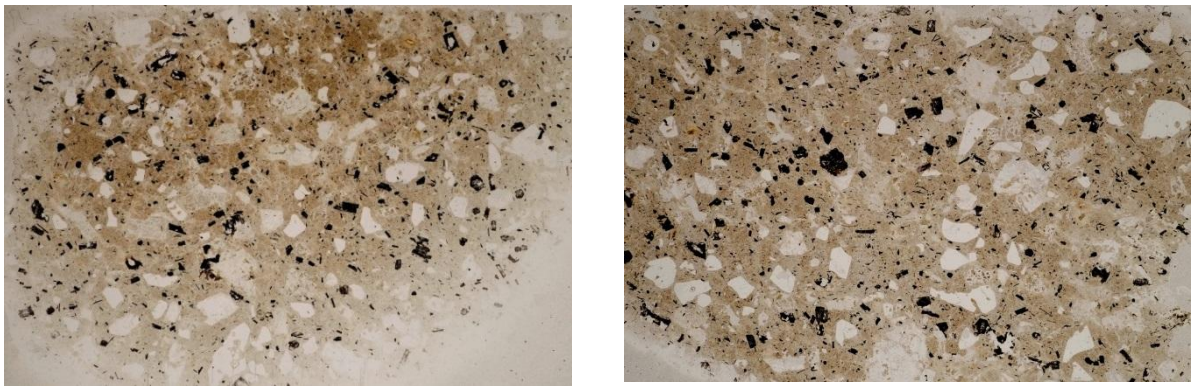

Figure 4.98: Thin sections of the sample 18A: a) section cut parallel to the stratification; b) section cut perpendicular to the stratification. Vertical side: 25 mm.

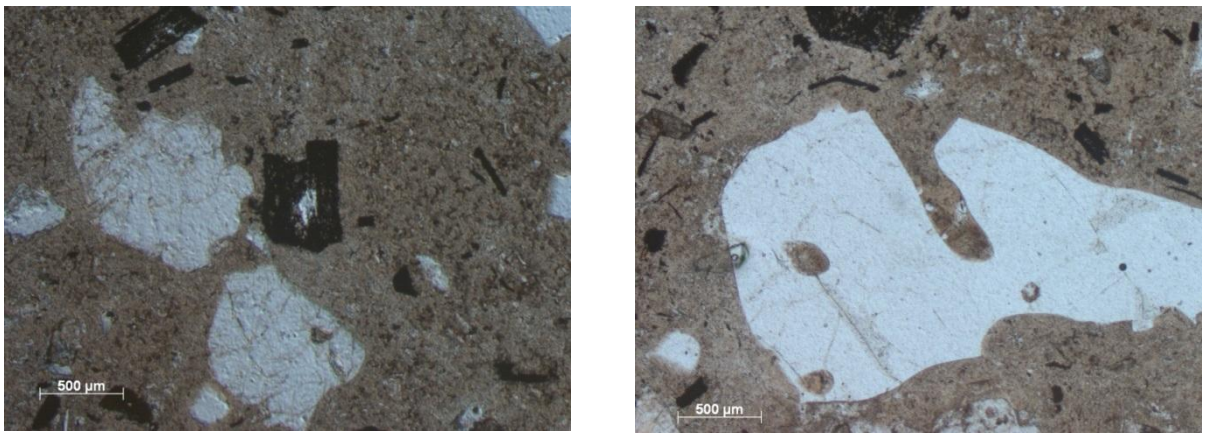

Figure 4.99: Thin sections of the sample 18A: a) altered biotite flake (in the middle and top left) in the section cut parallel to the stratification; b) embayed quartz crystal with some recrystallized melt drops in the section cut perpendicular to the stratification. The scale is on the pictures.

4.5.8 Formazione Werfen WER (4B)

This samples is a grain-supported carbonatic rock having a lot of bioclasts (packstone). As we can see in Fig. 4.100b, bioclasts are oriented parallel to the stratification of the rock.
Sometimes voids within bioclasts are filled by sparite (Fig. 4.101a). Also at higher magnification (Fig. 4.101b), no significative compositional differences between the perpendicular and parallel thin sections are found.

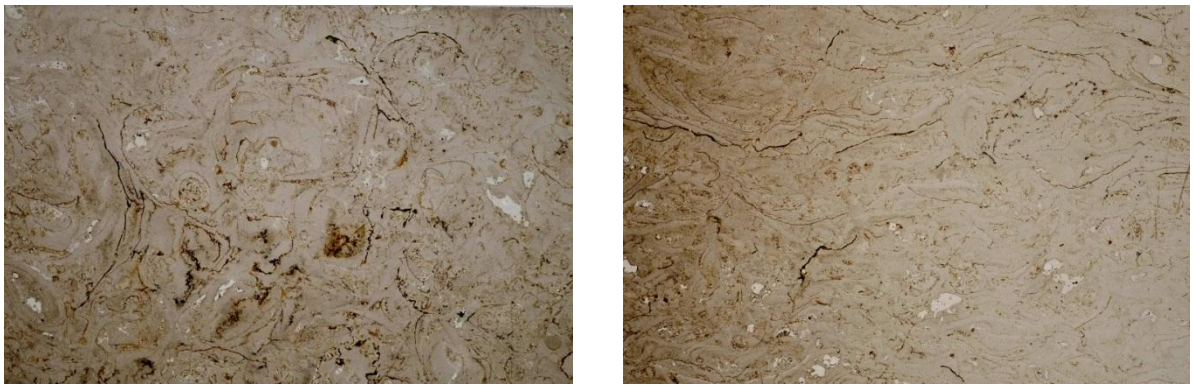

Figure 4.100: Thin sections of the sample 4B: a) section cut parallel to the stratification; b) section cut perpendicular to the stratification. Vertical side: 25 mm.

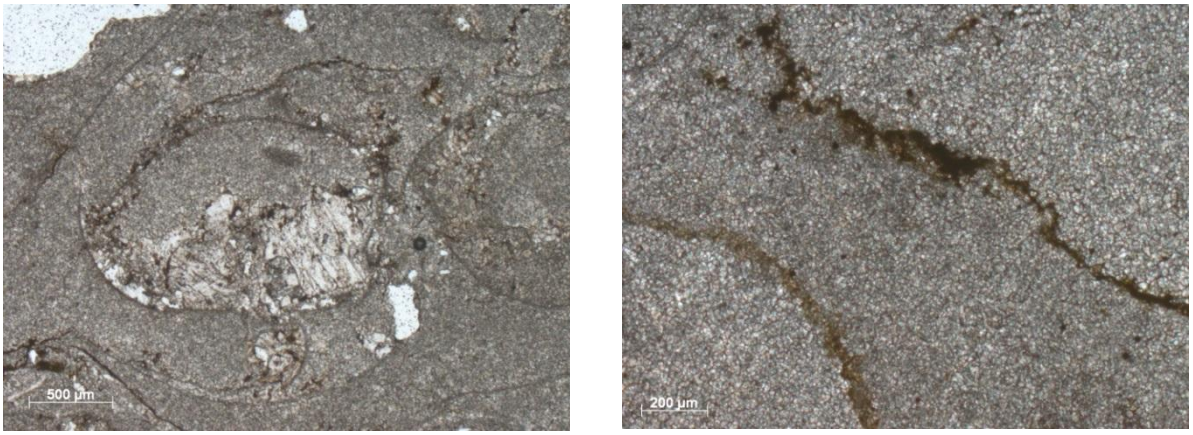

Figure 4.101: Thin sections of the sample 4B: a) section cut parallel to the stratification: sparite filling porosity within bioclasts; b) section cut perpendicular to the stratification: opaque minerals along fractures. The scale is on the pictures.

4.5.9 Formazione Werfen WER (5A)

This sample can be classified as a grainstone because of its grain supported structure. Few cavities filled by calcite are present (Fig. 4.102). A lot of veins filled by sparitic calcite, are present.
Oxides and hydroxides minerals form red-brownish oriented haloes on the parallel as well as perpendicular thin section (Fig. 4.102a, b).
At higher magnification (Fig. 4.103a), we can easily distinguish the calcite crystals. In the section cut perpendicular to the stratification (Fig. 4.103b) it is visible the hydroxides deposition along the crystal boundaries.
The structural and compositional features of the samples do not show evident differences on the two differently oriented surfaces.

Figure 4.102: Thin sections of the sample 5A: a) section cut parallel to the stratification; b) section cut perpendicular to the stratification. Vertical side: 25 mm.

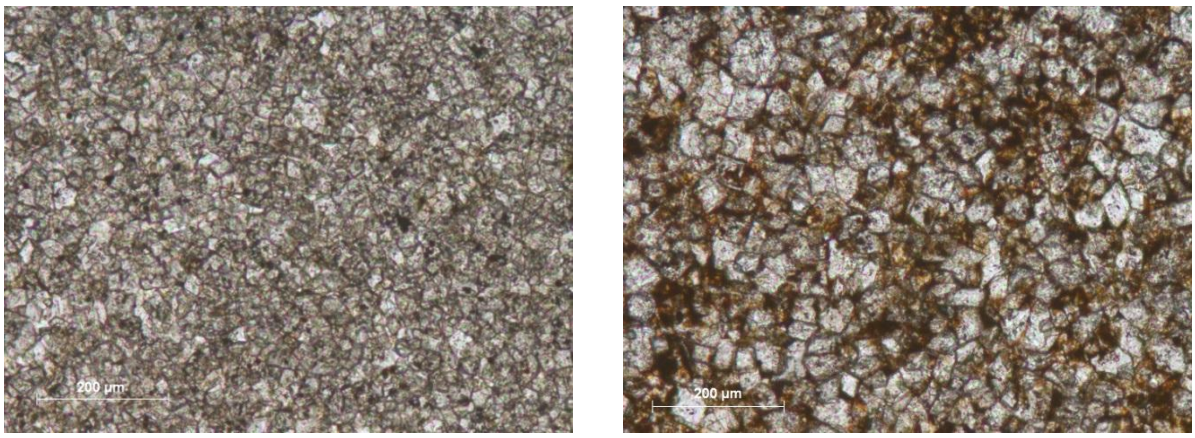

Figure 4.103: Thin sections of the sample 5A: a) section cut parallel to the stratification; b) section cut perpendicular to the stratification. The scale is on the pictures.

4.5.10 Formazione Werfen WER (6A)

This samples is a grain-supported carbonatic rock (grainstone). Most of the grains are peloids (Fig. 4.104, 4.105a); only few bioclasts occur.
A lot of cavities, the so-called fenestrae, are present. They show a tendency to be elongate parallel to the bedding (Fig. 4.104b). Fenestrae of this type may form from the decay of organic matter associated with algal stromatolites. The bottom of these cavities is filled by micrite, whereas the upper part by sparite (Fig. 4.104b, 4.105.b).
No significative compositional differences between the perpendicular and parallel thin sections are found.

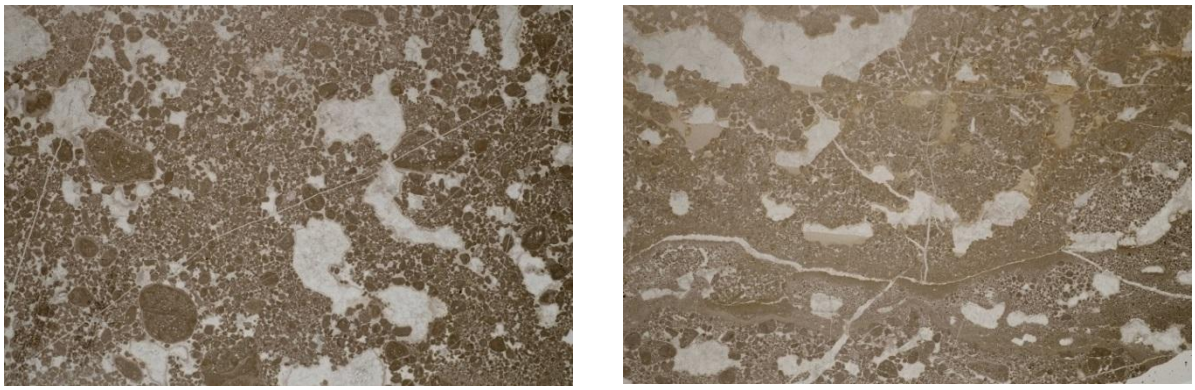

Figure 4.104: Thin sections of the sample 6A: a) section cut parallel to the stratification; b) section cut perpendicular to the stratification. Vertical side: 25 mm.

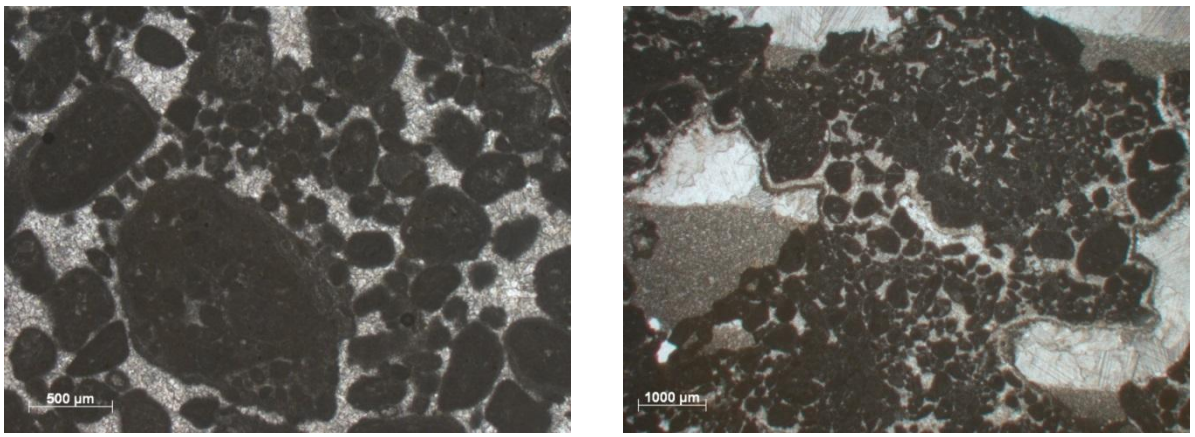

Figure 4.105: Thin sections of the sample 6A: a) section cut parallel to the stratification; b) section cut perpendicular to the stratification. The scale is on the pictures.

4.5.11 Formazione Werfen WER (6C)

This sample features a mud-supported structure and can be classified as a wackstone (Fig. 4.106). Grains are made up by peloids and bioclasts (Fig. 4.107a). The stratification is not evident neither at millimetric scale nor at micrometric one. Some cavities filled by sparitic calcite are found. A lot of veins occur in the samples (Fig. 4.106). Some of them are filled by two different kind of sparite (Fig. 4.107).
No significative compositional differences between the perpendicular and parallel thin sections are found.

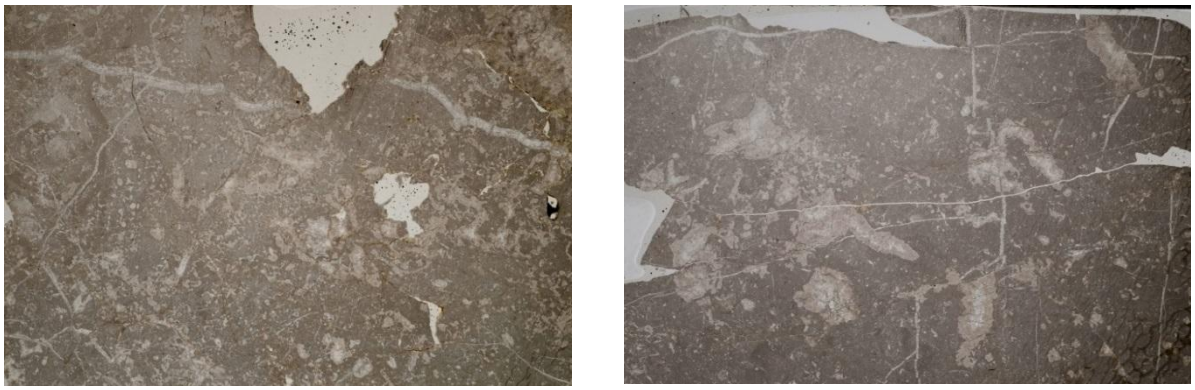

Figure 4.106: Thin sections of the sample 6C: a) section cut parallel to the stratification; b) section cut perpendicular to the stratification. Vertical side: 25 mm.

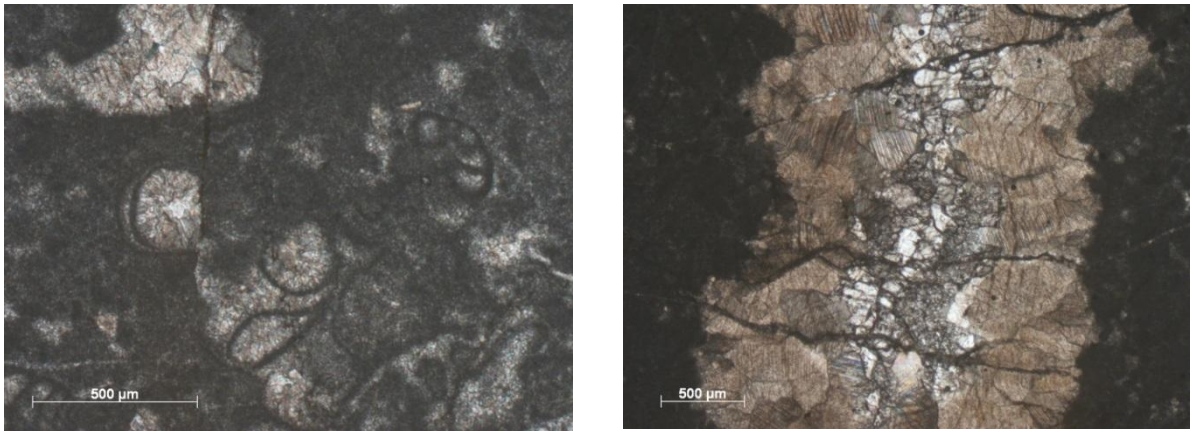

Figure 4.107: Thin sections of the sample 6C: a) bioclasts in the section cut parallel to the stratification; b) vein in the section cut perpendicular to the stratification. The scale is on the pictures.

4.5.12 Formazione del Giovo GIV3 (26A)

Dolostone. This sample can be classified as a grainstone because of its grain supported structure. The grains have a dolomitic composition. A lot of cavities filled by calcite are present (Fig. 4.108).
At higher magnification, we can easily distinguish the dolomite crystals in the section cut parallel to the stratification (Fig. 4.109a) and in the section cut perpendicular to the stratification (Fig. 4.109b). As we can see, at microscopic scale no orientation is visible
The structural and compositional features of the samples do not show evident differences on the two differently oriented surfaces.

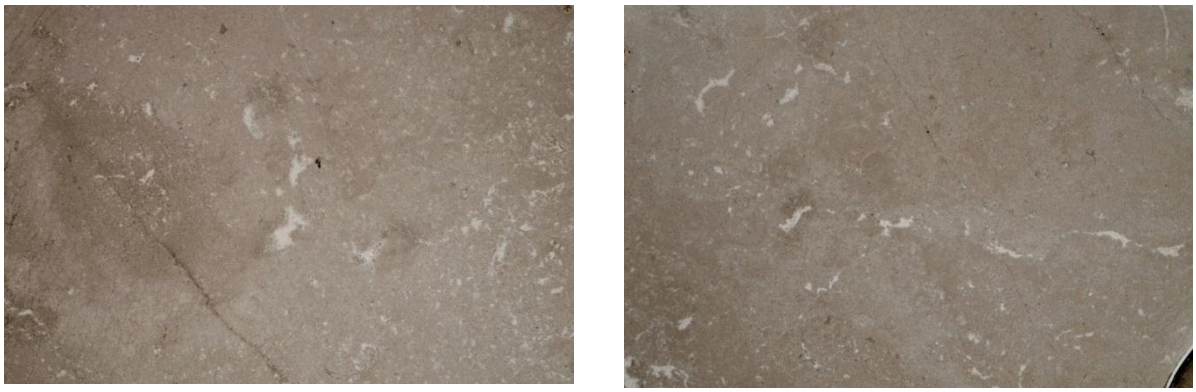

Figure 4.108: Thin sections of the sample 26A: a) section cut parallel to the stratification; b) section cut perpendicular to the stratification. Vertical side: 25 mm.

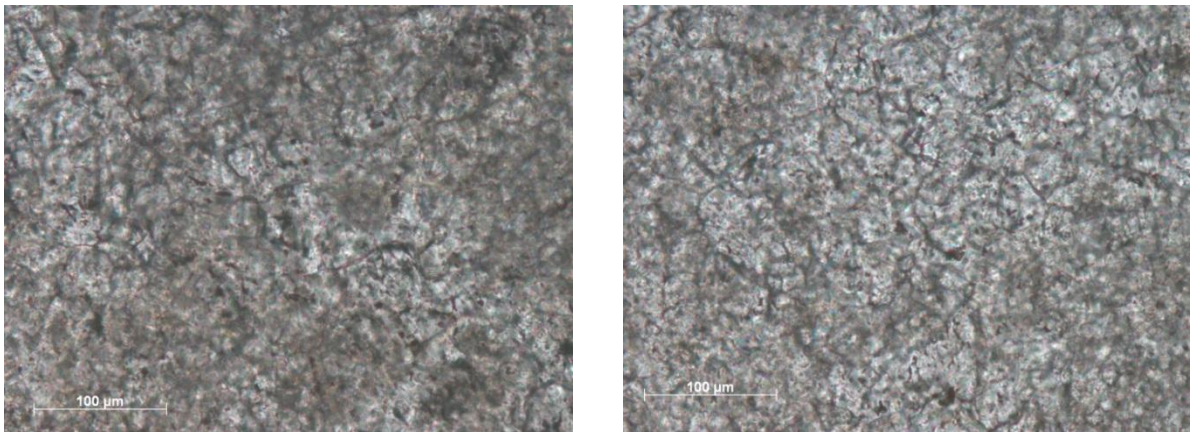

Figure 4.109: Thin sections of the sample 26A: a) section cut parallel to the stratification; b) section cut perpendicular to the stratification. The scale is on the pictures.

4.5.13 Formazione del Contrin CTR (19A)

Dolostone. Part of the sample can be classified as a grainstone (lighter portions in Fig. 4.110) because of its grain supported structure and the absence of carbonatic mud. Grains are made up by dolomite. Another part of the sample, a little bit darker, contains dolomitic micritic mud and can be classified as a mudstone. No oriented structures are visible. A lot of veins filled by sparitic calcite, are present. Opaque minerals are found in small black grains. Oxides and hydroxide minerals form red-brownish haloes.
At higher magnification, we can easily distinguish the mud-supported domains (Fig. 4.111a) and the grain-supported ones (Fig. 4.111b).
The structural and compositional features of the samples do not show evident differences on the two differently oriented surfaces.

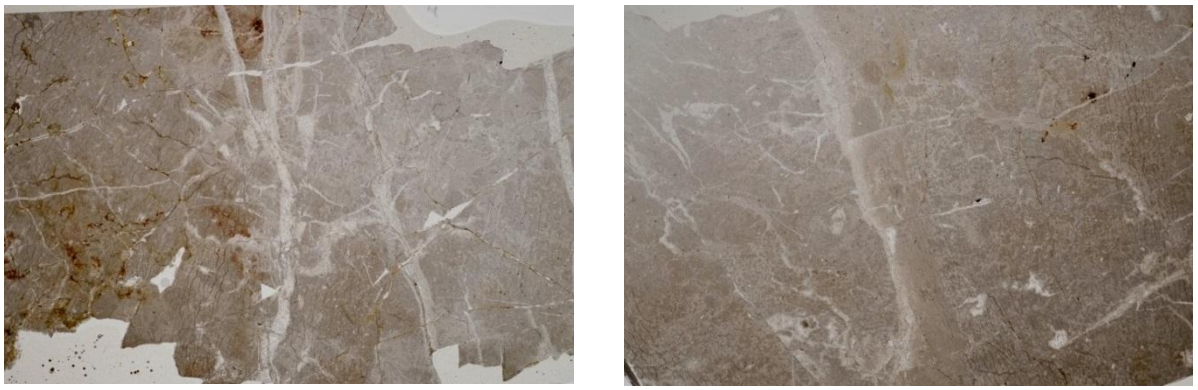

Figure 4.110: Thin sections of the sample 19A: a) section cut parallel to the stratification; b) section cut perpendicular to the stratification. Vertical side: 25 mm.

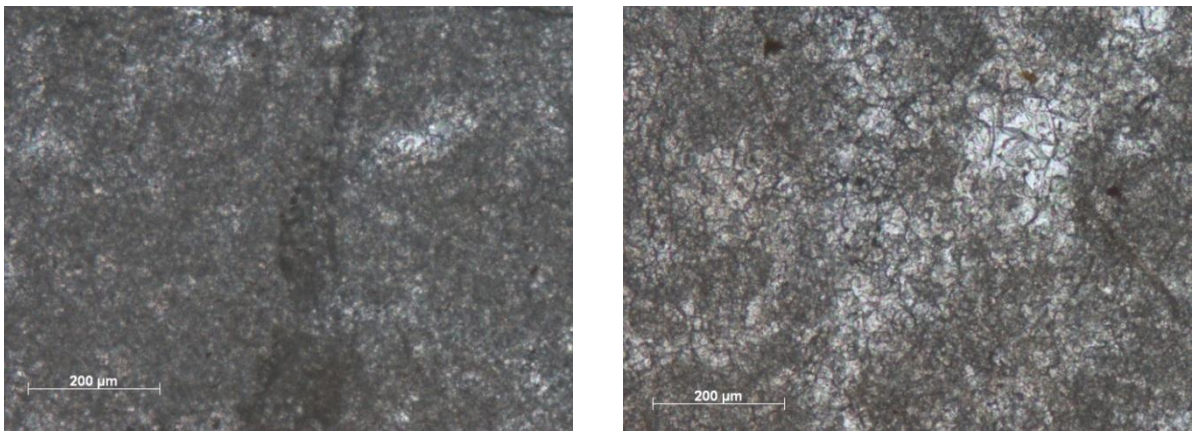

Figure 4.111: Thin sections of the sample 19A: a) micritic domain; b) dolomite grains. The scale is on the pictures.

4.5.14 Calcare di Nago NAG (23A)

This samples is a grain-supported carbonatic rock having a lot of bioclasts (packstone). As we can see in Fig. 4.112b, bioclasts are oriented in the thin section cut perpendicularly to the stratification.
Also at higher magnification (Fig. 4.113), no significative compositional differences between the perpendicular and parallel thin sections are found.

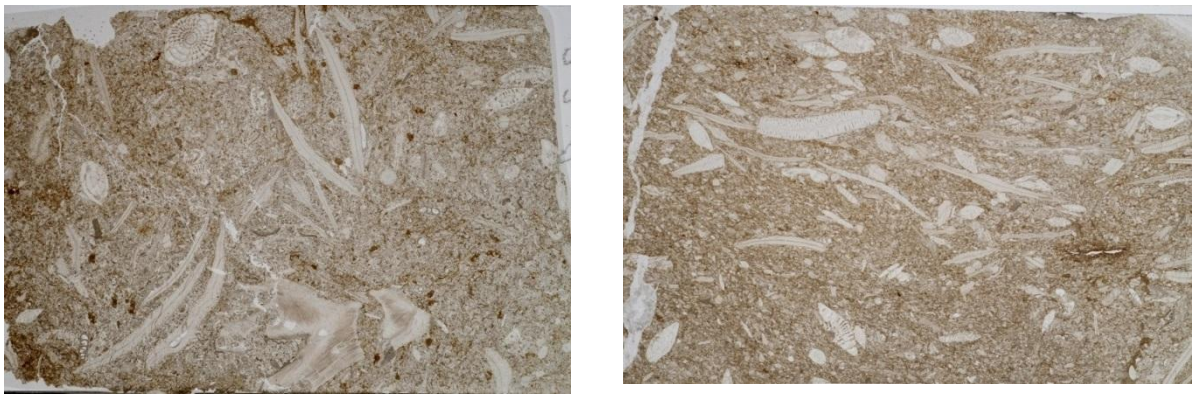

Figure 4.112: Thin sections of the sample 23A: a) section cut parallel to the stratification; b) section cut perpendicular to the stratification. Vertical side: 25 mm.

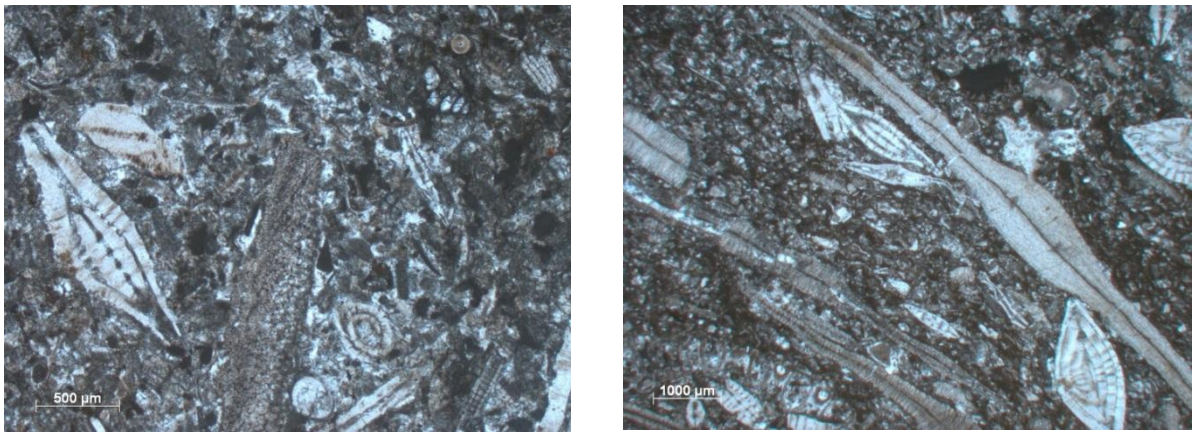

Figure 4.113: Thin sections of the sample 23A: a) section cut parallel to the stratification; b) section cut perpendicular to the stratification. The scale is on the pictures.

4.5.15 Formazione dello Sciliar SCI (20A)

This sample features a mud-supported structure and can be classified as a wackstone. The mud has a dolomitic composition. Grains are made up by peloids. The stratification is not evident neither at millimetric scale nor at micrometric one. A lot of sparite veins occur in the samples (white portions in Fig. 4.114). Most of the veins show an irregular thickness and shape, others are thinner and constant in thickness.
At higher magnification some cavities filled by sparitic calcite are found (Fig. 4.115a).
The structural and compositional features of the samples do not show evident differences on the two differently oriented surfaces.

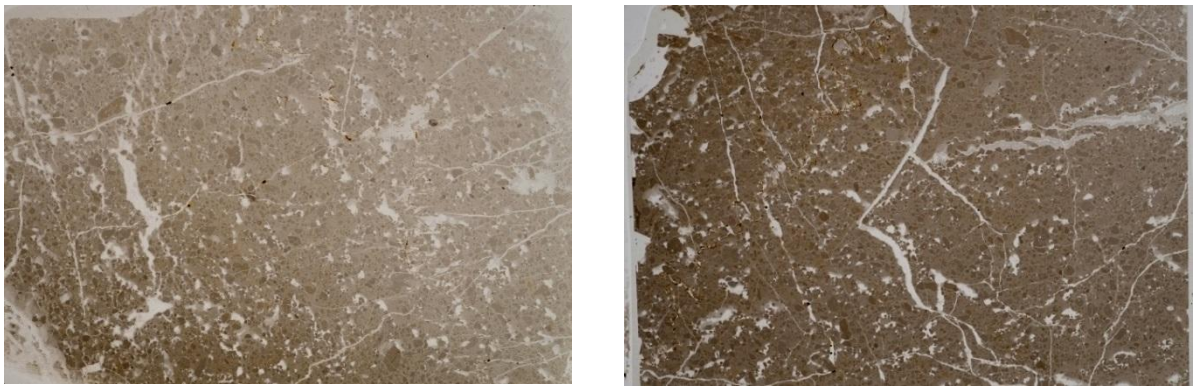

Figure 4.114: Thin sections of the sample 20A: a) section cut parallel to the stratification; b) section cut perpendicular to the stratification. Vertical side: 25 mm.

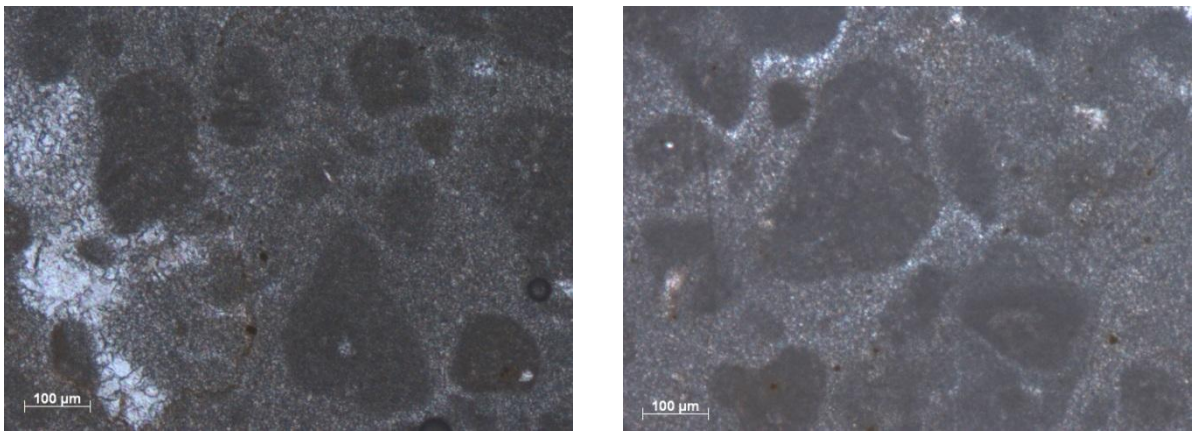

Figure 4.115: Thin sections of the sample 20A: a) peloids and porosity filled by spariti calcite in the section cut parallel to the stratification; b) peloids in the section cut perpendicular to the stratification. The scale is on the pictures.

4.5.16 Calcare di Malcesine MCE (22A)

This samples can be classified as a packstone because of its grain-supported structure. Grains are mainly formed by small bioclasts. Only a small amount of grains are made up by micritic materials.
No evident orientation of granules is present. Some brownish faint “shadows” are present (Fig. 4.116) but they do not show any peculiar orientation and relationships with the stratification of the rock. Maybe they are due to the occurrence of a small amount of oxides/hydroxides.
At higher magnification a slightly oriented structure is visible.

Figure 4.116: Thin sections of the sample 22A: a) section cut parallel to the stratification; b) section cut perpendicular to the stratification. Vertical side: 25 mm.

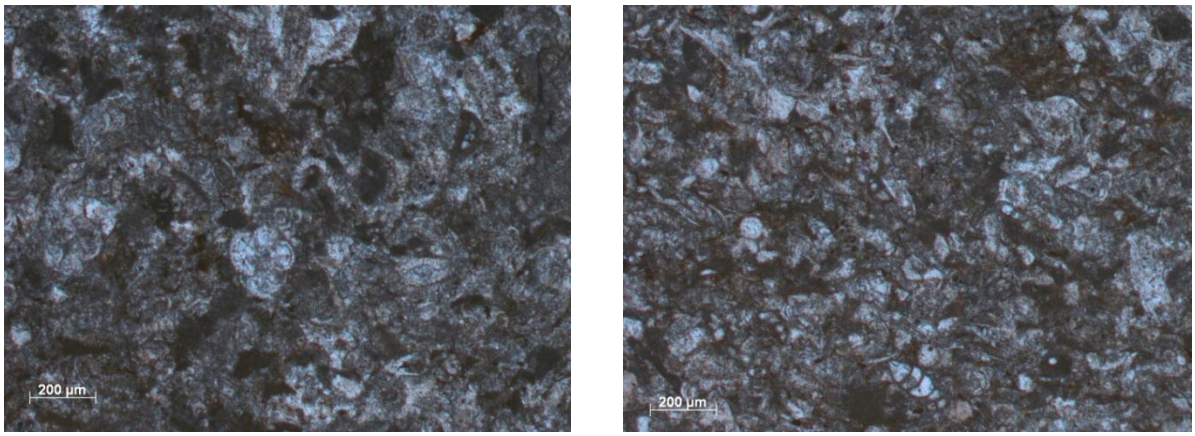

Figure 4.117: Thin sections of the sample 22A: a) section cut parallel to the stratification; b) section cut perpendicular to the stratification. The scale is on the pictures.

4.5.17 Filoni a quarzo e calcite f_a (2A)

This acidic volcanoclastic rock is formed by large grains (50%) and cryptocrystalline groundmass (50%) (Fig. 4.118). Grains are made up by: quartz, plagioclase, alkali feldspars, volcanic rocks fragments, biotite and opaque minerals.
No significative compositional differences between the perpendicular and parallel thin sections are found.

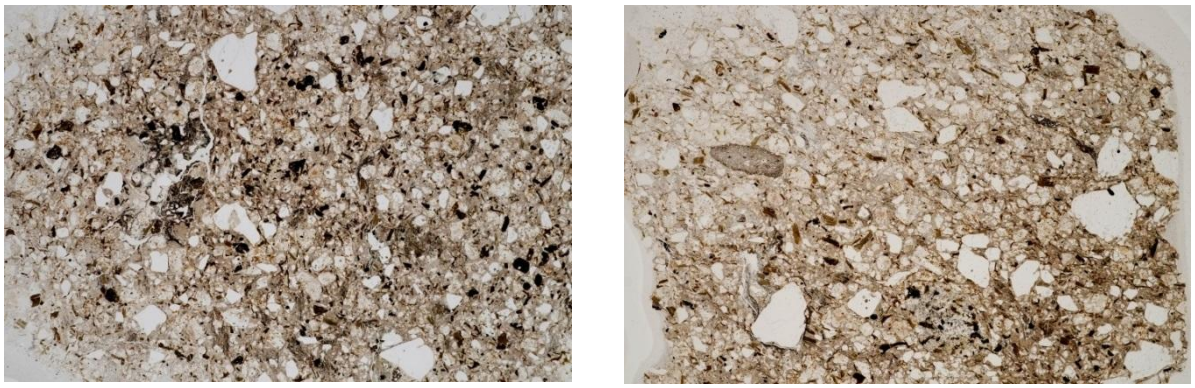

Figure 4.118: Thin sections of the sample 2A: a) section cut parallel to the stratification; b) section cut perpendicular to the stratification. Vertical side: 25 mm.

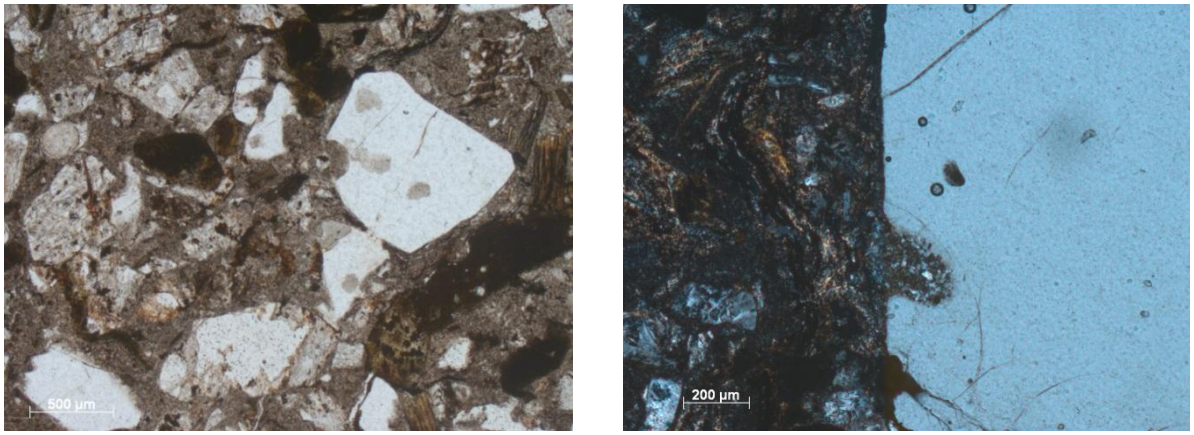

Figure 4.119: Thin sections of the sample 2A: a) recrystallized melt drops within quartz in the section cut parallel to the stratification; b) embayed quartz crystal in the section cut perpendicular to the stratification. The scale is on the pictures.

4.5.18 Calcare di Malcesine MCE (15B)

This samples can be classified as a grainstone because of its grain-supported structure and the absence of micrite. Grains are mainly formed by bioclasts and quartz grains (Fig. 120). A weak orientation of granules in visible in Fig. 4.120b.
No significative compositional differences between the perpendicular and parallel thin sections are found.

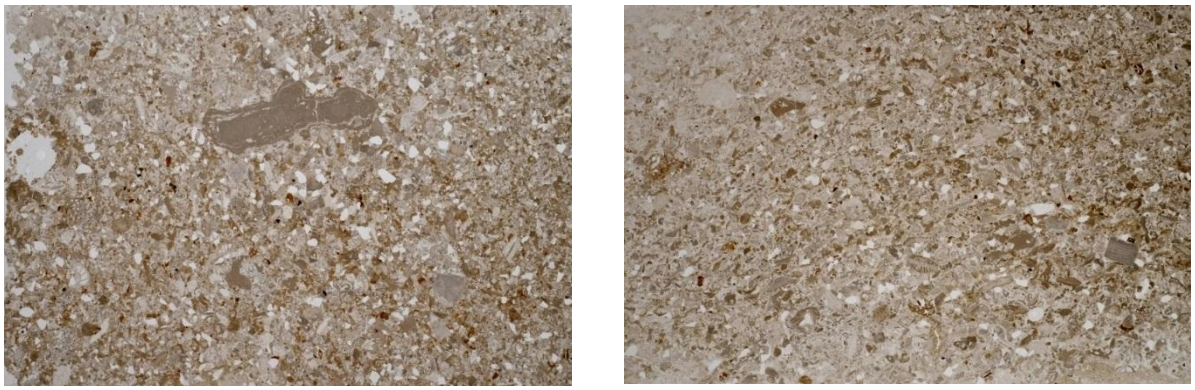

Figure 4.120: Thin sections of the sample 15B: a) section cut parallel to the stratification; b) section cut perpendicular to the stratification. Vertical side: 25 mm.

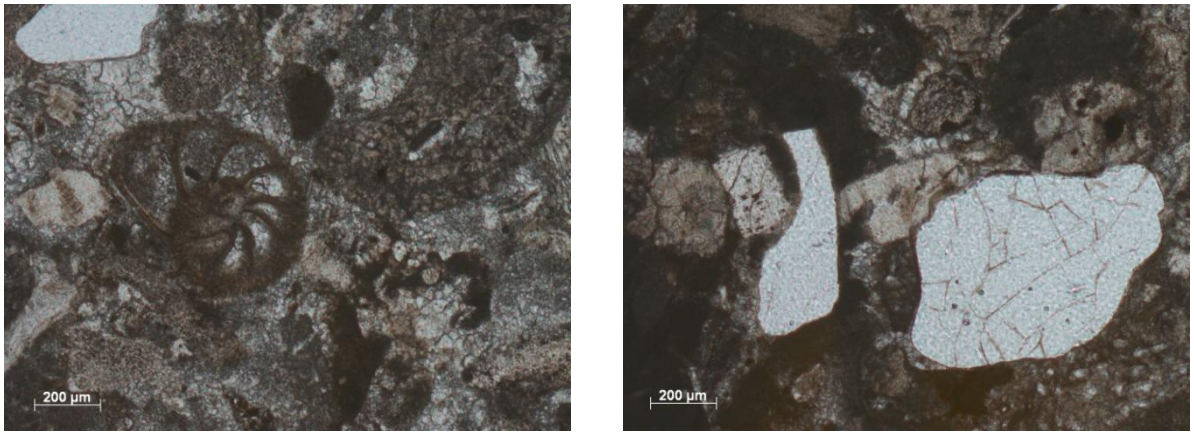

Figure 4.121: Thin sections of the sample 15B: a) bioclasts in section cut parallel to the stratification; b) quartz grains in section cut perpendicular to the stratification. The scale is on the pictures.

4.5.19 Filladi e Filladi quarzifere VFS (10A)

This phyllite shows an evident structural anisotropy: a plane, locally ondulated, schistosity (Fig. 4.122) occurs. The schistosity is given by the iso-orientation of muscovite flakes. The microstructure of this samples is characterized by a layering due to the alternance of lepidoblastic bands formed by muscovite and granoblastic ones, formed by quartz and albite (grey-white portion in Fig. 4.123a). Albitic porphyroblastesis also occur in this samples (Fig. 4.123b).

Due to the occurrence of alternating lepidoblastic and granoblastic bands, this rock show significative compositional differences between the perpendicular end parallel thin sections.

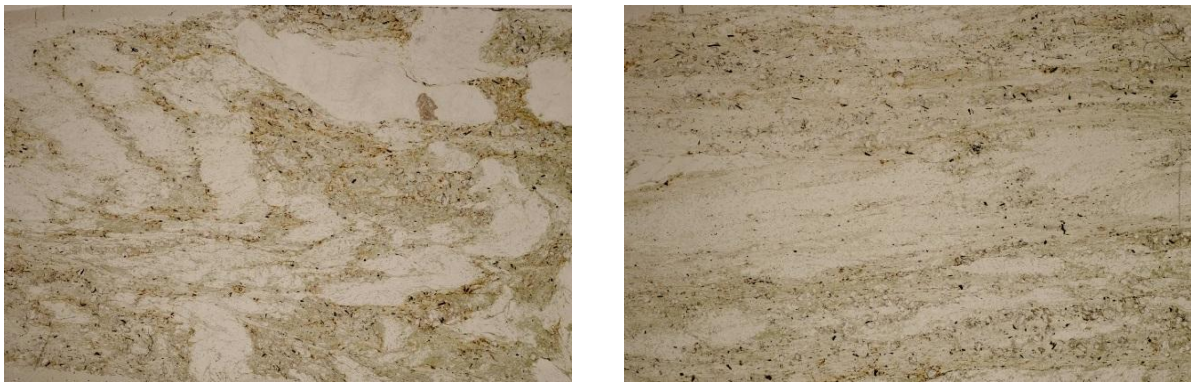

Figure 4.122: Thin sections of the sample 10A: a) section cut parallel to the stratification; b) section cut perpendicular to the stratification. Vertical side: 25 mm.

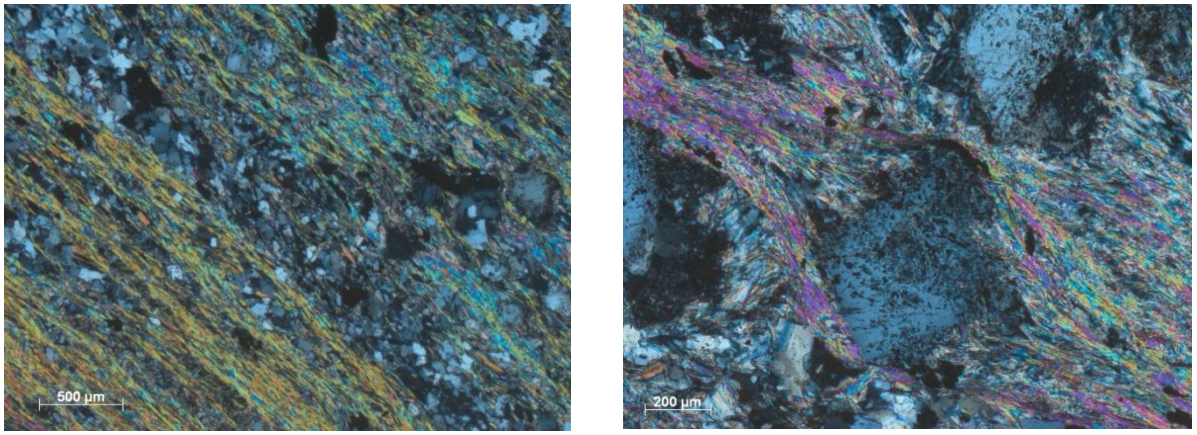

Figure 4.123: Thin sections of the sample 10A: a) lepidoblastic and granoblastic bands in section cut perpendicular to the metamorphic foliation; b) albite porphyroblast growth within lepidoblastic domain. The scale is on the pictures.

4.5.20 Gruppo Vulcanico Atesino - Fm Buss LUB (28A)

This acidic volcanoclastic rock is formed by large grains (25%) and micro-crystalline groundmass (75%) (Fig. 4.124). Grains are made up by: plagioclase, glomerocrystals, quartz, biotite, inosilicate, and opaque minerals. The inosilicate is transformed into chlorite maybe for the intense hydrothermal alteration affecting this sample.
No significative compositional differences between the perpendicular and parallel thin sections are found.

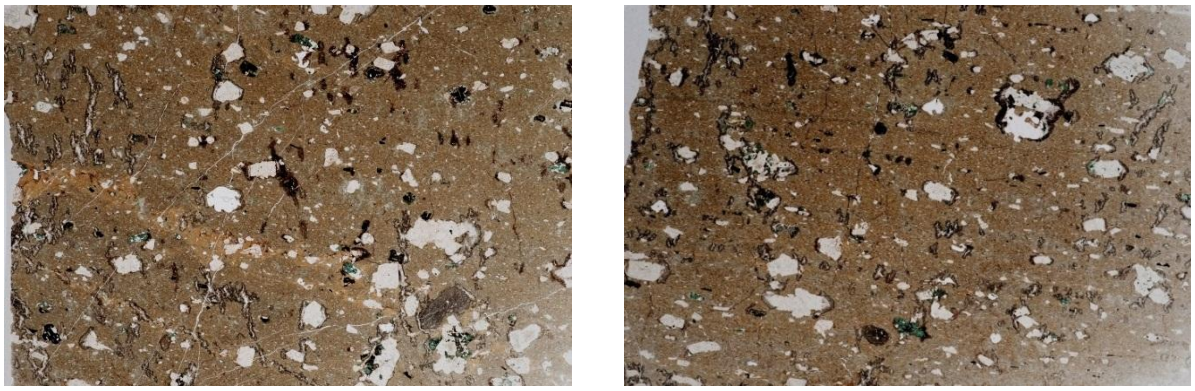

Figure 4.124: Thin sections of the sample 28A: a) section cut parallel to the stratification; b) section cut perpendicular to the stratification. Vertical side: 25 mm.

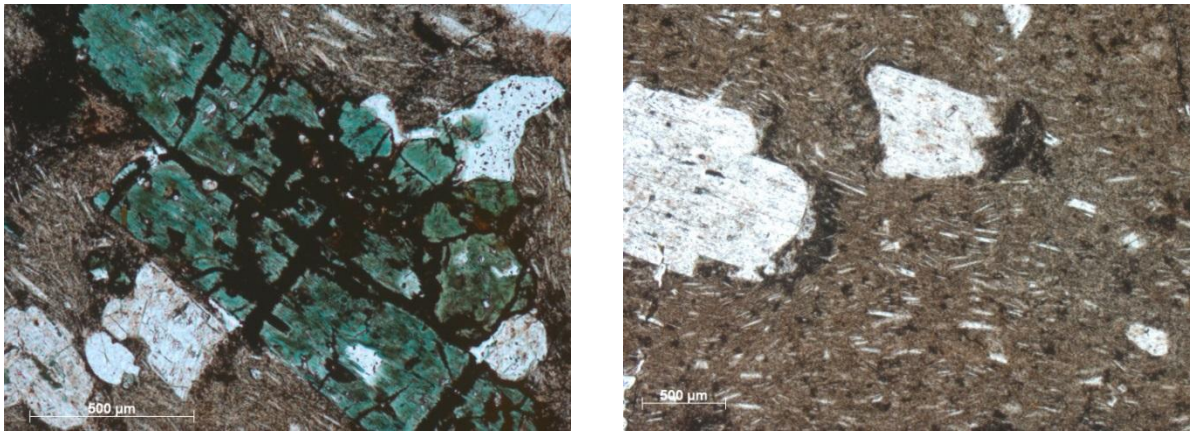

Figure 4.125: Thin sections of the sample 28A: a) Inosilicate altered into chlorite in the section cut parallel to the stratification; b) micro-crystalline groundmass, made up by small iso-oriented plagioclases, in the section cut perpendicular to the stratification. The scale is on the pictures.

4.5.21 Gruppo Vulcanico Atesino – Fm Castelliere ICT (29A)

This acidic volcanoclastic rock is formed by large grains (50%) and micro-crystalline groundmass (50%) (Fig. 4.126). Grains are made up by: plagioclase, alkali feldspars, quartz, biotite and opaque minerals.
No significative compositional differences between the perpendicular and parallel thin sections are found.

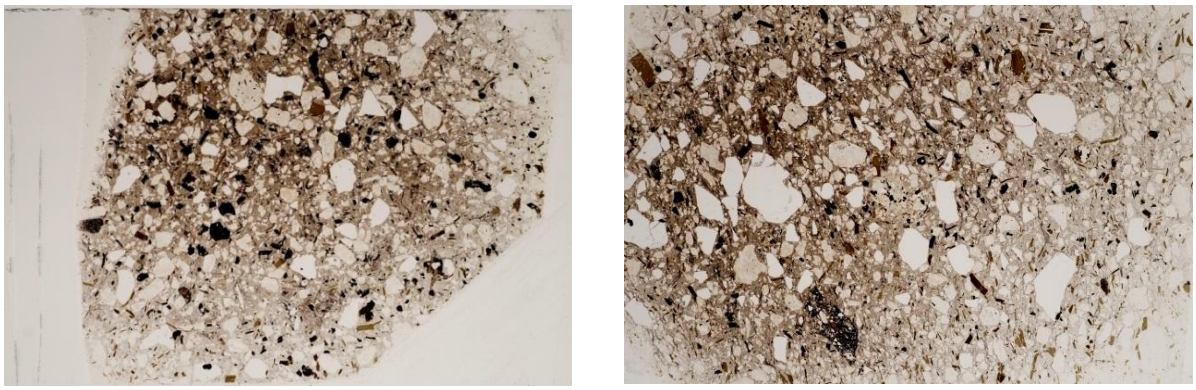

Figure 4.126: Thin sections of the sample 29A: a) section cut parallel to the stratification; b) section cut perpendicular to the stratification. Vertical side: 25 mm.

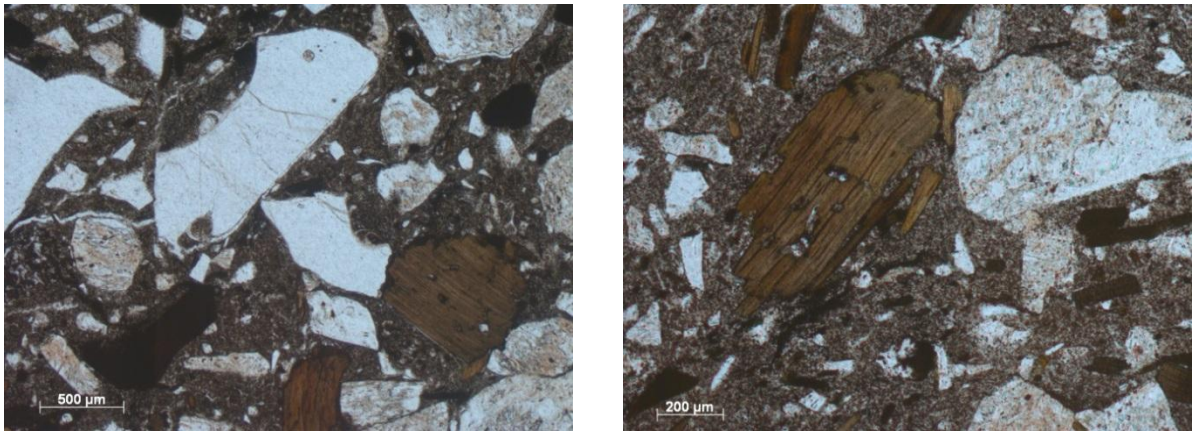

Figure 4.127: Thin sections of the sample 29A: a) section cut parallel to the stratification; b) section cut perpendicular to the stratification. The scale is on the pictures.

5. Results

There were analyzed 4 dolomites, 12 limestones, 4 volcanic rocks and 1 metamorphic (phyllite) rock. For every sample 2 measures of thermal properties were taken, one for each flat surface, where possible.

5.1 Density and porosity

In Table 5.1 are shown the measured values of apparent density and open porosity averaged for the three samples of each lithology. There were used three samples for each lithology to measure density and porosity. For unconsolidated sediments it was not possible to measure density and porosity.

Table 5.1: Values of apparent density and open porosity for the sampled lithologies.

Formation	Lithology	Code	Apparent density (g/cm^3)	Open porosity	Average apparent density (g/cm^3)	Average open porosity
Dolomia Principale	Dolomite	12A-1	2,783	2,19	2,768	2,40
		12A-2	2,773	2,26		
		12A-3	2,749	2,75		
Gruppo dei calcari grigi - Formazione di Rotzo	Limestone	16A-1	2,746	0,48	2,769	0,63
		16A-2	2,793	0,86		
		16A-3	2,768	0,55		
Scaglia Rossa	Limestone	14A-1	2,532	6,47	2,537	6,28
		14A-2	2,538	6,22		
		14A-3	2,540	6,14		
Formazione di Chiusole	micritic limestone	24A-1	2,615	1,88	2,621	2,03
		24A-2	2,626	2,00		
		24A-3	2,621	2,21		
Gruppo dei calcari grigi - Formazione di Monte Zugna	Limestone	8A-1	2,699	0,35	2,850	0,49
		8A-2	2,700	0,53		
		8A-3	3,151	0,59		
Rosso Ammonitico veronese	Limestone	17A-1	2,680	0,99	2,681	0,99
		17A-2	2,682	0,95		
		17A-3	2,682	1,04		
Gruppo vulcanico atesino - Formazione di Ora	Rhyolite	18A-1	2,542	4,11	2,539	4,17
		18A-2	2,537	4,28		
		18A-3	2,538	4,12		
Formazione di Werfen - Membri di Tesero e Mazzin	Calcarenite	4B-1	2,621	3,34	2,631	3,00
		4B-2	2,637	2,80		
		4B-3	2,635	2,85		
	Marly	5A-1	2,527	10,26	2,532	10,26

	limestone	5A-2	2,525	10,51		
		5A-3	2,544	10,01		
	Micritic limestone	6A-1	2,695	0,39	2,698	0,34
		6A-2	2,699	0,33		
		6A-3	2,699	0,31		
	Micritic limestone	6C-1	2,698	0,49	2,697	0,47
		6C-2	2,694	0,46		
		6C-3	2,698	0,46		
Formazione di Giovo - Membro del Monte Ozol	Dolomite	26A-1	2,829	0,49	2,833	0,38
		26A-2	2,838	0,32		
		26A-3	2,831	0,33		
Formazione del Contrin	Dolomite	19A-1	2,803	1,58	2,799	1,67
		19A-2	2,794	1,75		
Calcare di Nago	Limestone	23A-1	2,677	1,08	2,677	1,11
		23A-2	2,674	1,19		
		23A-3	2,679	1,05		
Formazione dello Scillar	Dolomite	20A-1	2,785	1,90	2,793	1,69
		20A-2	2,801	1,43		
		20A-3	2,794	1,73		
Calcare di Malcesine	Calcarenite	22A-1	2,619	2,70	2,640	1,98
		22A-2	2,662	1,18		
		22A-3	2,640	2,07		
Filoni a quarzo e calcite	Volcanoclastic rock	2A-1	2,245	15,89	2,265	14,88
		2A-2	2,265	14,70		
		2A-3	2,284	14,06		
Calcare di Malcesine	Calcarenite	15B-1	2,590	4,02	2,593	3,89
		15B-2	2,589	4,04		
		15B-3	2,601	3,61		
Unità della Valsugana - Filladi	Phyllite	10A-1	2,776	0,81	2,780	0,81
		10A-2	2,783	0,81		
Gruppo vulcanico atesino - Formazione di Buss	Andesite	28A-1	2,613	2,57	2,611	2,41
		28A-2	2,602	2,52		
		28A-3	2,617	2,15		
Gruppo vulcanico atesino - Formazione del Castelliere	Riodacite	29A-1	2,475	7,56	2,483	7,28
		29A-2	2,484	7,19		
		29A-3	2,489	7,10		

Density in all lithologies has a small variation; in fact it ranges from the minimum of 2,265 g/cm^3 of volcanoclastic rock to the maximum of 2,85 g/cm^3 of limestone of M. Zugna Formation. Even within the single rock the variability is very low, affecting only the second decimal.

Instead, porosity shows a great variability in rock samples, ranging from 0,34% for micritic

limestone (Werfen formation) to 14,88% of volcanoclastic rock.

In Table 5.2 are shown the values of density and porosity averaged for rock type (limestone, dolomite, volcanic and metamorphic). Dolomite and limestone have the highest values (metamorphic it is less representative) of density, volcanic the lowest. Porosity values are more heterogeneous, with the highest values for volcanic rock (7,19%) and the lowest for metamorphic rocks (0,81).

Table 5.2: Values of apparent density and open porosity for the different rock types.

Lithology	Code	ρ (g/cm3)		Φ (%)	
		Sample value	Mean Value	Sample value	Mean Value
Dolomite	12A	2,77	2,80	2,40	1,54
	26A	2,83		0,38	
	19A	2,80		1,67	
	20A	2,79		1,69	
Limestone	5A	2,53	2,66	10,26	2,62
	6A	2,70		0,34	
	6C	2,70		0,47	
	23A	2,68		1,11	
	16A	2,77		0,63	
	14A	2,54		6,28	
	24A	2,62		2,03	
	8A	2,85		0,49	
	17A	2,68		0,99	
	4B	2,63		3,00	
	22A	2,64		1,98	
	15B	2,59		3,89	
Volcanic	2A	2,27	2,47	14,88	7,19
	28A	2,61		2,41	
	29A	2,48		7,28	
	18A	2,54		4,17	
Metamorphic	10A	2,78	2,78	0,81	0,81

5.2 Thermal properties

In the following tables are shown the values of the thermal properties of the rock and unconsolidated sediment samples: thermal conductivity, volumetric heat capacity and thermal diffusivity. Heat capacity is isotropic, so the values obtained in parallel and normal direction are averaged.

5.2.1 Rock thermal conductivity

For rocks are displayed, where possible, the values of parallel and normal thermal conductivity. For some samples it was not possible to measure both $\lambda_{parallel}$ and λ_{normal} because of the small size of the rock. The surface probe requires a circular area with minimum diameter of 6 cm, and some samples were too small to allow a correct measurement.

Table 5.3: values of parallel and normal thermal conductivity in dry and wet conditions for rock samples.

Code	Lithology	Formation	λ_{dry} (W/m K)		λ_{wet} (W/m K)	
			Parallel	Normal	Parallel	Normal
12A	dolomite	Dolomia Principale	3,34	-	4,76	-
16A	limestone	Gruppo dei calcari grigi - Formazione di Rotzo	2,65	2,88	3,23	3,14
14A	limestone	Scaglia Rossa	-	2,17	-	2,95
24A	Micritic limestone	Formazione di Chiusole	2,47	2,28	2,26	2,65
8A	limestone	Gruppo dei calcari grigi - Formazione di Monte Zugna	2,42	2,97	2,95	3,04
17A	limestone	Rosso Ammonitico veronese	2,91	2,78	3,22	3,02
18A	rhyolite	Gruppo vulcanico atesino - Formazione di Ora	2,17	2,17	2,49	2,48
4B	calcarenite	Formazione di Werfen - Membri di Tesero e Mazzin	2,42	-	2,60	-
5A	Marly limestone	Formazione di Werfen - Membri di Tesero e Mazzin	-	2,13	-	3,39
6A	Micritic limestone	Formazione di Werfen - Membri di Tesero e Mazzin	2,68	2,76	2,81	3,00
6C	Micritic limestone	Formazione di Werfen - Membri di Tesero e Mazzin	2,64	2,58	2,96	2,84
26A	dolomite	Formazione di Giovo - Membro del Monte Ozol	4,99	-	5,66	-
19A	dolomite	Formazione del Contrin	4,25	2,36	4,26	4,55
23A	limestone	Calcare di Nago	2,48	2,47	2,78	2,29
20A	dolomite	Formazione dello Scillar	3,82	3,70	4,09	4,39
22A	calcarenite	Calcare di Malcesine	2,54	2,40	2,90	2,53
2A	volcanoclastic rock	Filoni a quarzo e calcite	1,35	1,26	1,97	2,01
15B	calcarenite	Calcare di Malcesine	2,36	2,32	2,12	2,69

10A	phyllite	Unità della Valsugana - Filladi	-	1,19	-	2,13
28A	andesite	Gruppo vulcanico atesino - Formazione di Buss	2,14	2,00	2,30	2,23
29A	riodacite	Gruppo vulcanico atesino - Formazione del Castelliere	1,76	-	2,17	-

The highest values of dry thermal conductivity are obtained for the dolomite (26A) of Giovo Formation (4,99 W/m K, parallel), the smaller ones for Phyllites (10A) of Valsugana unit (1,19 W/m K, normal).
In wet conditions, the highest values are obtained for the dolomite (26A) of Giovo Formation (5,66 W/m K, parallel), the smaller ones for the volcanoclastic rock (2A) (1,99 W/m K, normal).

In Table 5.4 are shown the values of dry and wet thermal conductivity (both parallel and normal) averaged for rock type (limestone, dolomite, volcanic and metamorphic). Dolomites have the highest values (around 4 W/m K, both parallel and normal), volcanic rocks the lowest (about 1,8 W/m K in dry conditions, about 2,2 W/m K in wet conditions).

Table 5.4: values of parallel and normal thermal conductivity in dry and wet conditions for each lithology.

Lithology	Code	$\lambda_{dry\_parallel}$ (W/m K)		λ_{dry_normal} (W/m K)		$\lambda_{wet\_parallel}$ (W/m K)		λ_{wet_normal} (W/m K)	
		Sample value	Mean Value	Sample value	Mean Value	Sample value	Mean Value	Sample value	Mean Value
Dolomite	12A	3,34	4,10	-	3,03	4,76	4,69	-	4,47
	26A	4,99		-		5,66		-	
	19A	4,25		2,36		4,26		4,55	
	20A	3,82		3,70		4,09		4,39	
Limestone	5A	-	2,56	2,13	2,52	-	2,78	3,39	2,87
	6A	2,68		2,76		2,81		3,00	
	6C	2,64		2,58		2,96		2,84	
	23A	2,48		2,47		2,78		2,29	
	16A	2,65		2,88		3,23		3,14	
	14A	-		2,17		-		2,95	
	24A	2,47		2,28		2,26		2,65	
	8A	2,42		2,97		2,95		3,04	
	17A	2,91		2,79		3,22		3,02	
	4B	2,46		-		2,60		-	
	22A	2,54		2,40		2,90		2,53	
	15B	2,36		2,32		2,12		2,69	
Volcanic	2A	1,35	1,86	1,26	1,81	1,97	2,23	2,01	2,24
	28A	2,14		2,00		2,30		2,23	
	29A	1,76		-		2,17		-	
	18A	2,17		2,17		2,49		2,48	
Metamorphic	10A	-	-	1,19	1,19	-	-	2,13	2,13

In Figures 5.1, 5.2, 5.3 and 5.4 are shown the boxplots of dry parallel, dry normal, wet parallel and wet normal thermal conductivity for dolomites, limestones, volcanic and metamorphic rocks. Dolomites, that show a great variability in dry conditions, for λ_{normal} in wet conditions have values very similar, while limestones, despite the great number of samples, show a small variability.

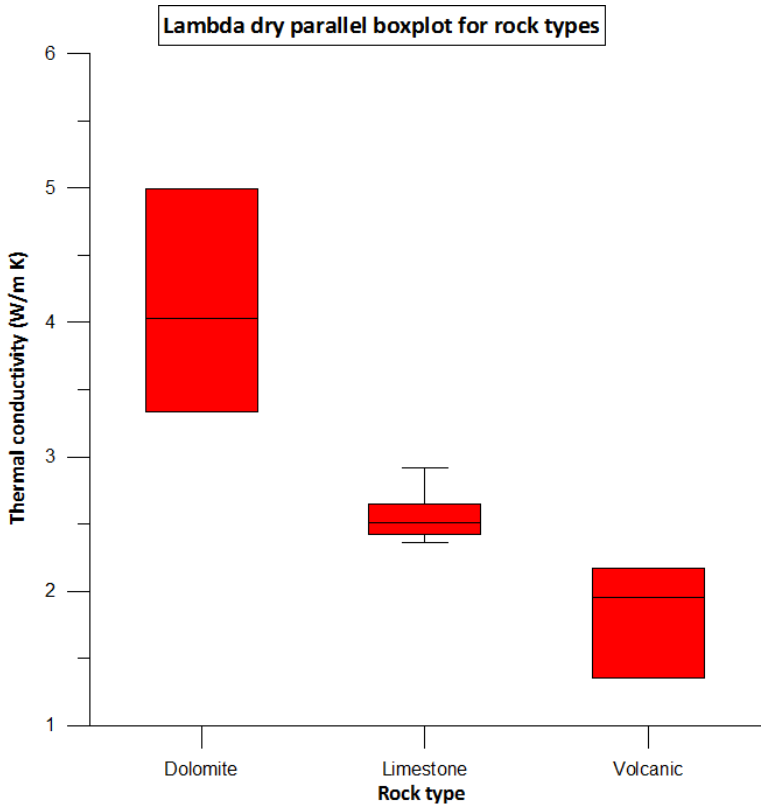

Figure 5.1: boxplot of parallel thermal conductivity in dry conditions for rock types.

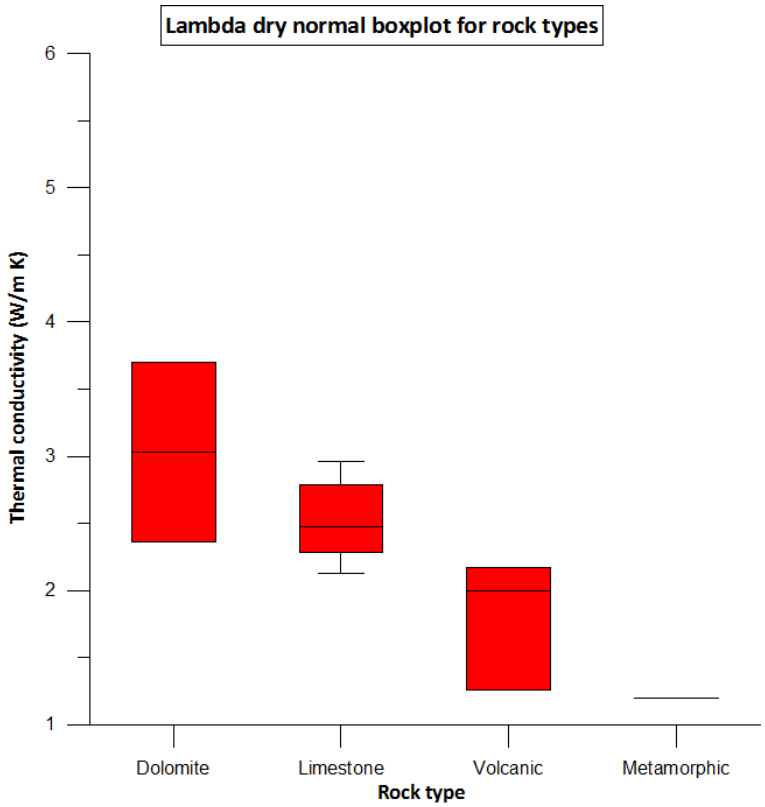

Figure 5.2: boxplot of normal thermal conductivity in dry conditions for rock types.

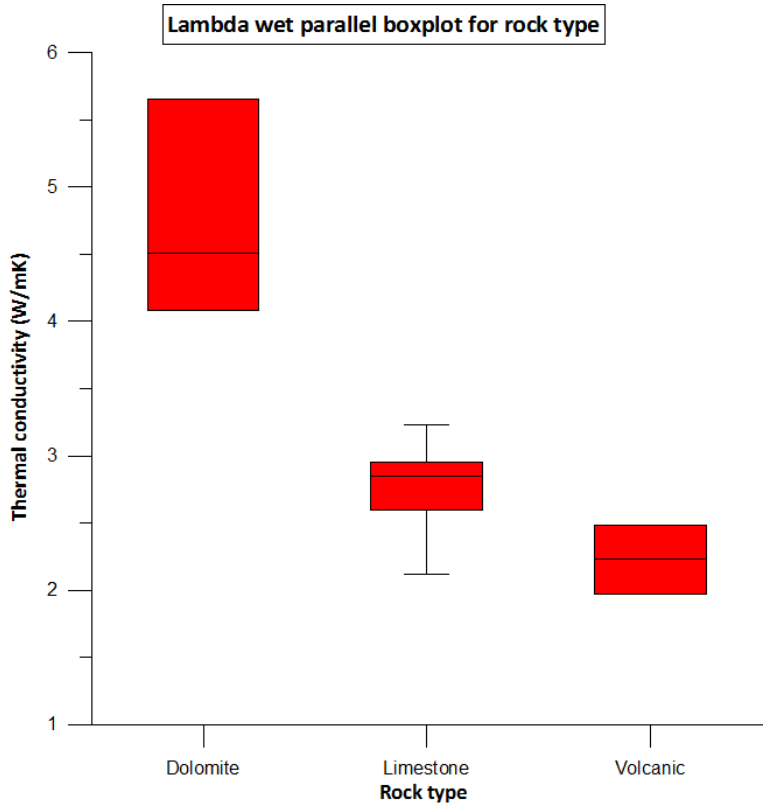

Figure 5.3: boxplot of parallel thermal conductivity in wet conditions for rock types.

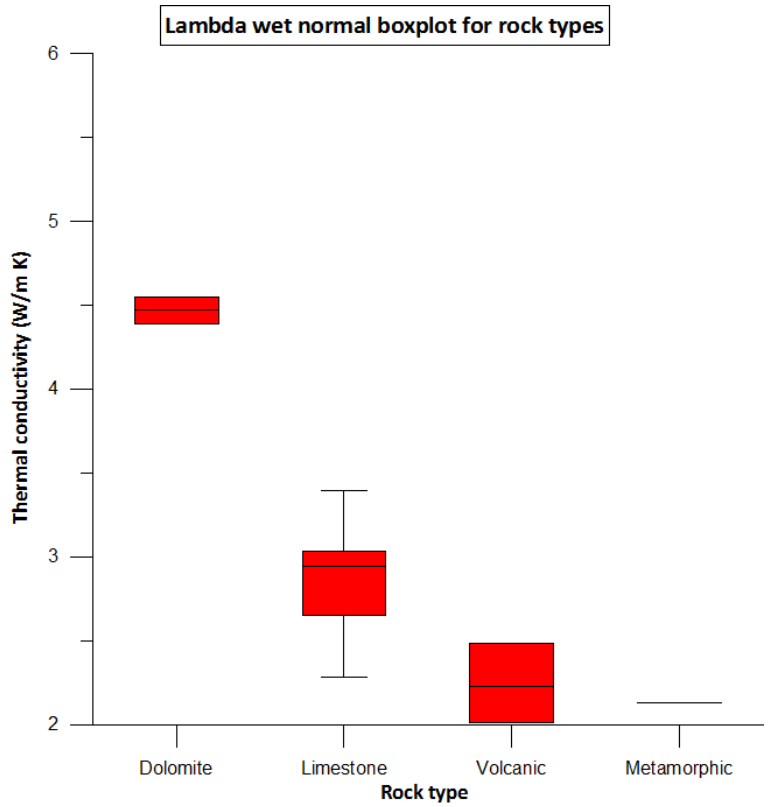

Figure 5.4: boxplot of normal thermal conductivity in wet conditions for rock types.

In Tables 5.5 and 5.6 are shown the values of thermal conductivity in dry and wet conditions obtained via literature search. The search was done on about 20 authors; only values of rocks of the similar lithology of collected samples were selected, narrowing to 9 authors. As a consequence, the number of values is limited especially for volcanic and metamorphic rock, but it can be expanded. The values are aggregated into the four rock types as done with measured data (Barry-Macaulay et al., 2013; Alishaev et al., 2012; Gomes et al., 2005; Gunn et al., 2005; Lee et al., 1998; Jones, 2003; Witte et al., 2002; Diao et al., 2004; Gangyan, 2003). There were found literature values for rocks both in wet and dry conditions.

Table 5.5: values of thermal conductivity in dry conditions for each lithology from bibliographic research.

Lithology	λ_dry (W/m K)	
	Sample value	Mean Value
Dolomite	3,14	3,92
	2,28	
	4,71	
	4,61	
	4,85	
Limestone	1,94	2,63
	1,63	
	3,33	
	3,33	
	3,53	

	2,33	
	2,49	
	2,85	
	2,27	
	2,89	
	2,30	
Volcanic	2,90	2,90
Metamorphic	1,90	2,26
	2,61	

Table 5.6: values of thermal conductivity in wet conditions for each lithology from bibliographic research.

Lithology	**λ_wet (W/m K)**	
	Sample value	**Mean Value**
Dolomite	5,10	4,52
	2,45	
	5,18	
	5,34	
Limestone	3,56	3,00
	3,68	
	3,71	
	2,55	
	2,63	
	2,90	
	2,49	
	2,94	
	2,53	
Volcanic	3,53	3,53
Metamorphic	-	-

For dolomites the bibliographic values ranges (2,28 – 4,81 W/m K dry, 2,45 – 5,34 W/m K wet) are similar to measured values ranges (2,36 – 4,99 W/m K dry, 4,09 – 5,66 W/m K wet), and also the mean correspond. The presence of values of thermal conductivity both in bibliographic and measured values around 2 W/m K, that is quite low for a dolomite, is probably due to dolomites with other minerals with lower λ.

For limestones the bibliographic values ranges (1,63 – 3,53 W/m K dry, 2,49 – 3,71 W/m K wet) are greater than measured values ranges (2,13 – 2,97 W/m K dry, 2,12 – 3,39 W/m K wet), although the mean is very close. This is due to the fact that limestones from literature are from different countries and different geological ages, while the sampled limestones are all from Jurassic/Cretaceous period and therefore have quite the same compression rate.

For volcanic and metamorphic rock there are not enough data to make a proper comparison, but it can be seen that literature and measured values are similar.

5.2.2 Rock volumetric heat capacity

The highest values of volumetric heat capacity in dry conditions are obtained for the dolomite (26A) of Giovo Formation (2,37 10^{-6} J/m^{3}K), the smaller ones for Phyllites (10A) of Valsugana unit (1,3472 10^{-6} J/m^{3}K).
In wet conditions, the highest values are obtained for the dolomite (26A) of Giovo Formation (2,93 10^{-6} J/m^{3}K), the smaller ones for Phyllites (10A) of Valsugana unit (1,43 10^{-6} J/m^{3}K).

Table 5.7: values of averaged volumetric heat capacity in dry and wet conditions for rock samples.

Code	Lithology	Formation	$c_{p,dry}$ 10^{-6} (J/m^3 K)	$c_{p,wet}$ 10^{-6} (J/m^3 K)
12A	dolomite	Dolomia Principale	2,03	2,50
16A	limestone	Gruppo dei calcari grigi - Formazione di Rotzo	2,12	2,35
14A	limestone	Scaglia Rossa	1,86	2,48
24A	Micritic limestone	Formazione di Chiusole	2,09	2,17
8A	limestone	Gruppo dei calcari grigi - Formazione di Monte Zugna	2,03	2,16
17A	limestone	Rosso Ammonitico veronese	2,15	2,44
18A	rhyolite	Gruppo vulcanico atesino - Formazione di Ora	1,94	2,16
4B	calcarenite	Formazione di Werfen - Membri di Tesero e Mazzin	2,17	2,50
5A	Marly limestone	Formazione di Werfen - Membri di Tesero e Mazzin	1,92	2,66
6A	Micritic limestone	Formazione di Werfen - Membri di Tesero e Mazzin	2,13	2,32
6C	Micritic limestone	Formazione di Werfen - Membri di Tesero e Mazzin	2,01	2,12
26A	dolomite	Formazione di Giovo - Membro del Monte Ozol	2,37	2,93
19A	dolomite	Formazione del Contrin	1,97	2,14
23A	limestone	Calcare di Nago	2,09	2,00
20A	dolomite	Formazione dello Scillar	2,33	2,69
22A	calcarenite	Calcare di Malcesine	2,09	2,29
2A	volcanoclastic rock	Filoni a quarzo e calcite	1,68	1,88
15B	limestone	Calcare di Malcesine	2,10	2,00
10A	phyllite	Unità della Valsugana - Filladi	1,35	1,43
28A	andesite	Gruppo vulcanico atesino - Formazione di Buss	2,02	2,25
29A	riodacite	Gruppo vulcanico atesino - Formazione del Castelliere	1,85	2,12

In Table 5.8 are shown the values of dry and wet volumetric heat capacity averaged for rock

type (limestone, dolomite, volcanic and metamorphic). Dolomites have the highest values (around 2,2 10^{-6} W/m K in dry conditions and 2,6 10^{-6} W/m K in wet conditions), metamorphic rocks the lowest (1,35-1,43 10^{-6} W/m K).

Table 5.8: values of averaged volumetric heat capacity in dry and wet conditions for lithology.

Lithology	Code	cp_dry 10^-6 (J/m3 K)		cp_wet 10^-6 (J/m3 K)	
		Sample value	Mean Value	Sample value	Mean Value
Dolomite	12A	2,03	2,18	2,50	2,57
	26A	2,37		2,93	
	19A	1,97		2,14	
	20A	2,33		2,69	
Limestone	5A	1,92	2,06	2,66	2,29
	6A	2,13		2,32	
	6C	2,01		2,12	
	23A	2,09		2,00	
	16A	2,12		2,35	
	14A	1,86		2,48	
	24A	2,09		2,17	
	8A	2,03		2,16	
	17A	2,15		2,44	
	4B	2,17		2,50	
	22A	2,09		2,29	
	15B	2,10		2,00	
Volcanic	2A	1,68	1,88	1,88	2,10
	28A	2,02		2,25	
	29A	1,85		2,12	
	18A	1,94		2,16	
Metamorphic	10A	1,35	1,35	1,43	1,43

In Figures 5.5 and 5.6 are shown the boxplots of dry and wet volumetric heat capacity for dolomites, limestones, volcanic and metamorphic rocks. Dolomites show a great variability, while limestones tend to have very similar values.

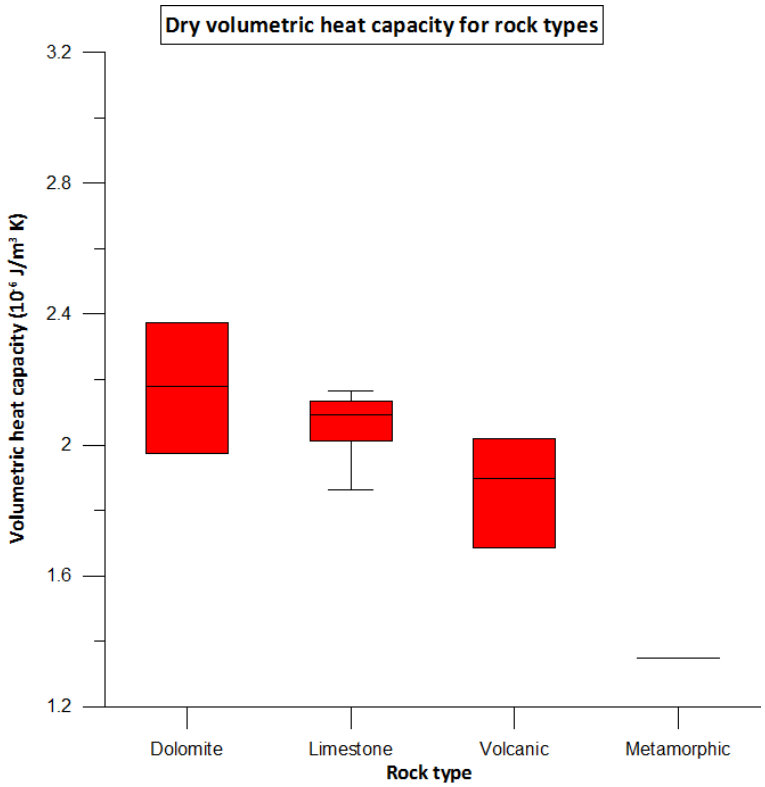

Figure 5.5: boxplot of volumetric heat capacity in dry conditions for rock types.

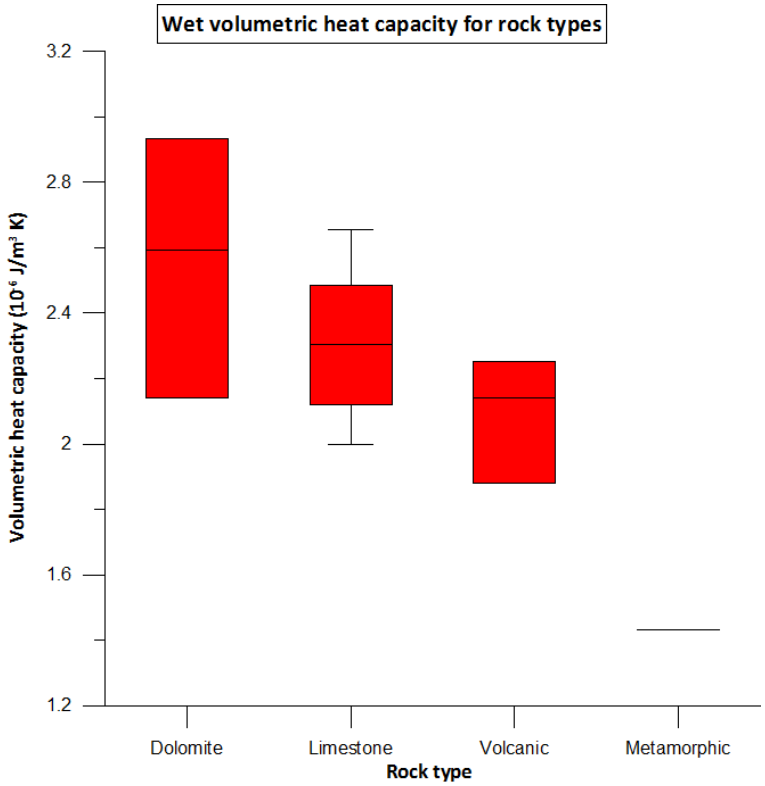

Figure 5.6: boxplot of volumetric heat capacity in dry conditions for rock types.

5.2.3 Rock thermal diffusivity

The highest values of thermal diffusivity in dry conditions are obtained for the dolomite (26A) of Giovo Formation (2,11 10^6 m^2/s), the smaller ones for Phyllites (10A) of Valsugana unit (0,89 10^6 m^2/s).
In wet conditions, the highest values are obtained for the dolomite (19A) of Contrin Formation (2,09 10^6 m^2/s), the smaller ones for andesite (28A) of Buss Formation (1,00 10^6 m^2/s).

Table 5.9: values of parallel and normal thermal diffusivity in dry and wet conditions for rock samples.

Code	Lithology	Formation	κ_{dry} 10^6 (m^2/s)		κ_{wet} 10^6 (m^2/s)	
			Parallel	Normal	Parallel	Normal
12A	dolomite	Dolomia Principale	1,65	-	1,91	-
16A	limestone	Gruppo dei calcari grigi - Formazione di Rotzo	1,31	1,30	1,38	1,33
14A	limestone	Scaglia Rossa	-	1,17	1,19	-
24A	Micritic limestone	Formazione di Chiusole	1,13	1,14	1,20	1,08
8A	limestone	Gruppo dei calcari grigi - Formazione di Monte Zugna	1,35	1,31	1,41	1,36
17A	limestone	Rosso Ammonitico veronese	1,30	1,35	1,22	1,34
18A	rhyolite	Gruppo vulcanico atesino - Formazione di Ora	1,10	1,13	1,24	1,26
4B	calcarenite	Formazione di Werfen - Membri di Tesero e Mazzin	1,12	-	1,04	-
5A	Marly limestone	Formazione di Werfen - Membri di Tesero e Mazzin	-	1,11	1,28	-
6A	Micritic limestone	Formazione di Werfen - Membri di Tesero e Mazzin	1,28	1,27	1,28	1,22
6C	Micritic limestone	Formazione di Werfen - Membri di Tesero e Mazzin	1,31	1,28	1,34	1,40
26A	dolomite	Formazione di Giovo - Membro del Monte Ozol	2,11	-	1,93	-
19A	dolomite	Formazione del Contrin	1,76	1,53	2,02	2,09
23A	limestone	Calcare di Nago	1,19	1,19	1,26	1,27
20A	dolomite	Formazione dello Scillar	1,61	1,62	1,70	1,48
22A	calcarenite	Calcare di Malcesine	1,12	1,24	1,22	1,15
2A	volcanoclastic rock	Filoni a quarzo e calcite	0,79	0,76	1,11	1,01
15B	calcarenite	Calcare di Malcesine	1,13	1,09	1,20	1,20

10A	phyllite	Unità della Valsugana - Filladi	-	0,89	1,49	-
28A	andesite	Gruppo vulcanico atesino - Formazione di Buss	1,05	1,00	1,00	1,01
29A	riodacite	Gruppo vulcanico atesino - Formazione del Castelliere	0,95	-	1,02	-

In Table 5.10 are shown the values of dry and wet thermal diffusivity (both parallel and normal) averaged for rock type (limestone, dolomite, volcanic and metamorphic). Dolomites have the highest values (around 1,7 10^6 m^2/s), volcanic rocks the lowest (around 1 10^6 m^2/s).

Table 5.10: values of thermal diffusivity in wet conditions for rock samples.

Lithology	Code	$\kappa_{dry\_parallel}$ 10^6 (m^2/s)		κ_{dry_normal} 10^6 (m^2/s)		$\kappa_{wet\_parallel}$ 10^6 (m^2/s)		κ_{wet_normal} 10^6 (m^2/s)	
		Sample value	Mean Value	Sample value	Mean Value	Sample value	Mean Value	Sample value	Mean Value
Dolomite	12A	1,65	1,78	-	1,58	1,91	1,89	-	1,78
	26A	2,11		-		1,93		-	
	19A	1,76		1,53		2,02		2,09	
	20A	1,61		1,62		1,70		1,48	
Limestone	5A	-	1,22	1,11	1,22	1,28	1,25	-	1,26
	6A	1,28		1,27		1,28		1,22	
	6C	1,31		1,28		1,34		1,40	
	23A	1,19		1,19		1,26		1,27	
	16A	1,31		1,30		1,38		1,33	
	14A	-		1,17		1,19		-	
	24A	1,13		1,14		1,20		1,08	
	8A	1,35		1,31		1,41		1,36	
	17A	1,30		1,35		1,22		1,34	
	4B	1,12		-		1,04		-	
	22A	1,12		1,24		1,22		1,15	
	15B	1,13		1,09		1,20		1,20	
Volcanic	2A	0,79	0,97	0,76	0,96	1,11	1,09	1,01	1,09
	28A	1,05		1,00		1,00		1,01	
	29A	0,95		-		1,02		-	
	18A	1,10		1,13		1,24		1,26	
Metamorphic	10A	-	-	0,89	0,89	1,49	1,49	-	-

In Figures 5.7, 5.8, 5.9 and 5.10 are shown the boxplots of dry parallel, dry normal, wet parallel and wet normal thermal diffusivity for dolomites, limestones, volcanic and metamorphic rocks. It is remarkable to see that the dolomites and volcanic rocks have a wider range, while limestones remain more around the same value.

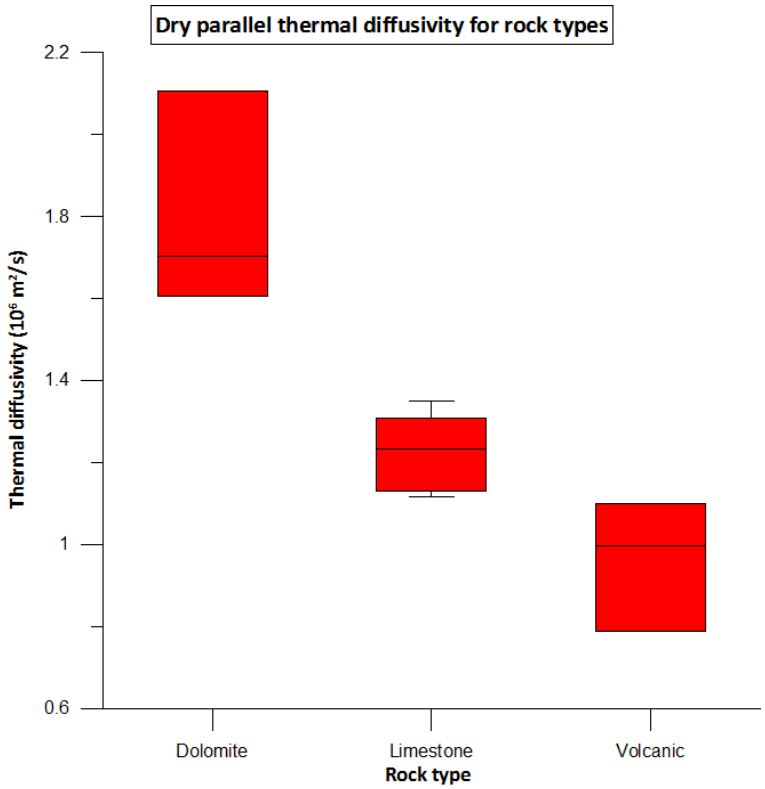

Figure 5.7: boxplot of parallel thermal diffusivity in dry conditions for rock types.

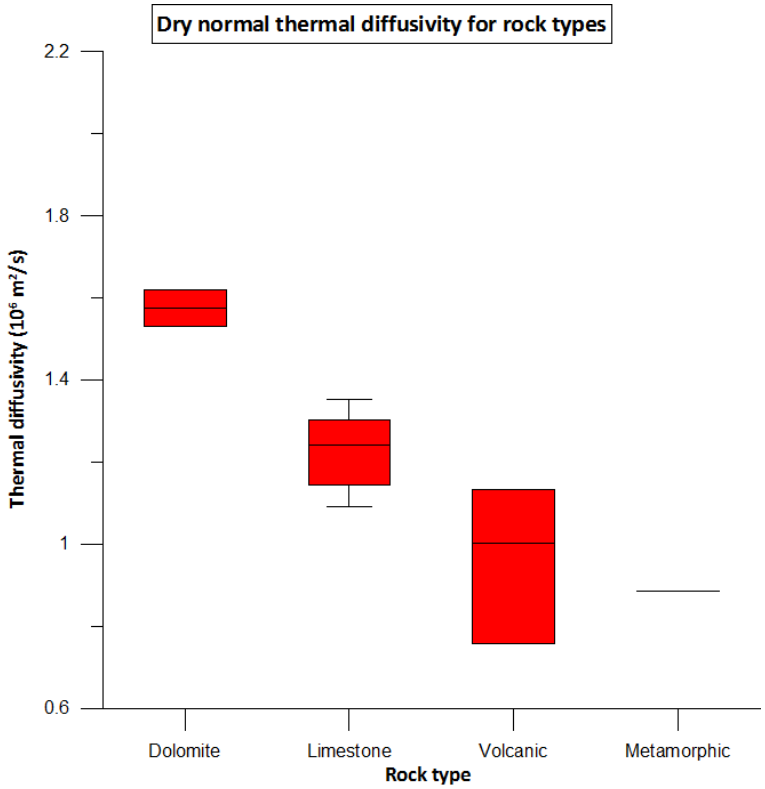

Figure 5.8: boxplot of normal thermal diffusivity in dry conditions for rock types.

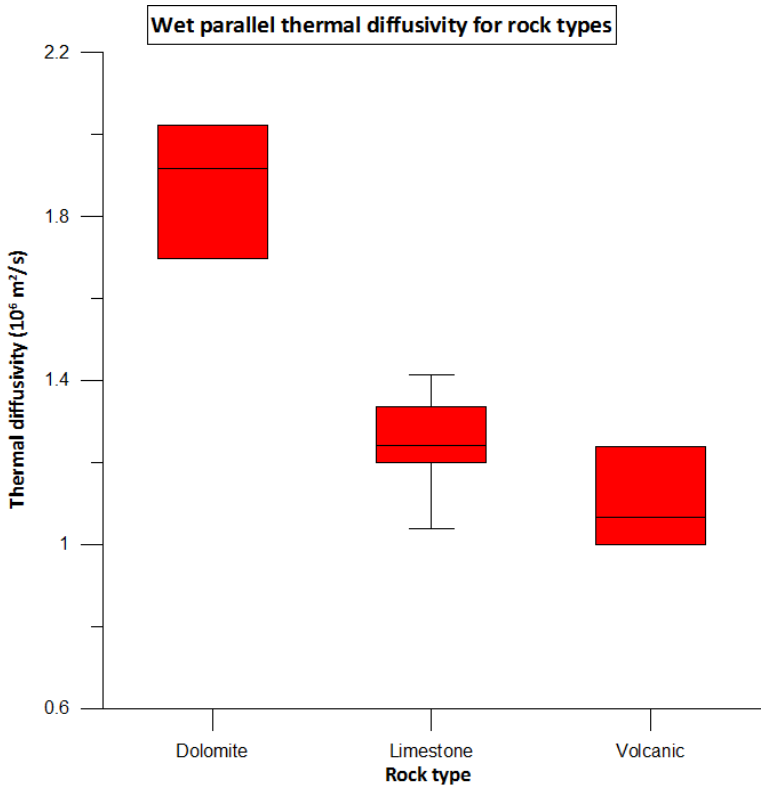

Figure 5.9: boxplot of parallel thermal diffusivity in wet conditions for rock types.

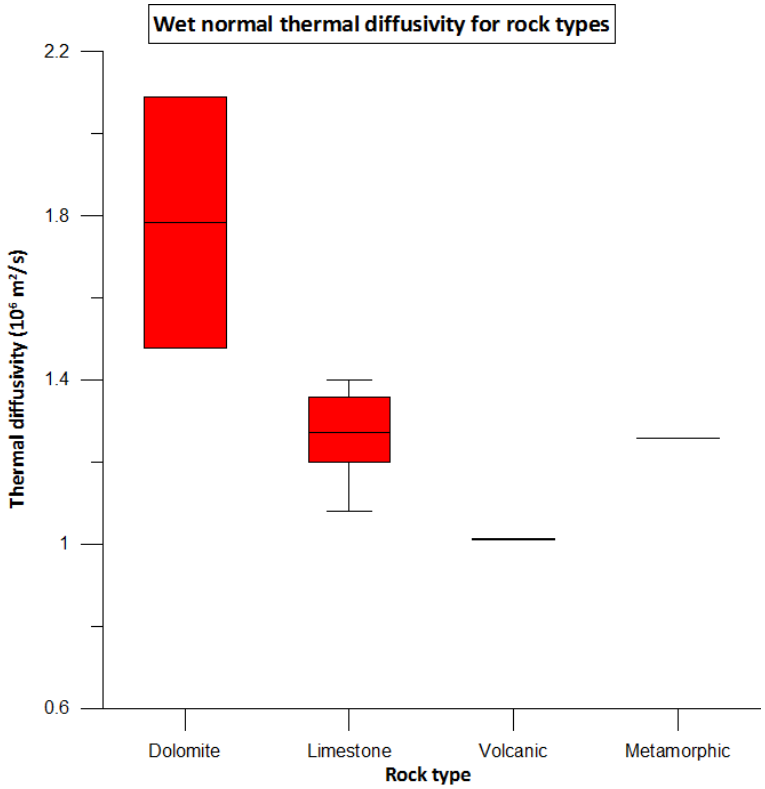

Figure 5.10: boxplot of normal thermal diffusivity in wet conditions for rock types.

5.2.4 Unconsolidated sediments

In Tables 5.11 and 5.12 are shown the values of thermal conductivity, volumetric heat capacity and thermal diffusivity for the unconsolidated sediments in dry and wet condition respectively.

The highest values of thermal conductivity in dry conditions are obtained for the silt and clay of glacial deposit (0,55 W/m K), the smallest for the silt and clay of debris/alluvial deposit (0,28 W/m K). See Table 4.2 for the description of the samples.
In wet conditions the highest values are obtained for the sand of landslide deposit (1,67 W/m K), the smallest for the silt and clay of debris/alluvial deposit (1,00 W/mK).

The highest values of volumetric heat capacity in dry conditions are obtained for the silt and clay of glacial deposit (1,54 10^{-6} J/m^3K), the smallest for the silt and clay of debris/alluvial deposit (1,46 10^{-6} J/m^3K).
In wet conditions the highest values are obtained for the sand of landslide deposit (2,20 10^{-6} J/m^3K), the smallest for the silt and clay of debris/alluvial deposit (1,94 10^{-6} J/m^3K).

The highest values of thermal diffusivity in dry conditions are obtained for the silt and clay of glacial deposit (0,36 m^2/s), the smallest for the silt and clay of debris/alluvial deposit (0,19 10^6 m^2/s).
In wet conditions the highest values are obtained for the sand of debris/alluvial fan (0,76 10^6 m^2/s), the smallest for the sand of alluvial/fluvioglacial deposit (0,51 10^6 m^2/s).

Table 5.11: values of thermal properties in dry conditions for unconsolidated sediments.

Code	Formation	Description	λ_{dry} (W/m K)	c_{p_dry} 10^{-6} (J/m^3 kg)	κ_{dry} 10^6 (m^2/s)
10B	Glacial deposit	Silt and clay	0,55	1,54	0,36
20B	Alluvional/fluvioglacial deposit	Sand	0,38	1,51	0,25
27A	Landslide deposit	Sand	0,34	1,51	0,23
6D	Slope deposit	Sand	0,40	1,48	0,27
25A	Alluvial/fluvioglacial fan	Sand	0,31	1,49	0,21
21A	Mixed fan: debris flow and alluvial	Sand	0,46	1,49	0,31
31A	Mixed deposit: debris and alluvial	Silt and clay	0,28	1,46	0,19
13A	Colluvial deposit	Silt and clay	0,46	1,50	0,31

Table 5.12: values of thermal properties in wet conditions for unconsolidated sediments.

Code	Formation	Description	λ_{wet} (W/m K)	c_{p_wet} 10^{-6} (J/m^3 kg)	κ_{wet} 10^6 (m^2/s)
10B	Glacial deposit	Silt and clay	1,48	2,16	0,69
20B	Alluvional/fluvioglacial deposit	Sand	1,05	2,05	0,51
27A	Landslide deposit	Sand	1,59	2,13	0,75
6D	Slope deposit	Sand	1,35	2,12	0,64

25A	Alluvial/fluvioglacial fan	Sand	1,07	2,02	0,53
21A	Mixed fan: debris flow and alluvial	Sand	1,67	2,20	0,76
31A	Mixed deposit: debris and alluvial	Silt and clay	1,00	1,94	0,52
13A	Colluvial deposit	Silt and clay	1,28	2,05	0,63

In Tables 5.13 and 5.14 are shown the values of dry and wet thermal diffusivity, volumetric heat capacity and thermal diffusivity averaged for soil type (sands, silt and clay). Sand and silt and clay have similar mean values of all thermal properties both in dry and wet conditions. This is due to the strong influence of saturating fluids in porous medium as soils are, assuming that they all have quite the same mineralogical composition. Water, for example, with its thermal conductivity value of 0,6 W/m K, makes that the values of thermal conductivity are bigger than 1 W/m K.

Table 5.13: values of thermal properties in dry conditions for unconsolidated sediments typologies.

Lithology	Code	λ_{dry} (W/m K)		cp_{dry} 10^{-6} (J/m^3 K)		κ_{dry} 10^{6} (m^2/s)	
		Measured value	Mean value	Measured value	Mean value	Measured value	Mean value
Sand	20B	0,38	0,38	1,51	1,50	0,25	0,25
	27A	0,34		1,51		0,23	
	6D	0,40		1,48		0,27	
	25A	0,31		1,49		0,21	
	21A	0,46		1,49		0,31	
Silt and clay	31A	0,28	0,43	1,46	1,50	0,19	0,29
	13A	0,46		1,50		0,31	
	10B	0,55		1,54		0,36	

Table 5.14: values of thermal properties in wet conditions for unconsolidated sediments typologies.

Lithology	Code	λ_{wet} (W/m K)		cp_{wet} 10^{-6} (J/m^3 K)		κ_{wet} 10^{6} (m^2/s)	
		Measured value	Mean value	Measured value	Mean value	Measured value	Mean value
Sand	20B	1,05	1,35	2,05	2,10	0,51	0,64
	27A	1,59		2,13		0,75	
	6D	1,35		2,12		0,64	
	25A	1,07		2,02		0,53	
	21A	1,67		2,20		0,76	
Silt and clay	31A	1,00	1,26	1,94	2,05	0,52	0,61
	13A	1,28		2,05		0,63	
	10B	1,48		2,16		0,69	

In Figures 5.11, 5.12, 5.13, 5.14, 5.15 and 5.16 are shown the boxplots of dry and wet thermal conductivity, volumetric heat capacity and thermal diffusivity for sands, and silts and clays. Generally all thermal properties are more dispersed for each soil type in wet condition compared to dry conditions.

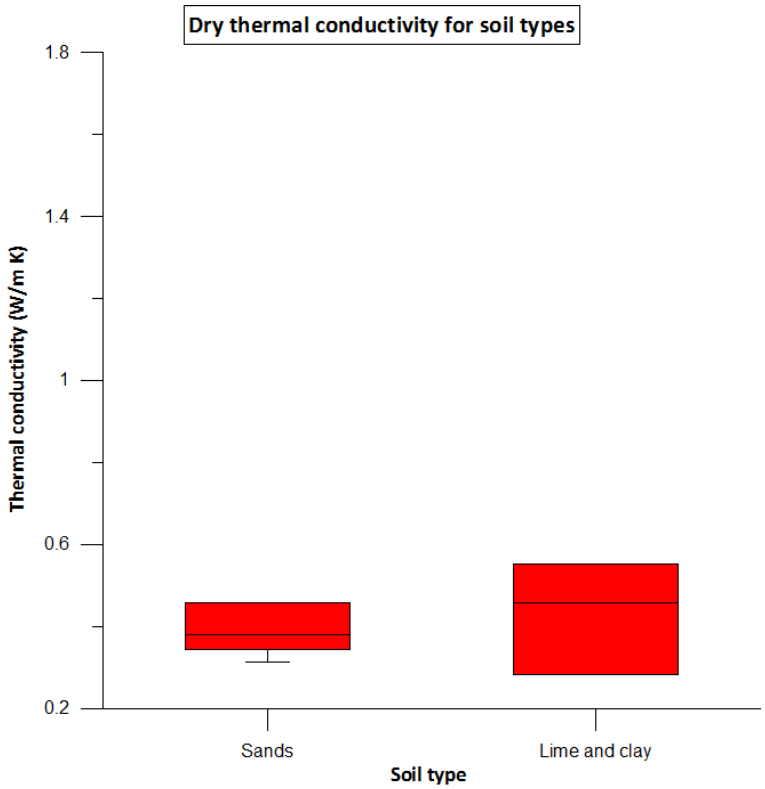

Figure 5.11: boxplot of thermal conductivity in dry conditions for soil types.

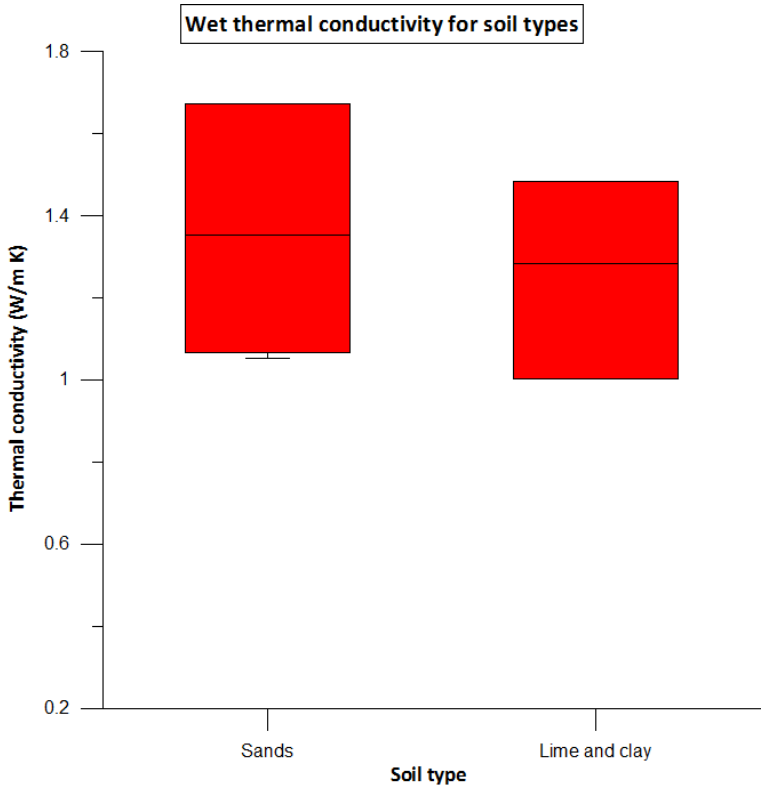

Figure 5.12: boxplot of thermal conductivity in wet conditions for soil types.

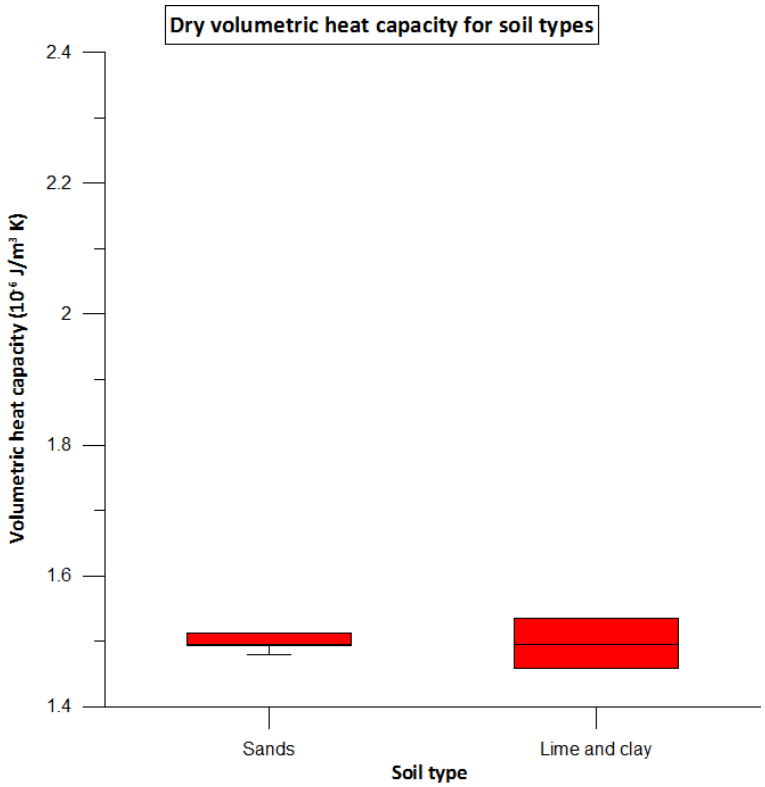

Figure 5.13: boxplot of volumetric heat capacity in dry conditions for soil types.

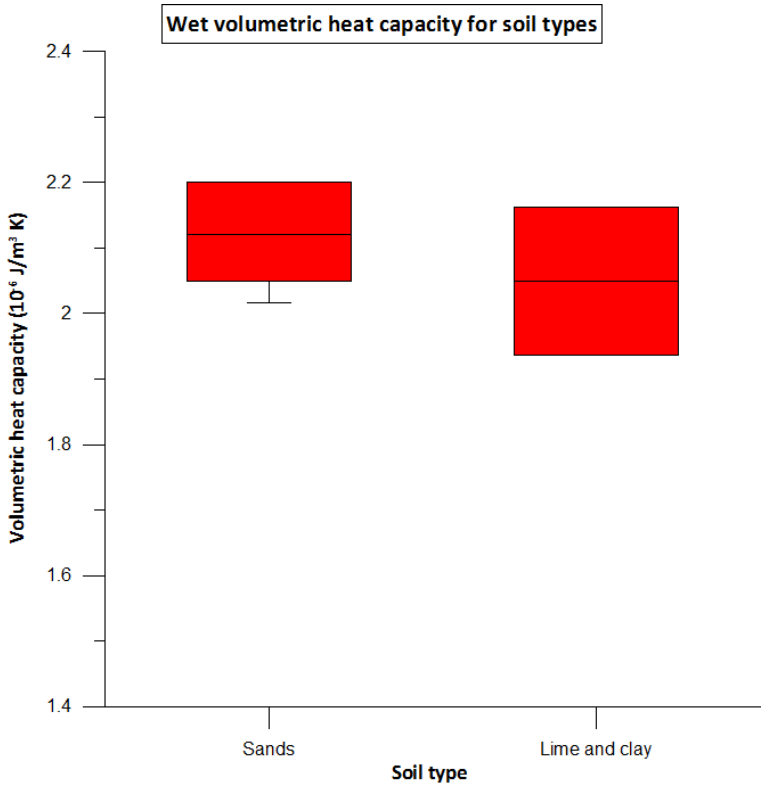

Figure 5.14: boxplot of volumetric heat capacity in wet conditions for soil types.

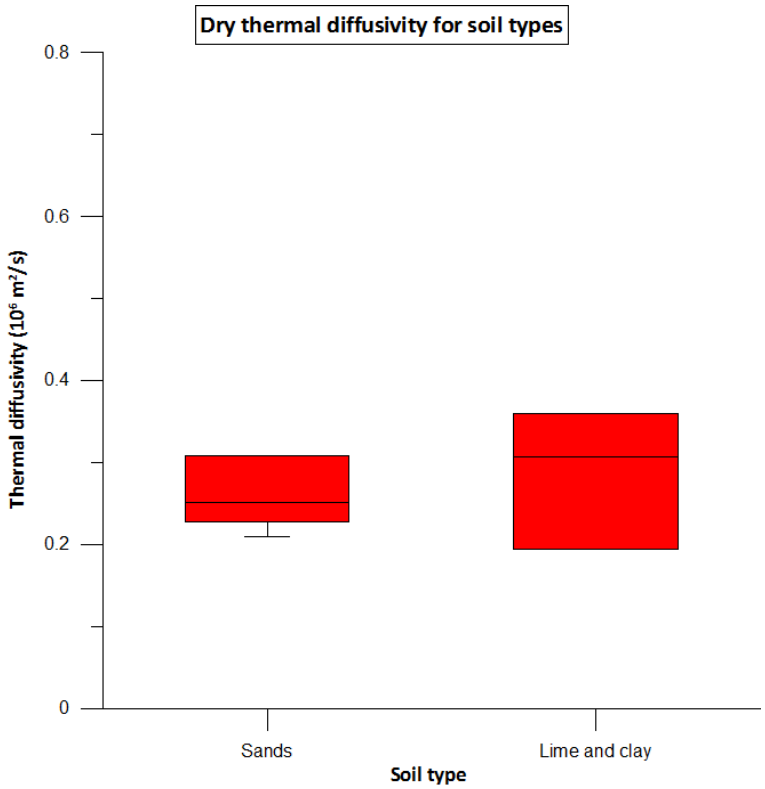

Figure 5.15: boxplot of thermal diffusivity in dry conditions for soil types.

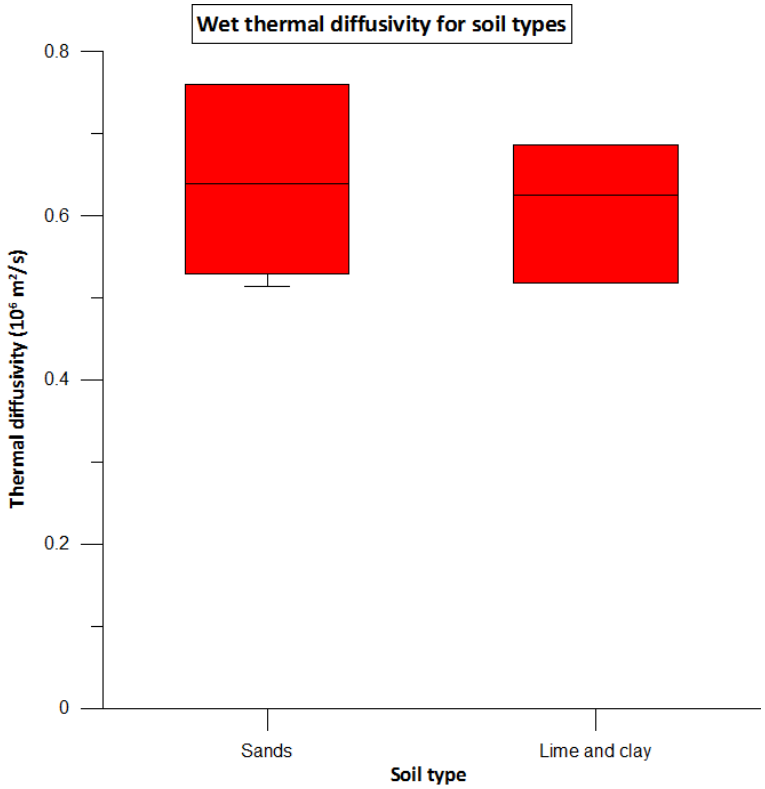

Figure 5.16: boxplot of thermal diffusivity in wet conditions for soil types.

6. Data discussion

Data collected on the thermo-physical properties of rocks and soils are useful in the determination of the relations between the various parameters. The ISOMET 2114 measures directly the thermal conductivity, while thermal diffusivity and volumetric heat capacity are obtained indirectly using reference standards of density (see eq. 3.7).

6.1 Thermal conductivity

From the distinction between the measurements made in the direction parallel and perpendicular to the stratification was then calculated the anisotropy factor A_λ in dry conditions. Most of the rocks analyzed can be considered isotropic, because of their anisotropy factor is very near to one. In fact, the ratio A_λ generally falls in the range 0,9 - 1,11, with the exception of the dolomite (sample 19A) belonging to Contrin formation, which has a factor of anisotropy equal to 1,79. This is probably due to the presence of fault lines through the outcrop, that may have caused oriented cracks. For phyllite, which is certainly anisotropic for its elevated schistosity, it was not possible to calculate $\lambda_{parallel}$ due to the small size of the sample. In general for sedimentary and volcanic rocks is not highlighted any remarkable deviation from the value of 1 of the anisotropy factor. In table 6.1 are shown the values of the anisotropy factor A_λ, where possible.

Table 6.1: factor of anisotropy A_λ for rock samples in dry conditions.

Code	Lithology	Formation	λ_dry (W/m K)		
			parallel	normal	Aλ
12A	dolomite	Dolomia Principale	3,34	-	-
16A	limestone	Gruppo dei calcari grigi - Formazione di Rotzo	2,65	2,88	0,92
14A	limestone	Scaglia Rossa	-	2,17	-
24A	Micritic limestone	Formazione di Chiusole	2,47	2,28	1,08
8A	limestone	Gruppo dei calcari grigi - Formazione di Monte Zugna	2,42	2,97	0,82
17A	limestone	Rosso Ammonitico veronese	2,91	2,78	1,05
18A	rhyolite	Gruppo vulcanico atesino - Formazione di Ora	2,17	2,17	1,00
4B	calcarenite	Formazione di Werfen - Membri di Tesero e Mazzin	2,42	-	-
5A	Marly limestone	Formazione di Werfen - Membri di Tesero e Mazzin	-	2,13	-
6A	Micritic limestone	Formazione di Werfen - Membri di Tesero e Mazzin	2,68	2,76	0,97
6C	Micritic limestone	Formazione di Werfen - Membri di Tesero e Mazzin	2,64	2,58	1,03
26A	dolomite	Formazione di Giovo - Membro del Monte Ozol	4,99	-	-
19A	dolomite	Formazione del Contrin	4,25	2,36	1,80

23A	limestone	Calcare di Nago	2,48	2,47	1,00
20A	dolomite	Formazione dello Scillar	3,82	3,70	1,03
22A	calcarenite	Calcare di Malcesine	2,54	2,40	1,06
2A	volcanoclastic rock	Filoni a quarzo e calcite	1,35	1,26	1,07
15B	calcarenite	Calcare di Malcesine	2,36	2,32	1,02
10A	phyllite	Unità della Valsugana - Filladi	-	1,19	-
28A	andesite	Gruppo vulcanico atesino - Formazione di Buss	2,14	2,00	1,07
29A	riodacite	Gruppo vulcanico atesino - Formazione del Castelliere	1,76	-	-

In section 3.2, dedicated to the thermo-physical properties of materials, we have already seen what is the dependence of the thermal conductivity as a function of temperature, pressure, porosity, saturation, anisotropy. Taking these concepts into consideration for data obtained from laboratory measurements, Figures 6.1 and 6.2 show the variation of the parallel and normal thermal conductivity measured in dry and wet conditions with porosity for rock samples aggregated in sedimentary, volcanic and metamorphic rocks, making also a comparison between them. Porosity is important for the thermal conductivity, because the saturating fluid significantly influences the total thermal conductivity.

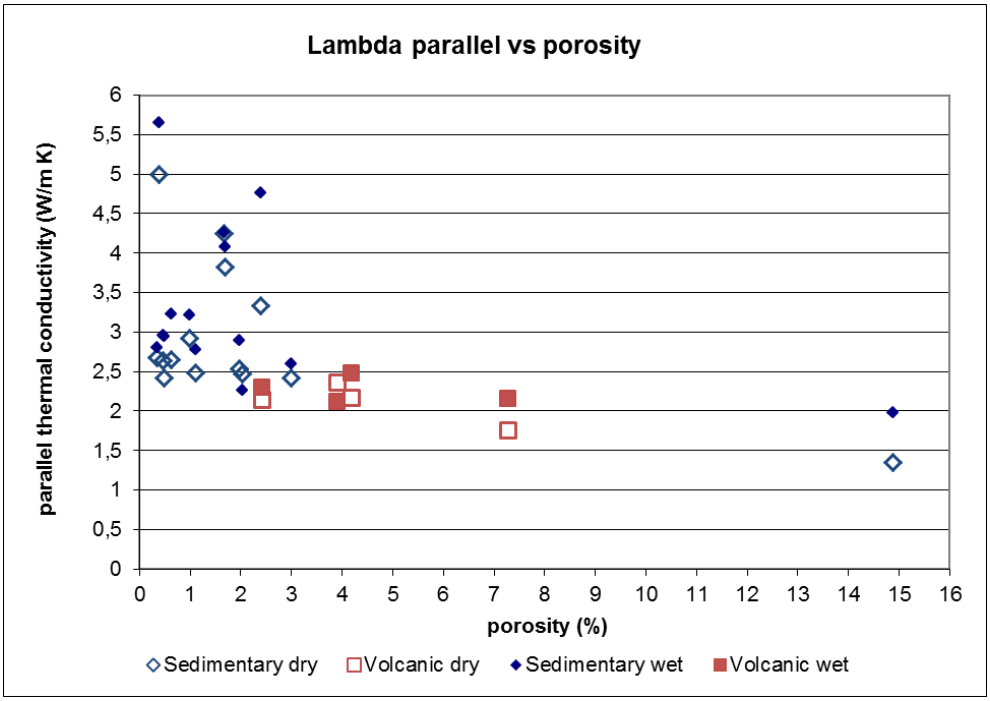

Figure 6.1: distribution of parallel thermal conductivity in dry and wet conditions vs porosity for sedimentary, volcanic and metamorphic rocks.

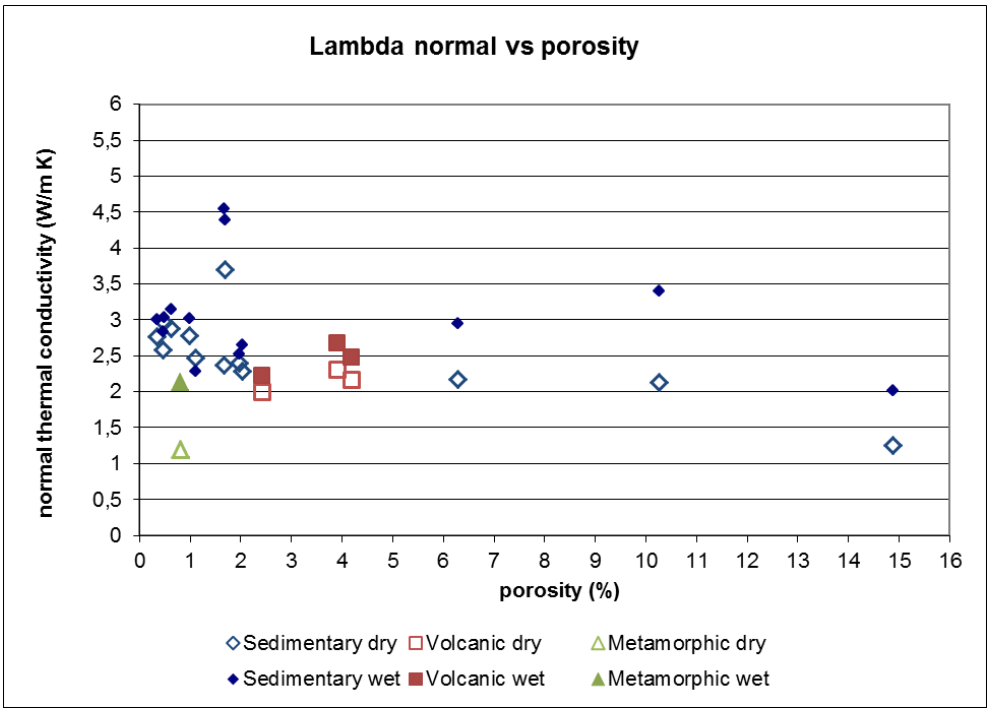

Figure 6.2: distribution of normal thermal conductivity in dry and wet conditions vs porosity for sedimentary, volcanic and metamorphic rocks.

As you would expect there is a decrease of thermal conductivity with increasing porosity in dry conditions, because air filling the voids is a poor thermic conductor, while a more irregular behavior of thermal conductivity with porosity is observed in wet conditions. Dolomites have a small variation in porosity but great in thermal conductivity, so they depend more on other factors than porosity. This is due to presence of cracks, crystals orientation and quartz intrusions, while limestones depend more on porosity. Volcanic rocks have porosity as main factor affecting thermal conductivity (see § 3.2.1).
The effect of saturation varies for porous or fractured rocks since the voids may or may not be interconnected. In any case the effect it is evident looking at the difference between dry and wet values: the thermal conductivity of the saturating fluid significantly influences the total thermal conductivity, so λ_{wet} is greater than λ_{dry}.

Rocks density depends on the composition (density of the mineral constituents), porosity and density of the pore fluids. Density and thermal conductivity are correlated (Fig. 6.3, 6.4); also for rocks containing quartz this effect can be attributed to the mineral. Quartz has a density of about 2630 kg/m^3 and a high thermal conductivity (7,7 W/mK). A higher content of this mineral phase entails greater thermal conductivity for a rock (Kukkonen I., Lindberg A., 1998).

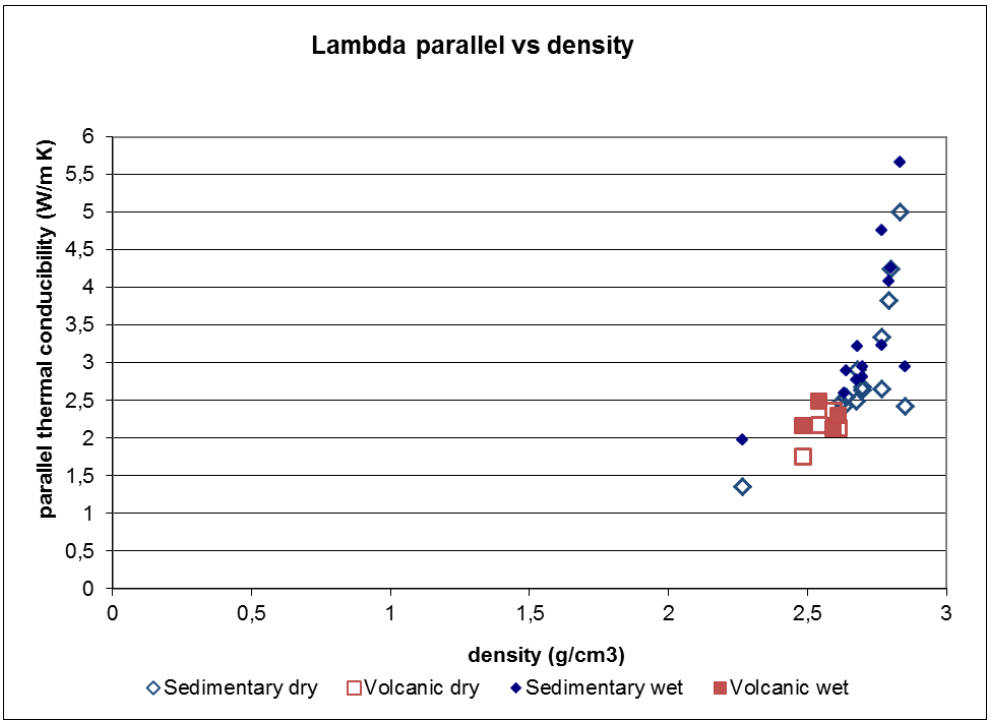

Figure 6.3: distribution of parallel thermal conductivity in dry and wet conditions vs density for sedimentary, volcanic and metamorphic rocks.

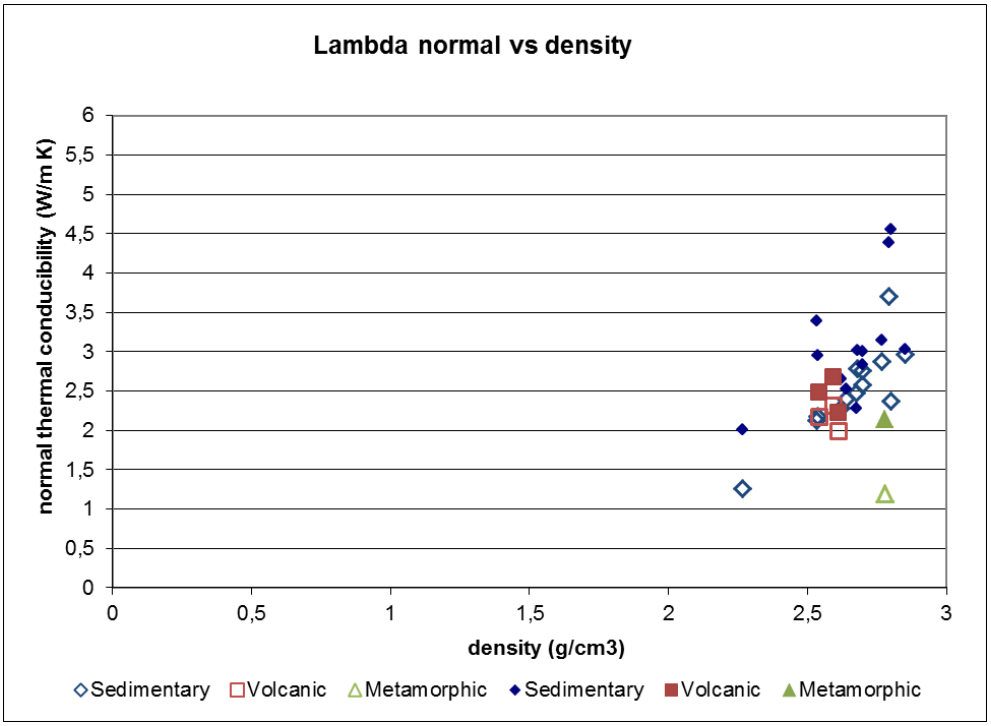

Figure 6.4: distribution of normal thermal conductivity in dry and wet conditions vs density for sedimentary, volcanic and metamorphic rocks.

Correlation between thermal conductivity and density is more evident for $\lambda_{parallel}$ rather than λ_{normal}. As for porosity, dolomites are distributed along a vertical line.

The relationship between thermal conductivity and density can be observed for both air and water saturated rocks. The air saturated samples showed a general exponential increase in

thermal conductivity as the density of the samples increases. This is attributed to the rock particles, because they have a much higher thermal conductivity than air which is 0,024 W/m K.

In wet conditions the thermal conductivity of the rocks increased due to the higher thermal conductivity of the water (0,6 W/m K) allowing greater heat flow. Nevertheless, density influences thermal conductivity more than the saturating fluid.

6.2 Volumetric heat capacity

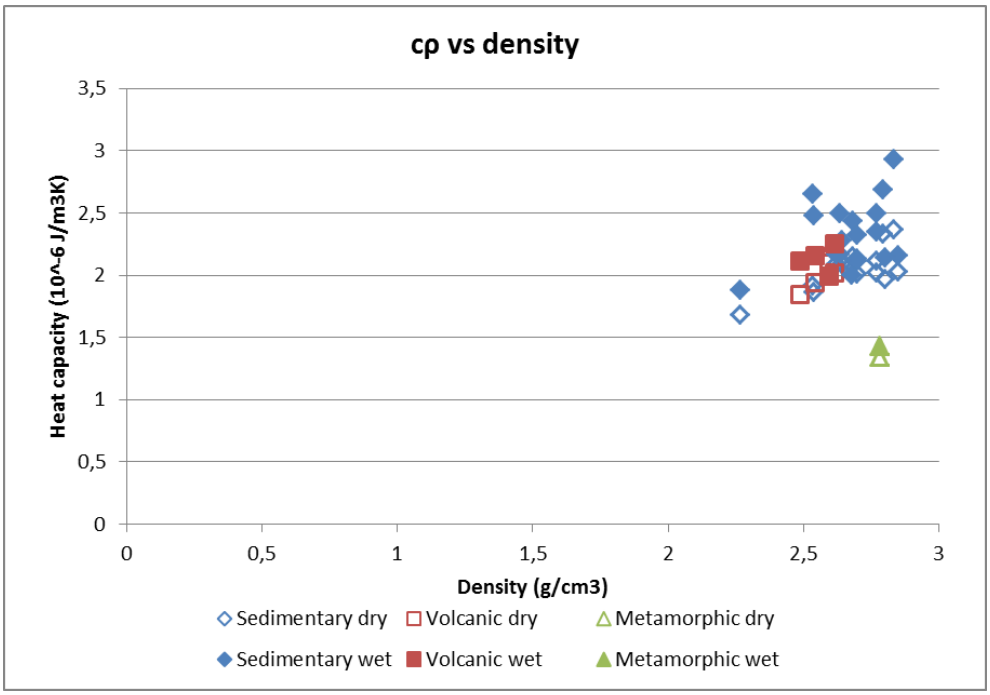

Figure 6.5: distribution of volumetric heat capacity in dry and wet conditions vs density for sedimentary, volcanic and metamorphic rocks.

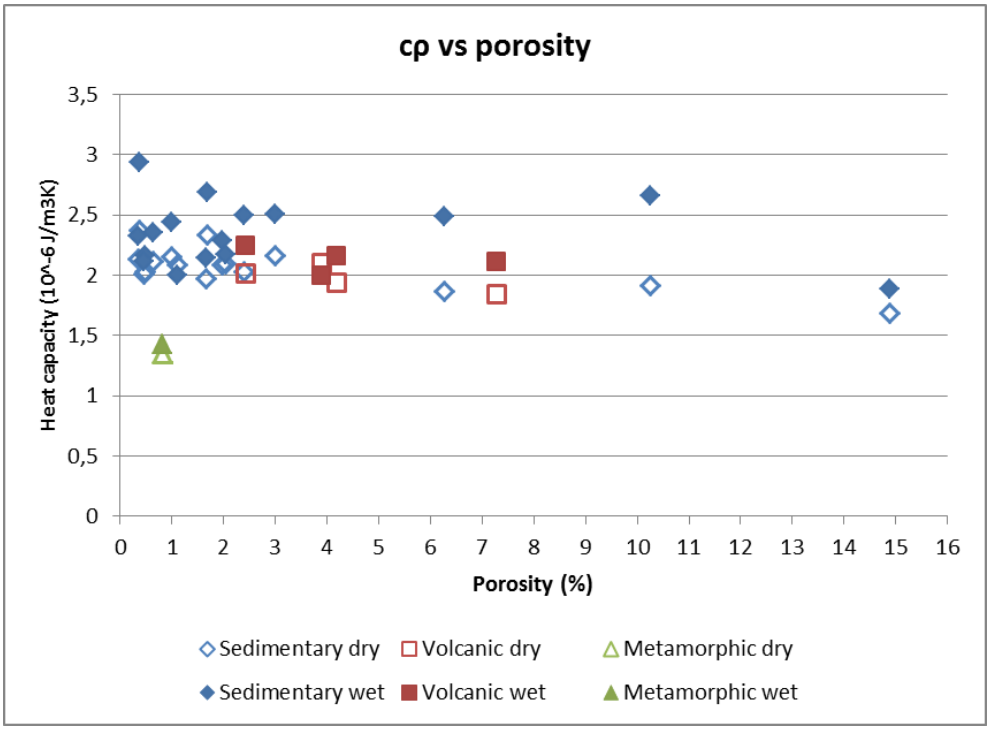

Figure 6.6: distribution of volumetric heat capacity in dry and conditions vs porosity for sedimentary, volcanic and metamorphic rocks.

Volumetric heat capacity is isotropic (Verrone, 2009) in contrast to thermal conductivity, so it was taken the mean of the values measured in the two faces of the rock samples. Since the amount of fluids present depends on the porosity, it is interesting to see the correlation between volumetric heat capacity and porosity measured (Fig. 6.6). It can be noticed that phyllite is far from the other values, out of an hypothetical correlation line; this is probably due to measurement errors (bad contact between sample and probe) or heterogeneities of the sample. It was taken only a measure perpendicular to stratification, and knowing that phyllite has a strong anisotropy the absence of parallel measure could have influenced the result.

6.3 Thermal diffusivity

Thermal diffusivity is linearly related to thermal conductivity (Fig. 6.7). This is not unexpected since the values of thermal conductivity can be used for the calculation of the thermal diffusivity according to the following equation:

(6.1) $$\kappa = \lambda/(\rho\, c_P)$$

where κ is the thermal diffusivity, λ the thermal conductivity, c_P is the specific heat and ρ the density, then the variables are not totally independent.

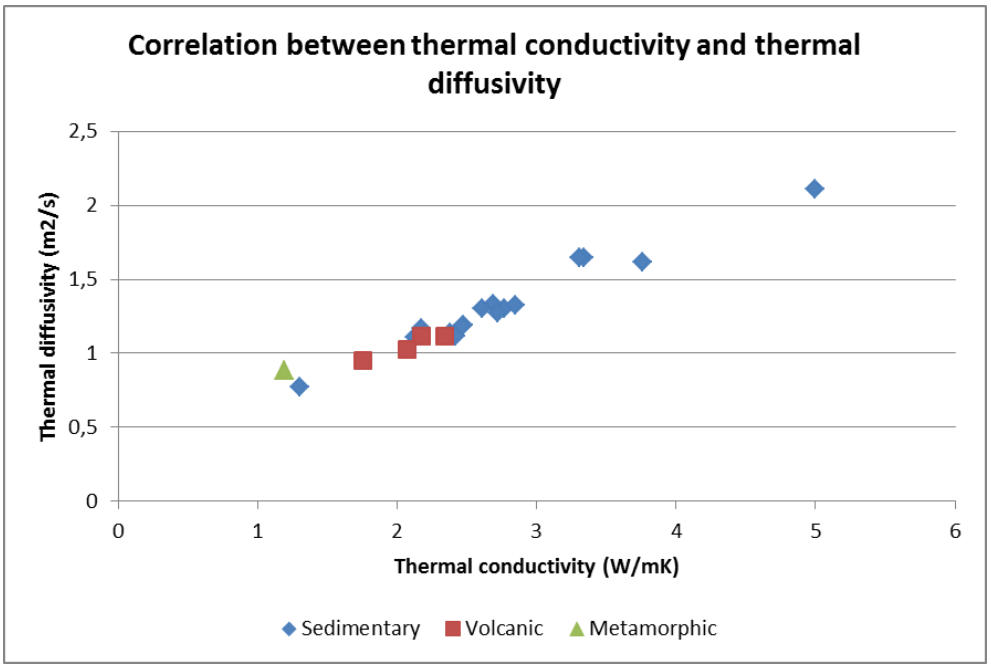

Figure 6.7: Correlation between measured thermal diffusivity and thermal conductivity.

For further research, it could be compared the thermal diffusivity measured by the instrument (with an indirect procedure) to that calculated form eq. (6.1), given λ and ρ from laboratory measurements and c_P from tabulated values.

Figures 6.8 and 6.9 show the relationship existing between the thermal diffusivity obtained in the laboratory and the density for the lithologies analyzed. It can be found an exponential behavior between the two parameters.

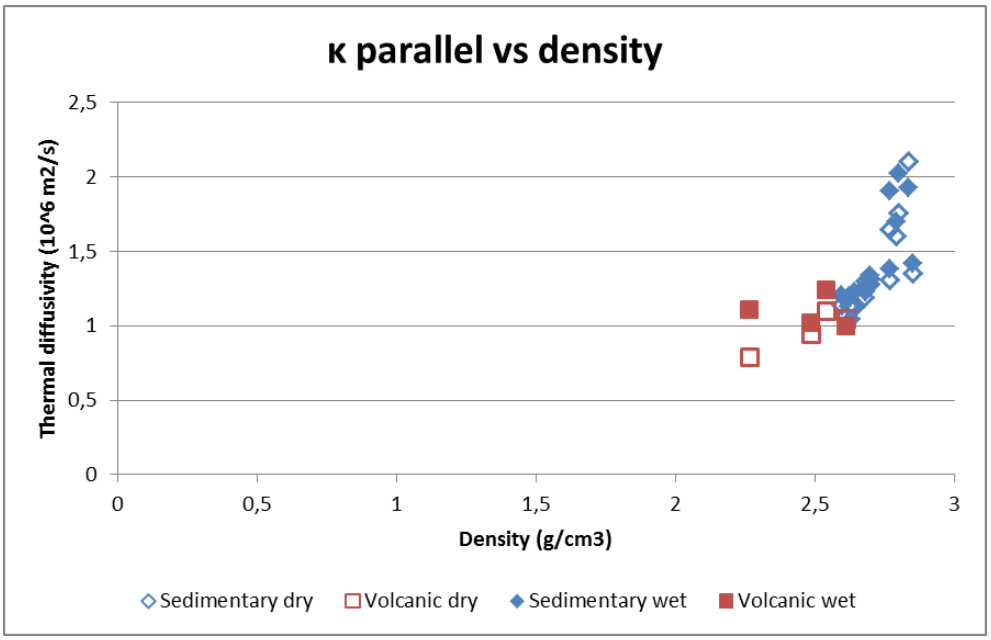

Figure 6.8: distribution of parallel thermal diffusivity in dry and wet conditions vs density for sedimentary, volcanic and metamorphic rocks.

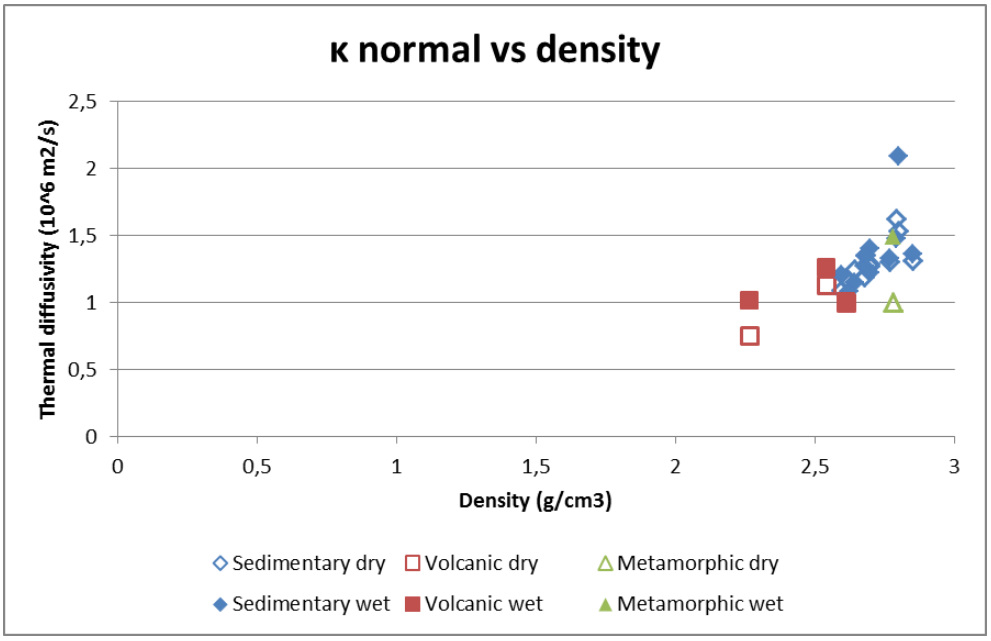

Figure 6.9: distribution of normal thermal diffusivity in dry and wet conditions vs density for sedimentary, volcanic and metamorphic rocks.

Figures 6.10 and 6.11 show the relationship existing between the thermal diffusivity obtained in laboratory and the density for the lithologies analyzed. It can be found a weak exponential behavior between the two parameters.

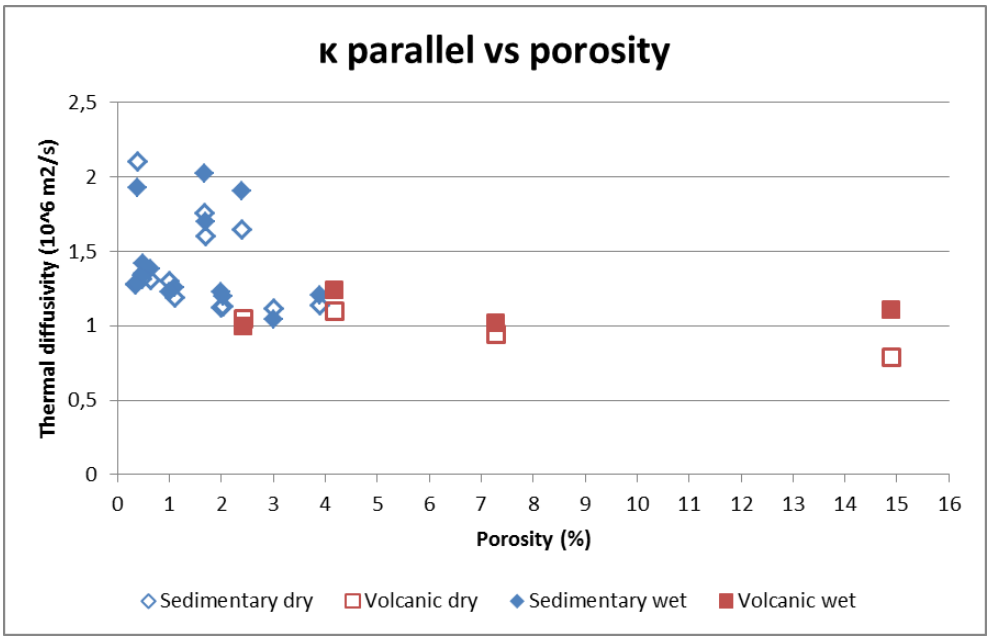

Figure 6.10: distribution of parallel thermal diffusivity in dry and wet conditions vs density for sedimentary, volcanic and metamorphic rocks.

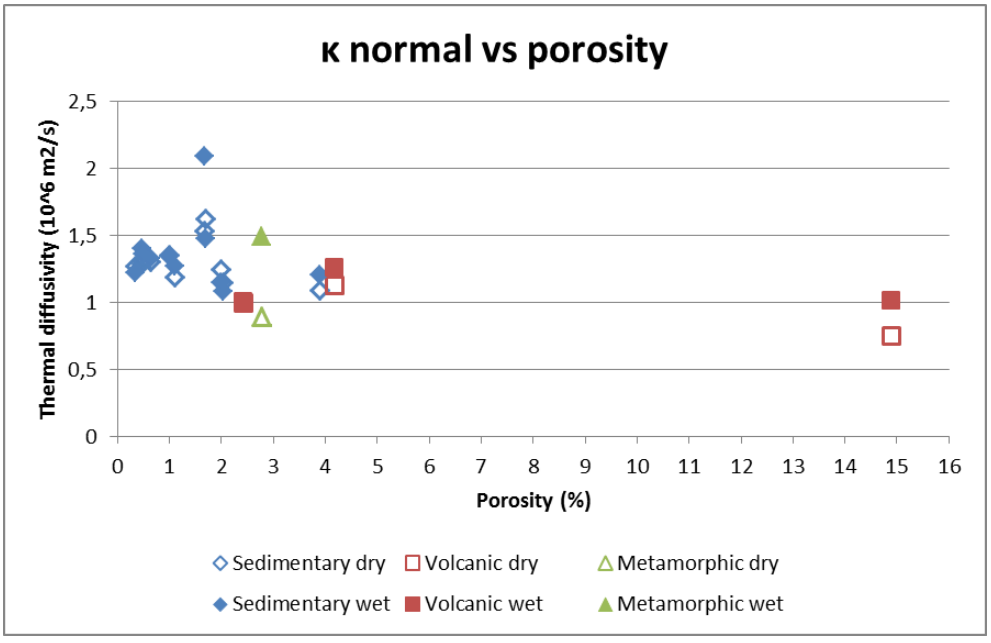

Figure 6.11: distribution of normal thermal diffusivity in dry and wet conditions vs density for sedimentary, volcanic and metamorphic rocks.

7. Conclusions

The thesis work has brought some results: it has created a first database of some of the lithologies present in the area of Trento, with their values of physical and thermal properties, that will be useful for the implementation of low enthalpy geothermal systems, in particular Borehole Thermal Energy Storage (BTES) systems.

Thermal conductivity describes the ability of a material to transmit heat, volumetric heat capacity describes the ability of a material to store heat increasing its temperature, and thermal diffusivity describes the ability of a material to conduct thermal energy relative to its ability to store thermal energy. These parameters, especially λ and κ, are useful in BTES systems to calculate properly the heat dispersion and the efficiency of the storage. Also, with values of density and porosity it was possible to verify the dependence of thermal properties with these two parameters.
Starting from literature search, measuring thermal properties in different conditions (dry, wet, parallel, normal) allows a more precise characterization of the rocks, enabling to use some values rather than others to be in a conservative side. For example it is recommendable to use dry parallel thermal conductivity when orientation of rock and presence of water are unknown.

The results obtained with the use of ISOMET 2114 instrumentation about thermal parameters of the rocks have a good correspondence with literature values. There are present some differences that reflect different methods of determination and the different mineral compositions of rock types analyzed by the various authors.
Also, for some samples only one surface was measured, and in presence of strong anisotropies this could have influenced significantly. A future study could be done widening the rock database: a greater number of samples, even of the same lithology, will provide enough data to properly study the behavior of sedimentary, volcanic and metamorphic rocks.

Taking measures of thermal properties with other instruments it would be interesting for comparing different procedures and methods. A different instrument can provide more accurate data, and if it requires a smaller flat surface for measurements, it would allow the measure on more of the collected samples.

With regard to thermal diffusivity, measured only in an indirect way by ISOMET, it would be interesting, having the possibility to get specific heat, to compare the thermal diffusivity calculated with equation (6.1) with instrument results, to test the reliability of ISOMET.

Further studies may involve a thermal characterization of the subsoil of Trento province using Geographical Information System (GIS), also taking into account the thickness of lithologies.

8. References

AA.VV. (?). Geoscambio nella provincia di Treviso.

Alishaev, M.G., Abdulagatov, I.M., & Abdulagatova, Z.Z. (2012). Effective thermal conductivity of fluid-saturated rocks. Experiment and modeling. *Engineering Geology, 135–136*, 24–39.

Avanzini, M., Bargossi, G., Borsato, A., & Selli L. (2010). Note illustrative della Carta Geologica d'Italia alla scala 1:50.000: Foglio 060 Trento.

Banks, D., Robins, N. S., & Robins, N. (2002). *An introduction to groundwater in crystalline bedrock*. Norges Geologiske Undersokelse.

Barry-Macaulay, D., Bouazza, A., Singh, R.M., Wang, B., & Ranjith, P.G. (2013). Thermal conductivity of soils and rocks from the Melbourne (Australia) region. *Engineering Geology, 164,* 131–138.

Bateman, R., Harris, A., & Park, A. (2011). MTPS sensor to determine thermal conductivity of geological samples. CTAS2011 conference.

Bateman, R, & Kuvandykova, D. (2010). A new transient method to measure thermal conductivity of asphalt. *C-Therm Technol*, *2*, 1-10.

Cha, J., Seo, J., & Kim, S. (2012). Building materials thermal conductivity measurement and correlation with heat flow meter, laser flash analysis and TCi. *Journal of thermal analysis and calorimetry*, *109*(1), 295-300.

Chieco, M. (2011). Geotermia a bassa entalpia: cenni introduttivi ed iniziative in Puglia. *Report 1/2011*.

Clauser, C. (2011). Thermal storage and transport properties of rocks, I: Heat capacity and latent heat. *Encyclopedia of Solid Earth Geophysics*, 1423-1431.

Clauser, C., & Huenges, E. (1995). Thermal conductivity of rocks and minerals. *AGU reference shelf*, *3*, 105-126.

De Carli, M., Del Bianco, R., Fellin, F., Manente, M., Tonon, M., & Zecchin, R. (2003). Sviluppi nelle pompe di calore: il terreno come sorgente termica. *Convegno Aicarr, Padova*.

Diao, N., Li, Q., & Fang, Z. (2004). Heat transfer in ground heat exchangers with groundwater advection. *International Journal of Thermal Sciences, 43*, 1203–1211.

Di Sipio, E., Chiesa, S., Destro, E., Galgaro, A., Giaretta, A., Gola, G., & Manzella, A. (2013). Rock thermal conductivity as key parameter for geothermal numerical models. *Energy Procedia*, *40*, 87-94.

Fondazione Bruno Kessler, Statuto.

Gangyan, G., Gorin, G., & Wagner, J. J. (2003). Physical properties of alpine rocks.

Gomes, A.J.L., & Hamza, V.M. (2005). Geothermal gradient and heat flow in the state of Rio de Janeiro. *Revista Brasileira de Geofisica, 23*(4), 325-347.

Gunn, D.A., Jones, L.D., Raines, M.G., Entwisle, D.C., & Hobbs, P.R.N. (2005). Laboratory measurement and correction of thermal properties for application to the rock mass. *Geotechnical and Geological Engineering , 23*, 773–791.

Hasnain, S. M. (1998). Review on sustainable thermal energy storage technologies, Part I: heat storage materials and techniques. *Energy Conversion and Management*, *39*(11), 1127-1138.

Jones, M.Q.W. (2003). Thermal properties of stratified rocks from Witwatersrand gold mining areas. *The South African Institute of Mining and Metallurgy,* 173-186.

Kukkonen, I., & Lindberg, A. (1998). Thermal properties of rocks at the investigation sites: measured and calculated thermal conductivity, specific heat capacity and thermal diffusivity. *Posiva working report 98-09e*.

Kušnerová, M., Valíček, J., Harničárová, M., Hryniewicz, T., Rokosz, K., Palková, Z., Václavík, V., Řepka, M., & Bendová, M. (2013). A Proposal for Simplifying the Method of Evaluation of Uncertainties in Measurement Results. *Measurement Science Review, 13*(1).

Lee, Y., & Deming, D. (1998). Evaluation of thermal conductivity temperature corrections applied in terrestrial heat flow studies. *Journal of geophysical research, 103*(B2), 2447-2454.

Lund, J. W. (2003). The USA geothermal country update. *Geothermics*, *32*(4), 409-418.

Lund, J. W. (2003). The use of downhole heat exchangers. *Geothermics*, *32*(4), 535-543.

Mottaghy, D., Vosteen, H. D., & Schellschmidt, R. (2008). Temperature dependence of the relationship of thermal diffusivity versus thermal conductivity for crystalline rocks. *International Journal of Earth Sciences*, *97*(2), 435-442.

Nordell, B., Grein, M., & Kharseh, M. (2007). Large-scale utilization of renewable energy requires energy storage. *International conference for renewable energies and sustainable development (ICRESD_07), Université Abou Bakr BELKAID—TLEMCEN, Algeria, May*, 21-24.

Norden, B. (2011). Geothermal Energy Utilization in Low-Enthalpy Sedimentary Environments. *Scientific Technical Report STR 11/06, Deutsches GeoForschungsZentrum GFZ.*

Özkahraman, H. T., Selver, R., & IsIk, E.C. (2004). Determination of the thermal conductivity of rock from P-wave velocity. *International Journal of Rock Mechanics & Mining Sciences, 41,* 703–708.

Park, C., Synn, J.H., Shin, H.S., Cheon, D.S., Lim, H.D., & Jeon, S.W. (2004). Experimental study on the thermal characteristics of rock at low temperatures. *International Journal of Rock Mechanics & Mining Sciences, 41*(3).

Popov, Y.A., Pribnow, D.F.C., Sass, J.H., Williams, C.F., & Burkhardt, H. (1999). Characterization of rock thermal conductivity by high-resolution optical scanning. *Geothermics 28*, 253-276.

Pouloupatis, P. D., Florides, G., & Tassou, S. (2011). Measurements of ground temperatures in Cyprus for ground thermal applications. *Renewable Energy*, *36*(2), 804-814.

Sass, J.H., Kennelly, J.P., Smith, E. P., & Wendt, W.E. (1984). Laboratory line-source methods for the measurement of thermal conductivity of rocks near room temperature. United States Department of the Interior geological survey.

UNI EN 1936:2001, Natural stone test method. Determination of real density and apparent density, and of total and open porosity.

Verrone, A., Bruno, R., & Tinti, F. (2009). Sistemi per la climatizzazione mediante pompe di calore geotermiche e pali energetici.

Witte, H.J.L., Van Gelder, G.J., & Spitler, J.D. (2002). In Situ Measurement of Ground Thermal Conductivity: A Dutch Perspective. *ASHRAE Transactions, 108*(1), 263-272.